TOPICS IN TWO-DIMENSIONAL SYSTEMS WITH SPIN-ORBIT INTERACTION

A Dissertation

by

MARIO FRANCISCO BORUNDA BERMÚDEZ

Submitted to the Office of Graduate Studies of
Texas A&M University
in partial fulfillment of the requirements for the degree of

DOCTOR OF PHILOSOPHY

December 2008

Major Subject: Physics

TOPICS IN TWO-DIMENSIONAL SYSTEMS WITH SPIN-ORBIT INTERACTION

A Dissertation

by

MARIO FRANCISCO BORUNDA BERMÚDEZ

Submitted to the Office of Graduate Studies of
Texas A&M University
in partial fulfillment of the requirements for the degree of

DOCTOR OF PHILOSOPHY

Approved by:

Chair of Committee,	Jairo Sinova
Committee Members,	Donald G. Naugle
	Wayne Saslow
	Raymond E. Schaak
Head of Department,	Edward Fry

December 2008

Major Subject: Physics

ABSTRACT

Topics in Two-Dimensional Systems with Spin-Orbit Interaction. (December 2008)
Mario Francisco Borunda Bermúdez, B.S., The University of Texas at El Paso
Chair of Advisory Committee: Dr. Jairo Sinova

This dissertation focuses on the study of spin-dependent transport in systems with strong spin-orbit coupling within their band structure. In particular we focus on the anomalous Hall effect, the spin Hall effect, and the Aharonov-Casher effect whose origins, are linked to the presence of spin-orbit coupling. Given the theoretical controversy surrounding these effects we further simplify our studies to semiconductor systems where the band structure is much simpler than in metallic systems with heavy elements. To obtain finite analytical results we focus on reduced dimensions (two and one dimensions) which can be explored experimentally. To set the stage, we discuss the origins of the strong spin-orbit coupling in semiconductors deriving the effective interaction from the Dirac equation. We discuss in detail the skew scattering contribution to the anomalous Hall effect in two-dimensional systems, which is dominant for systems with low impurity concentrations, and find that it is reduced when the two chiral subbands are partially occupied in an electron gas and vanishes for a hole gas, regardless of the band filling. We also present calculations for all contributing mechanisms. We propose a device to test this prediction and study the crossover from the intrinsic to the extrinsic anomalous Hall effect. We calculate all contributions to the anomalous Hall effect in electron systems using the Kubo-Streda formalism. We find that all contributions vanish when both subbands are occupied and that the skew scattering contribution dominates when only the majority subband is occupied. We calculate the interference effects due to spin-orbit interaction in mesoscopic ring

structures patterned from HgTe quantum wells related to the Aharonov-Casher effect and the spin Hall effect. We find that the transport properties are affected by the carrier density as well as the spin orbit interaction. We find that the conductivity is larger in hole gas systems. We also show that devices with inhomogenous spin orbit interaction exhibit an electrically controlled spin-flipping mechanism.

To my wife, Yolanda

ACKNOWLEDGMENTS

Appreciation and acknowledgements are due to a great family: my wife, Yolanda, my parents, Silvia and Mario, my sisters, Silvia, and Laura, my brother, Antonio, and of course, my daughters, Iris, and Julia. With their support, they made everything possible. I would like to thank all of the faculty and staff in the physics department who helped me in so many ways. I would like to especially thank the professors of the outstanding classes I have taken while at Texas A&M: Siu A. Chin, Alexander Finkelstein, Chia-Ren Hu, Leonid Keldysh, Valery Pokrovsky, Joseph Ross, and Wayne Saslow. Finally, I would like to thank the members of my committee: Donald Naugle, Wayne Saslow, and Raymond Schaak. I hope they enjoy reading this dissertation.

While obtaining the understanding needed for this dissertation, I was able to work and interact with a large number of collaborators: Ar. Abanov, L. Brey, V. K. Dugaev, J.-I. Inoue, T. Lück, A. H. MacDonald, L. W. Molenkamp, K. Nomura, S. Y. Rodriguez, C. Timm, K. Výborný, J. Wunderlich, and J. Zemen. In work related to the anomalous Hall effect, Tamara Nunner and Nikolai Sinitsyn garner a special recognition. I also worked closely with the members of the Sinova group: Ewelina M. Hankiewicz, Alexey A. Kovalev, Xin Liu, Xiong-Jun Liu, and Liviu Zarbo. Professor Tomas Jungwirth, who was part of all work presented here and whose collaboration was fundamental. Of course, none of the chapters of this work would have been possible without my extremely patient advisor, Professor Jairo Sinova. I will always look back to those moments when we had to iron away wrinkle after wrinkle in a calculation, and will fondly remember all of those times throughout my career. Without everyone mentioned above, I would have more embarrassing mistakes that those that are inadvertently left.

TABLE OF CONTENTS

CHAPTER Page

LIST OF FIGURES

FIGURE Page

CHAPTER I

INTRODUCTION

The study of solid sate devices relies in large part on the transport properties of materials. Usually, resistance is of an ohmic nature:

$$V = IR$$

The above equation means that the voltage drop between the ends of a piece of material is proportional to the current flowing in the material, with the proportionality constant being R, the resistance of the material. A finer approach reveals that the resistance depends on the geometry of the material, its chemical composition and atomic arrangement [1]:

$$R = \frac{\rho\ l}{A}\ \ [3D], \quad R = \frac{\rho\ l}{W}\ \ [2D] \tag{1.1}$$

The quantity ρ is the electrical resistivity of the material and encapsulates its electrical transport properties. The geometric aspect is enclosed in A, the cross-sectional area of the material in three dimensional systems. In two dimensional systems, W is the width of the material which plays the role of A in three dimensional systems. The length of the material is denoted by l in both situations. In addition, ρ itself is in general not a single coefficient but a tensor, whose inverse is the conductivity tensor relating the applied electric fields in all directions and the induced currents.

In this dissertation, we explore the effect of spin-orbit interactions and disorder scattering in the conductivity tensor of semiconductors with reduced dimensionalities. We are interested in the response of the two dimensional electron(hole) gas

---

The journal model is *Physical Review Letters*.

in systems of infinite and mesoscopic sizes for semiconductors where the chemical composition and atomic arrangements are such that the spin-orbit coupling plays an important role in their transport properties. The main motivation of this research is to understand spin-dependent electronic transport in these systems. Specifically, we aim to understand the basic physics of the anomalous Hall effects in two-dimensional bulk semiconductors and the spin Hall effect and Aharonov-Casher effect in one-dimensional mesoscopic ring structures.

The area of research which focuses among other thing, on controlling the spin-dependent transport using electrical means, is also know as spintronics [2]. Spintronics has made its way into technological applications e.g., increases in the storage capacity of computers (through the effect known as giant magnetoresistance) [3] and nonvolatile, low-power, high-density magnetic random access memory (MRAM) [4] which may soon replace dynamic random access memory (DRAM) in personal computers. The two effects mentioned take place in metals. However, the majority of modern electronic devices are based on semiconductors and more applications will be possible when semiconductor devices can employ the spin degree of freedom as another functional variable in computational processing.

We study the effects of spin-orbit interaction in semiconductors given that it allows for the electrical control of the spin degree of freedom through gating acting in low dimensionality devices. The spin-orbit interaction also gives rises to unusual transport effects such as the anomalous Hall effect in ferromagnets, the spin Hall effect in paramagnetic materials, and the Aharonov-Casher effect in mesoscopic ring structures. This dissertation is devoted to topics in two-dimensional semiconductor systems with spin-orbit interaction. Chapter II discusses the origins of the spin-orbit coupling in semiconductors whose simple band structure is reviewed and derive the effective interaction starting with the Dirac equation. The next two chapters

pertain to the anomalous Hall effect. In Chapter III, we discuss in detail the skew scattering contribution to the anomalous Hall effect. This contribution is dominant for systems with low impurity concentrations. Chapter IV continues the treatment of the anomalous Hall effect with calculations for all the contributing mechanisms of the anomalous Hall effect within a simple two-dimensional system with strong spin-orbit coupling. In Chapter V, we shift our attention to interference effects due to spin-orbit interaction in mesoscopic ring structures patterned from HgTe quantum wells related to the Aharonov-Casher effect and the spin Hall effect.

CHAPTER II

SPIN ORBIT COUPLING IN THE WEAK RELATIVISTIC LIMIT

Open a graduate level quantum mechanics book to the section where the spin-orbit (SO) interaction is presented and it is likely the author introduces SO coupling qualitatively and in the context of the fine structure of the hydrogen atom or more generally, the Alkali atoms. For example, both Sakurai [5] and Shankar [6] state that the SO interaction is a relativistic effect. The electron and the nuclei interact via a Coulomb-like interaction ($V_c(r) \propto -e^2 r^{-1}$). The electron experiences an electric field due to the central force ($e > 0$):

$$\mathbf{E} = -\frac{\nabla V_c(r)}{e} \tag{2.1}$$

Given that the electron moves at a velocity $\mathbf{v}$ under the influence of the electric field, an effective magnetic field is present:

$$\mathbf{B_{eff}} = -\frac{\mathbf{v}}{c} \times \mathbf{E} \tag{2.2}$$

Note that in the rest frame of the same electron, the nuclei moves at a velocity $(-\mathbf{v})$, so that the induced magnetic field can also be written as:

$$\mathbf{B_{eff}} = -\frac{e}{c}\frac{\mathbf{v} \times \mathbf{r}}{r^3} \tag{2.3}$$

Then, the interaction energy of the electron's magnetic moment ($\boldsymbol{\mu} = -e\mathbf{S}/mc$) with this field is:

$$\begin{aligned} H_{int} &= -\boldsymbol{\mu} \cdot \mathbf{B_{eff}} = \frac{e}{mcr^3}\boldsymbol{\mu} \cdot (\mathbf{p} \times \mathbf{r}) = -\frac{e}{mc}\frac{\boldsymbol{\mu} \cdot \mathbf{L}}{r^3} \\ &= \frac{e^2}{m^2c^2r^3}\mathbf{S} \cdot \mathbf{L} \end{aligned} \tag{2.4}$$

this interaction energy[1] is the contribution to the Hamiltonian due to the SO interaction except that it is double the magnitude of the measured effect. Usually, the textbook will offer an argument, mentioning the Thomas factor [7], and state the correct result:

$$H_{so} = \frac{e^2}{2m^2c^2r^3}\mathbf{S}\cdot\mathbf{L} \tag{2.5}$$

As noted in Shankar's book, the above equation can be derived from the Dirac equation [6]. One fundamental aspect often overlooked in textbooks is that in solids the SO interaction has an enhanced effect in the properties of the material and the effective strength of the SO interaction is related to the band structure considered. For instance, in two-dimensional semiconductor heterostructures, the spin degree of freedom can be profoundly affected by SO coupling. This being an important topic of the present dissertation, we use this chapter to derive the SO interaction, by looking at the details that are commonly skipped in the textbook literature [8, 9]. We follow here a different strategy that the usual one followed by textbooks. We first go in detail through the derivation of the weak relativistic limit of the Dirac equation and apply this afterwards to the band structure of semiconductors. In doing so we are first going to arrive to the so called Pauli Hamiltonian (Eq. (2.57)), whose derivation is shown in full detail in the subsection below, and find the connection with the effect of SO coupling on the band structure of semiconductors.

[1] Performing the same calculation but using Eq. 2.2 for the magnetic field, gives the interaction energy as [5]:

$$\begin{aligned} H_{int} &= -\boldsymbol{\mu}\cdot\mathbf{B_{eff}} = \boldsymbol{\mu}\cdot\left(\frac{\mathbf{v}}{c}\times\mathbf{E}\right) = -\left(\frac{e\mathbf{S}}{mc}\right)\cdot\left(\frac{\mathbf{p}}{mc}\times\frac{\nabla V_c(r)}{e}\right) \\ &= -\frac{\mathbf{S}}{mc}\cdot\left(\frac{\mathbf{p}}{mc}\times\frac{\mathbf{r}}{r}\frac{dV_c(r)}{dr}\right) = \frac{1}{m^2c^2}\frac{1}{r}\frac{dV_c(r)}{dr}(\mathbf{S}\cdot\mathbf{L}) \end{aligned}$$

A. Introduction to Dirac equation: from Schrödinger to Dirac

The Schrödinger equation as a quantum mechanical equation of motion is postulated in correspondence to classical mechanics. For instance for a free particle:

$$E = \frac{\mathbf{p}^2}{2m}, \tag{2.6}$$

and we know that the operators $E \to i\hbar\frac{\partial}{\partial t}$ and $\mathbf{p} \to -i\hbar\nabla$ so that

$$i\hbar\frac{\partial}{\partial t}\Psi(\mathbf{x},t) = -\frac{\hbar^2}{2m}\nabla^2\Psi(\mathbf{x},t). \tag{2.7}$$

Please note that throughout this chapter, whenever the gradient (∇) appears it is specifically acting on the immediate expression to its right and not as an operator; when acting as an operator we will write it as $i\mathbf{p}/\hbar$. To write a quantum relativistic equation of motion, a logical first step is:

$$E^2 = c^2\mathbf{p}^2 + m^2c^4 \tag{2.8}$$

$$\left(i\hbar\frac{\partial}{\partial t}\right)^2\Psi(\mathbf{x},t) = \left[c^2(-\hbar^2\nabla^2) + m^2c^4\right]\Psi(\mathbf{x},t) \tag{2.9}$$

$$0 = \left(\frac{1}{c^2}\frac{\partial^2}{\partial t^2} - \nabla^2 + \frac{m^2c^2}{\hbar^2}\right)\Psi(\mathbf{x},t) \tag{2.10}$$

$$\tag{2.11}$$

This is the Klein-Gordon (KG) equation. It is a scalar equation (particles with zero spin), but it has two groups of solutions each with either positive or negative energy. The continuity equation that follows from the KG equation is

$$\frac{\hbar}{2mc^2}\frac{\partial}{\partial t}\left(\Psi^*\frac{\partial\Psi}{\partial t} - \Psi\frac{\partial\Psi^*}{\partial t}\right) = \frac{\hbar}{2m}\nabla\left(\Psi^*\nabla\Psi - \Psi\nabla\Psi^*\right) \tag{2.12}$$

To maintain the usual probabilistic interpretation, we have to define the density as:

$$\varrho_{\text{KG}} \equiv \frac{i\hbar}{2mc^2}\left(\Psi^*\dot{\Psi} - \Psi\dot{\Psi}^*\right) \tag{2.13}$$

The density is negative for eigenstates of negative energy. We could simply say, that there are no physical states corresponding to these peculiar solutions, but it can be shown that after confining a particle to a finite volume its wave packet will always contain states with negative energy [10].

Another problem with the KG equation is the second time derivative, which impairs the causality of an equation of motion. In order to obtain an equation that yields the right probabilistic interpretation of the density, i.e. $\rho > 0$, the desired form of an equation of motion is:

$$i\hbar\frac{\partial\Psi}{\partial t} = H\Psi, \tag{2.14}$$

where

$$H = c\boldsymbol{\alpha}\mathbf{p} + \beta mc^2 \tag{2.15}$$

$$H^2 = c^2(-\hbar^2\nabla^2) + m^2c^4 = E^2 \tag{2.16}$$

Coefficients $\boldsymbol{\alpha}$ and β must be determined from this restriction. The condition above together with hermiticity of the Hamiltonian leads to conditions:

$$\{\alpha_j, \alpha_k\} = 2\delta_{jk}, \tag{2.17}$$

$$\{\alpha_j, \beta\} = 0, \text{ and} \tag{2.18}$$

$$\beta^2 = 1, \tag{2.19}$$

which form the so called Dirac algebra. Any matrices $\boldsymbol{\alpha}$ and β fulfilling these conditions are connected by a unitary transformation. The most commonly used representation in condensed matter physics is the Dirac realization:

$$\boldsymbol{\alpha} = \sigma_1 \otimes \boldsymbol{\sigma} \text{ and} \tag{2.20}$$

$$\beta = \sigma_3 \otimes 1, \tag{2.21}$$

which allows a simple spin interpretation (σ_j are Pauli matrices).

Now we are ready to write the Dirac equation for a free particle:

$$i\hbar\frac{\partial}{\partial t}\Psi(\mathbf{x},t) = (c\boldsymbol{\alpha}\cdot\mathbf{p} + \beta mc^2)\Psi(\mathbf{x},t) \tag{2.22}$$

It is a vector equation. The object $\Psi(\mathbf{x},t)$ has four components and it is called a bispinor. There are still solutions with positive and negative energy but now the continuity equation is

$$\frac{\partial}{\partial t}\left(\Psi^{+}\Psi\right) = -c\nabla\left(\Psi^{+}\boldsymbol{\alpha}\Psi\right). \tag{2.23}$$

This time, the density $\varrho_{\mathrm{D}} \equiv \Psi^{+}\Psi$ is positive for any solution (bispinor). That means the equation has a reasonable probabilistic interpretation. The problem of negative energies is addressed by quantum field theory. At the same time, the Dirac equation contains only the first derivative with respect to time so we can use it as a relativistic equation of motion in the following section.

B. From Dirac equation to spin orbit coupling

We start the derivation from the Dirac equation introduced in Eq. (2.22) and use the electromagnetic field described by potentials $\mathbf{A}$ and $V = -e\varphi$. These potentials enter the equation through the usual substitution:

$$\mathbf{p} \to \mathbf{p} - e\mathbf{A} \equiv \boldsymbol{\pi} \text{ and } \varepsilon \to \varepsilon + \mathbf{V}, \tag{2.24}$$

where

$$i\hbar\frac{\partial}{\partial t}\Psi(\mathbf{x},t) = \varepsilon\Psi(\mathbf{x},t). \tag{2.25}$$

In the Dirac realization the bispinor is written as

$$\Psi(\mathbf{x},t) = \begin{pmatrix} \varphi(\mathbf{x},t) \\ \chi(\mathbf{x},t) \end{pmatrix}, \tag{2.26}$$

where, as we will see below, χ is smaller than φ in the non-relativistic limit by a factor of v/c. We obtain then two coupled equations for the spinors

$$(i\hbar\frac{\partial}{\partial t} - V - mc^2)\varphi = c\ \boldsymbol{\sigma}\cdot(\mathbf{p} - e\mathbf{A})\chi = c\ \boldsymbol{\sigma}\cdot\boldsymbol{\pi}\chi \tag{2.27}$$

$$(i\hbar\frac{\partial}{\partial t} - V + mc^2)\chi = c\ \boldsymbol{\sigma}\cdot(\mathbf{p} - e\mathbf{A})\varphi = c\ \boldsymbol{\sigma}\cdot\boldsymbol{\pi}\varphi \tag{2.28}$$

Here, mc^2 is typically a large energy scale and V is usually smaller than this scale so we look for energy solutions where the non-rest mass energy,

$$E \equiv \varepsilon - mc^2, \tag{2.29}$$

is small ($|E| \ll mc^2$) i.e., the total energy is very close to the rest energy in this scale.

We proceed in two steps: First, we obtain the Dirac equation to first order in v/c. Afterwards, we obtain the Dirac equation to second order in v/c. Throughout this chapter we use the following identity:

$$\begin{aligned}(\boldsymbol{\sigma}\cdot\mathbf{X})(\boldsymbol{\sigma}\cdot\mathbf{Y}) &= \sum_{ij}\sigma_i X_i \sigma_j Y_j = \sum_{i=j}\sigma_i X_i \sigma_j Y_j + \sum_{i\neq j}\sigma_i X_i \sigma_j Y_j \\ &= \sum_i X_i Y_i + i\sum_k \varepsilon_{ijk}\sigma_k X_i Y_j = \mathbf{X}\cdot\mathbf{Y} + i\boldsymbol{\sigma}\cdot[\mathbf{X}\times\mathbf{Y}] \end{aligned} \tag{2.30}$$

which simplifies the operator algebra,

$$(\boldsymbol{\sigma}\cdot\mathbf{p})(\boldsymbol{\sigma}\cdot\mathbf{p}) = \mathbf{p}^2 \tag{2.31}$$

$$(\boldsymbol{\sigma}\cdot\boldsymbol{A})(\boldsymbol{\sigma}\cdot\mathbf{p}) = \boldsymbol{A}\cdot\mathbf{p} + i\boldsymbol{\sigma}\cdot[\boldsymbol{A}\times\mathbf{p}] \tag{2.32}$$

$$\begin{aligned}(\boldsymbol{\sigma}\cdot\mathbf{p})(\boldsymbol{\sigma}\cdot\boldsymbol{A}) &= \mathbf{p}\cdot\boldsymbol{A} + \mathbf{i}\boldsymbol{\sigma}\cdot[\mathbf{p}\times\boldsymbol{A}] = \mathbf{p}\cdot\boldsymbol{A} - \mathbf{i}\boldsymbol{\sigma}\cdot[\boldsymbol{A}\times\mathbf{p}] + \hbar\boldsymbol{\sigma}\cdot[\nabla\times\boldsymbol{A}] \\ &= \mathbf{p}\cdot\boldsymbol{A} - i\boldsymbol{\sigma}\cdot[\boldsymbol{A}\times\mathbf{p}] + \hbar\boldsymbol{\sigma}\cdot\boldsymbol{B}, \end{aligned} \tag{2.33}$$

yielding

$$(\boldsymbol{\sigma}\cdot(\mathbf{p}-e\boldsymbol{A}))^2=(\mathbf{p}-e\boldsymbol{A})^2-e\hbar\boldsymbol{\sigma}\cdot\boldsymbol{B}. \tag{2.34}$$

1. Dirac equation to first in order in v/c: Pauli Hamiltonian

To obtain the Dirac equation to first order in v/c we rewrite Eq. 2.28,

$$(i\hbar\frac{\partial}{\partial t}-V-mc^2)\chi+2mc^2\chi \;=\; c\,\boldsymbol{\sigma}\cdot(\mathbf{p}-e\boldsymbol{A})\varphi=c\,\boldsymbol{\sigma}\cdot\boldsymbol{\pi}\varphi \tag{2.35}$$

For $\epsilon\approx mc^2$, the *lower* spinor equation, can then be approximated by

$$\chi=\frac{c\,\boldsymbol{\sigma}\cdot(\mathbf{p}-e\boldsymbol{A})}{2mc^2}\varphi+O\left(\frac{v^2}{c^2}\right)=\frac{\boldsymbol{\sigma}\cdot\boldsymbol{\pi}}{2mc}\varphi+O\left(\frac{v^2}{c^2}\right) \tag{2.36}$$

Note that χ is a factor of v/c smaller than φ. Inserting the above equation into Eq. (2.27), results in an equation for the *upper* spinor:

$$(i\hbar\frac{\partial}{\partial t}-mc^2-V)\varphi=\frac{1}{2m}(\boldsymbol{\sigma}\cdot\boldsymbol{\pi})^2\varphi+O\left(\frac{v^2}{c^2}\right) \tag{2.37}$$

$$i\hbar\frac{\partial}{\partial t}\varphi=\frac{1}{2m}\boldsymbol{\pi}^2\varphi-\frac{e\hbar}{2m}\boldsymbol{\sigma}\cdot\boldsymbol{B}\varphi+(mc^2+V)\varphi \tag{2.38}$$

Eq. 2.38 is the Pauli Hamiltonian which gives the relativistic correction to order v/c and naturally gives the Zeeman contribution with the correct g-factor of 2.

2. Dirac equation to second order in v/c

In obtaining the Dirac equation to second order in v/c we need to first obtain the equation for the lower spinor (χ) up to second order. The first task consists of manipulating Eq. (2.28) by adding and subtracting $2mc^2\chi$:

$$(i\hbar\frac{\partial}{\partial t}-V-mc^2)\chi+2mc^2\chi=c\,\boldsymbol{\sigma}\cdot(\mathbf{p}-e\boldsymbol{A})\varphi \tag{2.39}$$

Then, solving for χ:

$$\chi = \frac{1}{2mc^2}\left[c\,\boldsymbol{\sigma}\cdot\boldsymbol{\pi}\varphi - (i\hbar\frac{\partial}{\partial t} - V - mc^2)\chi\right] \tag{2.40}$$

This provides a recursive way of obtaining higher corrections in (v/c) of the equation since now we can insert iteratively the first order approximation to the last term and obtain the second order equation for χ:

$$\chi = \frac{1}{2mc^2}\left[c\,\boldsymbol{\sigma}\cdot\boldsymbol{\pi}\varphi - (i\hbar\frac{\partial}{\partial t} - V - mc^2)\frac{1}{2mc}\boldsymbol{\sigma}\cdot\boldsymbol{\pi}\varphi\right] \tag{2.41}$$

We can then substitute this into Eq. 2.27 (re-written below) for the upper spinor (ϕ) and obtain:

$$\begin{aligned}(i\hbar\frac{\partial}{\partial t} - V - mc^2)\varphi &= c\,\boldsymbol{\sigma}\cdot\boldsymbol{\pi}\chi \\ &= \frac{(\boldsymbol{\sigma}\cdot\boldsymbol{\pi})^2}{2m}\varphi - \frac{\boldsymbol{\sigma}\cdot\boldsymbol{\pi}}{4m^3c^2}(i\hbar\frac{\partial}{\partial t} - V - mc^2)\boldsymbol{\sigma}\cdot\boldsymbol{\pi}\varphi \end{aligned} \tag{2.42}$$

Therefore, we need to evaluate the commutator of the expression $(i\hbar(\partial/\partial t) - V - mc^2)$with $\boldsymbol{\sigma}\cdot\boldsymbol{\pi}$ in order to use the substitution found from Eq. 2.37.

$$\begin{aligned}\left[(i\hbar\frac{\partial}{\partial t} - V - mc^2), \boldsymbol{\sigma}\cdot(\mathbf{p} - e\boldsymbol{A})\right] &= [i\hbar\frac{\partial}{\partial t}, -e\boldsymbol{\sigma}\cdot\boldsymbol{A}] + [-V, \boldsymbol{\sigma}\cdot\mathbf{p}] \\ &= -ie\hbar\boldsymbol{\sigma}\cdot\frac{\partial\boldsymbol{A}}{\partial t} - i\hbar\boldsymbol{\sigma}\cdot\nabla V \\ &= i\hbar e\boldsymbol{\sigma}\cdot\mathbf{E}(\mathbf{r},t) \end{aligned} \tag{2.43}$$

Thus,

$$\left(i\hbar\frac{\partial}{\partial t} - V - mc^2\right)\boldsymbol{\sigma}\cdot\boldsymbol{\pi} = \boldsymbol{\sigma}\cdot\boldsymbol{\pi}\left(i\hbar\frac{\partial}{\partial t} - V - mc^2\right) + i\hbar e\boldsymbol{\sigma}\cdot\mathbf{E}(\mathbf{r},t) \tag{2.44}$$

Substituting Eq. (2.44) and using Eq. (2.37), the Pauli Hamiltonian, in the last term of Eq. (2.42), we obtain

$$\left(i\hbar\frac{\partial}{\partial t} - V - mc^2\right)\varphi = \left[\frac{(\boldsymbol{\sigma}\cdot\boldsymbol{\pi})^2}{2m} - \frac{1}{8m^3c^2}(\boldsymbol{\sigma}\cdot\boldsymbol{\pi})^4 - \frac{i\hbar e}{4m^2c^2}(\boldsymbol{\sigma}\cdot\boldsymbol{\pi})\boldsymbol{\sigma}\cdot\mathbf{E}\right]\varphi \quad (2.45)$$

However, the equation presented above, which could be interpreted as the effective Hamiltonian for φ, is not Hermitian. The reason is that we have looked for an effective Hamiltonian that is a 2×2 matrix rather than the 4×4 which we started with. Remember that the particle state is described by Ψ and not φ alone,

$$\int \varphi^\dagger\varphi \neq 1 \quad (2.46)$$

Since it is the bispinor $\tilde{\varphi}$ which is normalized, starting from the normalization condition of Ψ:

$$\int \Psi^\dagger\Psi = 1 = \int \varphi^\dagger\varphi + \chi^\dagger\chi \approx \int \varphi^\dagger\left(1 + \frac{(\boldsymbol{\sigma}\cdot\boldsymbol{\pi})^2}{4m^2c^2}\right)\varphi = \int \tilde{\varphi}^\dagger\tilde{\varphi} + O\left(\frac{v^3}{c^3}\right) \quad (2.47)$$

where we used Eq. 2.36 and defined

$$\tilde{\varphi} \equiv \left(1 + \frac{(\boldsymbol{\sigma}\cdot\boldsymbol{\pi})^2}{8m^2c^2}\right)\varphi \equiv \hat{G}\varphi, \quad (2.48)$$

we can obtain an effective Hamiltonian for $\tilde{\varphi}$ rather than φ. To accomplish this, we need to go back to Eq. 2.42 and multiply it by the operator $\hat{G}$, acting from the left. The terms in the right hand side of Eq. 2.42 commutes with $\hat{G}$ or are terms that are already of order v^2/c^2 so we do not need to consider them:

$$\begin{aligned}\hat{G}&\left[\frac{(\boldsymbol{\sigma}\cdot\boldsymbol{\pi})^2}{2m} - \frac{1}{4m^3c^2}\boldsymbol{\sigma}\cdot\boldsymbol{\pi}(i\hbar\frac{\partial}{\partial t} - V - mc^2)\boldsymbol{\sigma}\cdot\boldsymbol{\pi}\right]\varphi \\ &= \left[\frac{(\boldsymbol{\sigma}\cdot\boldsymbol{\pi})^2}{2m} - \frac{1}{4m^3c^2}\boldsymbol{\sigma}\cdot\boldsymbol{\pi}(i\hbar\frac{\partial}{\partial t} - V - mc^2)\boldsymbol{\sigma}\cdot\boldsymbol{\pi}\right]\hat{G}\varphi + O\left(\frac{v^2}{c^2}\right) \quad (2.49)\end{aligned}$$

For the left hand side of Eq. 2.42, we need to calculate the commutator of $\hat{G}$ and $(i\hbar\frac{\partial}{\partial t} - V - mc^2)$:

$$\left[\hat{G}, (i\hbar\frac{\partial}{\partial t} - V - mc^2)\right] = \left[1 + \frac{(\boldsymbol{\sigma}\cdot\boldsymbol{\pi})^2}{8m^2c^2}, (i\hbar\frac{\partial}{\partial t} - V - mc^2)\right] \tag{2.50}$$

and,

$$\begin{aligned}
&\left[(\boldsymbol{\sigma}\cdot\boldsymbol{\pi})^2, (i\hbar\frac{\partial}{\partial t} - V - mc^2)\right] \\
&\quad = (\boldsymbol{\sigma}\cdot\boldsymbol{\pi})\left[(\boldsymbol{\sigma}\cdot\boldsymbol{\pi}), (i\hbar\frac{\partial}{\partial t} - V - mc^2)\right] + \left[(\boldsymbol{\sigma}\cdot\boldsymbol{\pi}), (i\hbar\frac{\partial}{\partial t} - V - mc^2)\right](\boldsymbol{\sigma}\cdot\boldsymbol{\pi}) \\
&\quad = -i\hbar e[(\boldsymbol{\sigma}\cdot\boldsymbol{\pi})(\boldsymbol{\sigma}\cdot\mathbf{E}) + (\boldsymbol{\sigma}\cdot\mathbf{E})(\boldsymbol{\sigma}\cdot\boldsymbol{\pi})]
\end{aligned} \tag{2.51}$$

We have computed the commutator explicitly, to obtain the effective Hamiltonian defined by $i\hbar\partial\tilde{\varphi}/\partial t = H_{\text{eff}}\tilde{\varphi}$:

$$\begin{aligned}
&\left(i\hbar\frac{\partial}{\partial t} - V - mc^2\right)\tilde{\varphi} + \left[\frac{(\boldsymbol{\sigma}\cdot\boldsymbol{\pi})^2}{8m^2c^2}, (i\hbar\frac{\partial}{\partial t} - V - mc^2)\right]\tilde{\varphi} \\
&\qquad = \left[\frac{(\boldsymbol{\sigma}\cdot\boldsymbol{\pi})^2}{2m} - \frac{1}{8m^3c^2}(\boldsymbol{\sigma}\cdot\boldsymbol{\pi})^4 - \frac{i\hbar e}{4m^2c^2}(\boldsymbol{\sigma}\cdot\boldsymbol{\pi})\boldsymbol{\sigma}\cdot\mathbf{E}\right]\tilde{\varphi},
\end{aligned} \tag{2.52}$$

We have obtained the final (although not simplified) expression for the effective Dirac Hamiltonian to v^2/c^2 order:

$$H_{\text{eff}} = \frac{(\boldsymbol{\sigma}\cdot\boldsymbol{\pi})^2}{2m} - \frac{1}{8m^3c^2}(\boldsymbol{\sigma}\cdot\boldsymbol{\pi})^4 + \frac{i\hbar e}{8m^2c^2}[-(\boldsymbol{\sigma}\cdot\boldsymbol{\pi})(\boldsymbol{\sigma}\cdot\mathbf{E}) + (\boldsymbol{\sigma}\cdot\mathbf{E})(\boldsymbol{\sigma}\cdot\boldsymbol{\pi})] \tag{2.53}$$

With the use of the identity Eq. 2.30, the last term can be rewritten:

$$\begin{aligned}
-(\boldsymbol{\sigma}\cdot\boldsymbol{\pi})(\boldsymbol{\sigma}\cdot\mathbf{E}) + (\boldsymbol{\sigma}\cdot\mathbf{E})(\boldsymbol{\sigma}\cdot\boldsymbol{\pi}) &= -\boldsymbol{\pi}\cdot\mathbf{E} - i\boldsymbol{\sigma}\cdot(\boldsymbol{\pi}\times\mathbf{E}) + \mathbf{E}\cdot\boldsymbol{\pi} + i\boldsymbol{\sigma}\cdot(\mathbf{E}\times\boldsymbol{\pi}) \\
&= i\hbar\nabla\cdot\mathbf{E} + i\boldsymbol{\sigma}\cdot(\mathbf{E}\times\boldsymbol{\pi}) - \hbar\boldsymbol{\sigma}\cdot(\nabla\times\mathbf{E}) + i\boldsymbol{\sigma}\cdot(\mathbf{E}\times\boldsymbol{\pi}) \\
&= i\hbar\nabla\cdot\mathbf{E} + i2\boldsymbol{\sigma}\cdot\mathbf{E}\times\boldsymbol{\pi} - \hbar\boldsymbol{\sigma}\cdot(\mathbf{E}\times\boldsymbol{\pi})
\end{aligned} \tag{2.54}$$

The $(\boldsymbol{\sigma}\cdot\boldsymbol{\pi})^4$ term can also be simplified since

$$(\boldsymbol{\sigma}\cdot\boldsymbol{\pi})^2 = \boldsymbol{\pi}^2 - e\hbar\boldsymbol{\sigma}\cdot\mathbf{B}, \tag{2.55}$$

thus,

$$\begin{aligned}(\boldsymbol{\sigma}\cdot\boldsymbol{\pi})^4 &= \boldsymbol{\pi}^4 - e\hbar(\boldsymbol{\pi}^2(\boldsymbol{\sigma}\cdot\mathbf{B}) + (\boldsymbol{\sigma}\cdot\mathbf{B})\boldsymbol{\pi}^2) + e^2\hbar^2\mathbf{B}^2 \\ &= \boldsymbol{\pi}^4 - e\hbar(\boldsymbol{\pi}\cdot(-i\hbar\nabla(\boldsymbol{\sigma}\cdot\mathbf{B}) + (\boldsymbol{\sigma}\cdot\mathbf{B})\boldsymbol{\pi}) + (\boldsymbol{\sigma}\cdot\mathbf{B})\boldsymbol{\pi}^2) + e^2\hbar^2\mathbf{B}^2 \\ &= \boldsymbol{\pi}^4 - e\hbar(-\hbar^2\nabla^2(\boldsymbol{\sigma}\cdot\mathbf{B}) - i2\hbar\nabla(\boldsymbol{\sigma}\cdot\mathbf{B})\cdot\boldsymbol{\pi} + 2(\boldsymbol{\sigma}\cdot\mathbf{B})\boldsymbol{\pi}^2) + e^2\hbar^2\mathbf{B}^2\end{aligned} \tag{2.56}$$

Using the above equation and Eq. (2.54), the expression for the effective Hamiltonian, which is also known as the Pauli Hamiltonian, becomes

$$\begin{aligned}H_{\text{eff}} &= mc^2 + V + \frac{1}{2m}\left[\boldsymbol{\pi}^2 - e\hbar(\boldsymbol{\sigma}\cdot\mathbf{B})\right] - \frac{\hbar}{8m^2c^2}\left[e\boldsymbol{\sigma}\cdot(2\mathbf{E}\times\boldsymbol{\pi} - i\hbar\frac{\partial\mathbf{B}}{\partial t}) + e\hbar\mathbf{B}^2\right. \\ &\left. -\frac{\hbar}{e}\nabla^2 V + \boldsymbol{\pi}^4 - e\hbar(-\hbar^2\nabla^2(\boldsymbol{\sigma}\cdot\mathbf{B}) - i2\hbar\nabla(\boldsymbol{\sigma}\cdot\mathbf{B})\cdot\boldsymbol{\pi} + 2(\boldsymbol{\sigma}\cdot\mathbf{B})\boldsymbol{\pi}^2)\right]\end{aligned} \tag{2.57}$$

The terms in the Pauli Hamiltonian (Eq. (2.57)) have a riveting interpretation. For instance, we see the kinetic energy term $\boldsymbol{\pi}^2/(2m)$ and its correction of order $(v/c)^2$ [9],

$$H_K = \frac{\boldsymbol{\pi}^2}{2m} - \frac{\boldsymbol{\pi}^4}{(2m)^3c^2} + O\left(\frac{v^4}{c^4}\right) \tag{2.58}$$

which compare satisfactorily to the classical relativistic kinetic energy,

$$\sqrt{c^2p^2 - m^2c^4} - mc^2 = \frac{p^2}{2m} - \frac{p^4}{8m^3c^2} + O\left(\frac{1}{c^4}\right) \tag{2.59}$$

We also obtained the Zeeman term, $e\hbar\boldsymbol{\sigma}\cdot\mathbf{B}/(2m)$, and its second order corrections:

$$H^{(2)}_{int} = \frac{(e\hbar\mathbf{B})^2}{(2m)^3c^2} + \frac{(\boldsymbol{\sigma}\cdot\mathbf{B})\boldsymbol{\pi}^2}{4m^3c^2} + ... \tag{2.60}$$

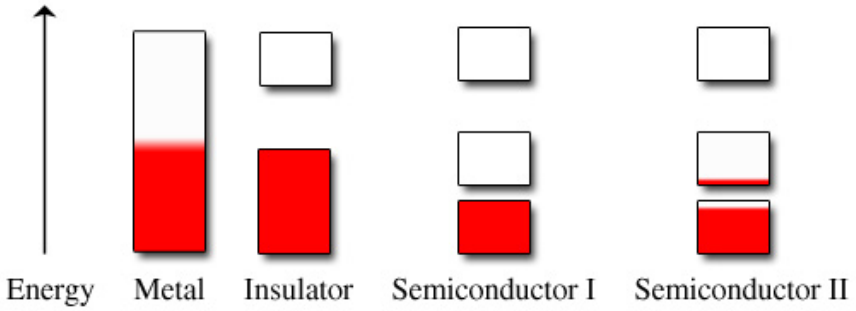

Fig. 1. Qualitative sketch of electron occupancy of allowed energy bands. Each of the energy bands is represented by a rectangle. The colored region in each rectangle indicates that at that energy level the band is occupied by charge carriers.

Further, by going to this order we have derived the Pauli SO coupling term:

$$H_{SO} = \frac{\hbar e}{(2mc)^2}\boldsymbol{\sigma} \cdot \mathbf{E} \times \boldsymbol{\pi} = \frac{\hbar e}{(2mc)^2}\boldsymbol{\sigma} \times \nabla V \cdot \mathbf{p} \tag{2.61}$$

For a spherical potential this term becomes:

$$H_{SO} = \frac{1}{2m^2c^2r}\frac{dV}{dr}\mathbf{S} \cdot \mathbf{L}. \tag{2.62}$$

The preceding equation makes it clear why this term is known as the spin-orbit term. The term proportional to $\nabla^2 V$ is called the Darwin term and it can be interpreted as a fast shaking of the particle at a length scale corresponding to its Compton wavelength, the so called *Zitterbewegung*.

C. Spin orbit coupling effects in bulk (3D) semiconductors

Just as the discrete energy levels are affected in atomic systems, spin-orbit coupling can affect the energy of the electrons in solid systems. For electrons in atomic systems, their energy states have gaps where no energy states are available. Once atoms are

brought close together, the nearby energy levels mix forming energy bands but many of the inherent energy gaps from the atomic structure remain. Hence, electrons in solids are restricted to sets of energy ranges. However, in contrast with the discrete energy levels of the atomic systems, the allowed energy states of the solid systems form continuous bands of allowed energy states. As seen in Figure 1, the energy bands are separated by gaps. The gaps can be the result of the interaction between the conduction electron and the ions in the crystal as well as the intrinsic energy gaps from the atomic levels. Solid state materials are classified in three groups depending on how these bands are filled. Materials with a partially filled (10% to 90 %) band behave as metals, as charge carriers in that band are mobile. Materials with a full band behave as insulators, as all states are filled and a large finite energy is needed to promote carriers to a higher band. In between a metal and an insulator we find the semiconductors, which have smaller gaps than the insulators.

The semiconductor I in Figure 1, illustrates the band scheme for a semiconductor at zero temperature. At such temperature, the main difference between an insulator and a semiconductor is the size of the band gap. The semiconductor II panel shows that carriers can be excited (thermally or optically) from an occupied band to an unoccupied band making the material conducting. Also, by inserting impurities or other means of additional carriers, the conductivity can be made non-zero even at zero temperature. These later type of semiconductors are known as extrinsic semiconductors.

In Figure 2, we present the band diagram of a direct gap semiconductor. It features one conduction band and three valence bands (p like electron states) usually known as the heavy holes band (hh), the light holes band (lh), and the split-off holes band (Δ). By assuming a perfectly periodic crystal, Bloch was able to establish that electrons in a lattice behave like plane waves whose amplitude is modulated with

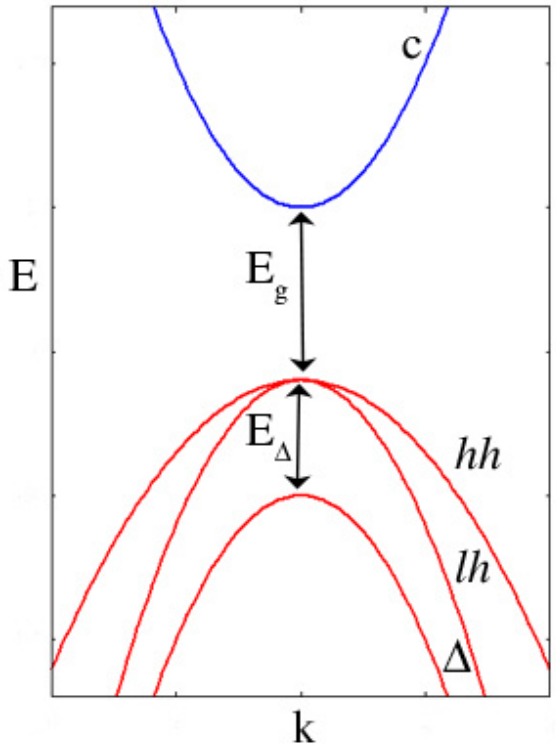

Fig. 2. Band edge structure of a simplified direct gap semiconductor. The blue band is the conduction band while bands in red represent the three valence bands: heavy holes (hh), light holes (lh), and split-off holes (Δ).

the period of the lattice [11]. Bloch's theorem (Eq. 2.64) allows the transformation of the original (infinite) Hamiltonian into an effective (finite) Hamiltonian. Band structure calculations usually make use of Bloch's theorem making it possible to study a single electron in a periodic potential. This reduction to a periodic one-electron problem is still a formidable problem. Thus, theoretical studies are carried out under several approximations such as the envelope function approximation, which describes carriers in the presence of slow-varying electromagnetic fields. The simplest of these approximations is the effective mass approximation [12], where the bands are assumed to be isotropic and parabolic. The curvature of each band in the neighborhood of the

point $k = 0$ defines the effective mass of the electrons in that band,

$$E_\mu(\mathbf{k}) = E_\mu^{(0)} + \frac{\hbar^2 k^2}{2m_\mu^*} \tag{2.63}$$

where μ is the band index ($\mu = c, hh, lh, \Delta$), $\mathbf{k}$ is the wave vector, and the effective masses for each band are given by m_μ^*. More details can be obtained by using the framework of $\mathbf{k} \cdot \mathbf{p}$ theory [13], which can account for non-parabolic bands, spin splitting, and the coupling between heave holes and light holes.

The wavefunction of the carriers can be expanded as

$$\Psi(\mathbf{x}) = \sum_{\mu,\sigma} \psi_{\mu,\sigma}(\mathbf{x}) u_\mu(\mathbf{x}) \left|\sigma\right\rangle \tag{2.64}$$

where ψ is the slowly varying envelope function, u is the periodic Bloch function, and $\left|\sigma\right\rangle$ is the spin eigenstate. In systems with spin-orbit interaction the spin quantum number (σ) is not a good number and as such we replace the label with the index n accommodating the orbital motion and the spin degree of freedom. Using the $\mathbf{k} \cdot \mathbf{p}$ theory, the Hamiltonian can be expanded along a high symmetry point. In the case of direct semiconductors, such as the one in Figure 2, the expansion is done around the $k = 0$ point, which in the crystallographic literature is known as the Γ point. In what follows we present how the $\mathbf{k} \cdot \mathbf{p}$ theory applies to bulk semiconductors, as was illustrated by Winkler [14]. From the lattice-periodic Bloch functions we can obtain a Schrödinger equation:

$$\left[\frac{p^2}{2m} + V + \frac{\hbar^2 k^2}{2m} + \frac{\hbar}{m}\mathbf{k} \cdot \mathbf{p}\right] u_{\mu k} = E_\mu(\mathbf{k}) u_{\mu k} = E_\mu(\mathbf{k}) \left|\mu \mathbf{k}\right\rangle \tag{2.65}$$

The potential V is the periodic potential present in the system. For a fixed wave vector ($\mathbf{k}_0$), the functions $\left|\mu \mathbf{k}_0\right\rangle$ and $\left|n \mathbf{k}_0\right\rangle$ are a complete orthonormal basis [14]. The

expansion then is:

$$|n\mathbf{k}_0\rangle = \sum_{\mu,\sigma=\uparrow,\downarrow} c^n_{\mu\sigma}(\mathbf{k}_0)\,|\mu\sigma\rangle \tag{2.66}$$

where the basis set at the band edge $|\mu\sigma\rangle$ contains no spin-orbit coupling, as the SO interaction will be treated as a small perturbation [14]. Since this is a perturbative approach, the best result is when the value of k is small. The dispersion relation $E_n(\mathbf{k})$ can be obtained from the algebraic eigenvalue problem,

$$\sum_{\mu',\sigma'}\left[\left(E_{\mu'}(\mathbf{k}=0)+\frac{\hbar^2k^2}{2m}\right)\delta\mu\mu'\delta_{\sigma\sigma'}+\frac{\hbar}{m}\mathbf{k}\cdot\mathbf{P}_{\mu\mu';\sigma\sigma'}+\Delta_{\mu\mu';\sigma\sigma'}\right]=E_n(\mathbf{k})c^n_{\mu\sigma}(\mathbf{k}) \tag{2.67}$$

where

$$\mathbf{P}_{\mu\mu';\sigma\sigma'}=\left\langle\mu\sigma\left|\left(\mathbf{p}+\frac{\hbar}{4mc^2}\boldsymbol{\sigma}\times\nabla V\right)\right|\mu'\sigma'\right\rangle, \tag{2.68}$$

$$\Delta_{\mu\mu';\sigma\sigma'}=\frac{\hbar}{4m^2c^2}\left\langle\mu\sigma\left|(\mathbf{p}\cdot\boldsymbol{\sigma}\times\nabla V)\right|\mu'\sigma'\right\rangle. \tag{2.69}$$

In Eq. (2.67), the off-diagonal terms proportional to $\mathbf{P}$ are mixing the states of the band edges $|\mu\mathbf{k}=0\rangle$. The mixing is stronger for energy bands that are closer together and for large k. The matrix elements of the SO interaction (Eq. 2.69) lift the degeneracy of bands even at $\mathbf{k}=0$. In semiconductors obeying the band edge structure in Figure 2, the valence bands all have the same orbital angular momentum ($l=1$). It is due to the SO interaction term that the degeneracy is lifted since the heavy holes and light holes states have total angular momentum $j=3/2$ while the split off holes have $j=1/2$.

The Hamiltonians describing semiconductor systems are in principle of infinite dimensional size. Therefore, it is wise to ignore bands that are far away from the valence and conduction band. For direct semiconductors such as those formed from the elements of the groups III and V (GaAs and InSb), and the II-IV compound CdTe, the smallest gap is at the Γ ($\mathbf{k}=0$) point. These materials can be described accurately

by the extended Kane model which is a 14×14 matrix and it is sometimes convenient to consider even smaller $\mathbf{k} \cdot \mathbf{p}$ models such as the 8×8 Kane Hamiltonian [13] or the six-band Kohn-Luttinger Hamiltonian [15], depending on the energy scale of interest in the problem at hand. The 8×8 Kane Hamiltonian would be able to describe the system depicted in Figure 2, while the six-band Kohn-Luttinger Hamiltonian is neglecting the conduction band. The four-band Kohn-Luttinger Hamiltonian is a further simplification made by ignoring the split-off holes valence band while still retaining the description of the heavy holes and light holes valence bands.

In the Kohn-Luttinger model one can choose the angular momentum quantization along the z-axis and order the $j = 3/2$ and $j = 1/2$ basis functions according to the total angular momentum eigenstates $|j, m_j\rangle$ [16]:

$$\begin{aligned} |1\rangle &= |3/2, 3/2\rangle, \qquad |2\rangle = |3/2, -1/2\rangle \\ |3\rangle &= |3/2, 1/2\rangle, \qquad |4\rangle = |3/2, -3/2\rangle \\ |5\rangle &= |1/2, 1/2\rangle, \qquad |6\rangle = |1/2, -1/2\rangle \end{aligned} \tag{2.70}$$

so that the six-band Hamiltonian, including spin-orbit coupling, can be expressed as:

$$H^L = \left(\begin{array}{cccc|cc} \mathcal{H}_{hh} & -c & -b & 0 & \frac{b}{\sqrt{2}} & c\sqrt{2} \\ -c^* & \mathcal{H}_{lh} & 0 & b & -\frac{b^*\sqrt{3}}{\sqrt{2}} & -d \\ -b^* & 0 & \mathcal{H}_{lh} & -c & d & -\frac{b\sqrt{3}}{\sqrt{2}} \\ 0 & b^* & -c^* & \mathcal{H}_{hh} & -c^*\sqrt{2} & \frac{b^*}{\sqrt{2}} \\ \hline \frac{b^*}{\sqrt{2}} & -\frac{b\sqrt{3}}{\sqrt{2}} & d^* & -c\sqrt{2} & \mathcal{H}_{so} & 0 \\ c^*\sqrt{2} & -d^* & -\frac{b^*\sqrt{3}}{\sqrt{2}} & \frac{b}{\sqrt{2}} & 0 & \mathcal{H}_{so} \end{array}\right) \tag{2.71}$$

In Eq. (2.71), the four-band model Hamiltonian is highlighted. The Kohn-Luttinger eigenenergies are measured down from the top of the valence band, i.e. they are hole

energies. The expressions which define the quantities that appear in H^L are

$$\mathcal{H}_{hh} = \frac{\hbar^2}{2m}\big[(\gamma_1+\gamma_2)(k_x^2+k_y^2)+(\gamma_1-2\gamma_2)k_z^2 \tag{2.72}$$

$$\mathcal{H}_{lh} = \frac{\hbar^2}{2m}\left[(\gamma_1-\gamma_2)(k_x^2+k_y^2)+(\gamma_1+2\gamma_2)k_z^2\right] \tag{2.73}$$

$$\mathcal{H}_{so} = \frac{\hbar^2}{2m}\gamma_1(k_x^2+k_y^2+k_z^2)+\Delta_{so} \tag{2.74}$$

$$b = \frac{\sqrt{3}\hbar^2}{m}\gamma_3 k_z(k_x-ik_y) \tag{2.75}$$

$$c = \frac{\sqrt{3}\hbar^2}{2m}\big[\gamma_2(k_x^2-k_y^2)-2i\gamma_3 k_x k_y\big] \tag{2.76}$$

$$d = -\frac{\sqrt{2}\hbar^2}{2m}\gamma_2\big[2k_z^2-(k_x^2+k_y^2)\big]\ . \tag{2.77}$$

The numerical value of the parameters used depends on the system being studied, for instance in the binary compound gallium arsenide (GaAs), $\gamma_1 = 6.98$, $\gamma_2 = 2.06$ and $\gamma_3 = 2.93$ [17].

In metals, the multi-band nature of the Hamiltonian is needed due to the complexity of the band structures and wavefunctions. For semiconductors an effective Hamiltonian that includes the SO effects can be derived if one is interested only in the conduction band electrons [18]. In essence, this simple two-band model works for narrow gap materials. The work presented in this dissertation uses such effective two-band models. In what follows we present the perturbation method used by Nozières and Lewiner [19] to construct such an effective Hamiltonian.

We start with a single electron wavefunction projected on a complete basis,

$$\psi_{n,\mathbf{k}} = e^{i\mathbf{k}\cdot\mathbf{r}}u_{n0}(\mathbf{r}) \tag{2.78}$$

where u_{n0} is the Bloch function of the crystal at the zone center. The next step consists of dividing ψ into two components: (1) ψ_1 are components that belong to the conduction band and (2) ψ_2 are the components that belong to the other bands.

The Hamiltonian is partitioned into 2 by 2 matrix operators and the Schrödinger equation can be written as

$$\begin{aligned} i\hbar\frac{\partial\psi_1}{\partial t} &= H_1\psi_1 + h\psi_2 \\ i\hbar\frac{\partial\psi_2}{\partial t} &= h^\dagger\psi_1 + H_2\psi_2. \end{aligned} \tag{2.79}$$

The matrix element H_1 is the intraband Hamiltonian for the conduction electrons. Then, assume that H_g describes the band gap at the zone center and H_2 can be defined as

$$H_2 = H_g + H_2' \tag{2.80}$$

where H_2' is the intraband Hamiltonian for the other bands. By choosing the zero of the energy at the bottom of the conduction band we can assume that H_1 is of the order of the conduction electron energy (ϵ_F). The key assumption is that the band gap is much larger than ϵ_F. Nozières and Lewiner [19] make an expansion in powers of H_g^{-1}. The procedure involves eliminating ψ_2 from Eq. (2.79) and construction of an effective Schrödinger equation for ψ_1. Solving the second equation in Eq. (2.79) by iteration, to second order in H_g^{-1},

$$\psi_2 = -\frac{1}{H_2}h^\dagger\psi_1 - \frac{i}{H_2^2}\left(\frac{\partial h^\dagger}{\partial t}\psi_1 + h^\dagger\frac{\partial\psi_1}{\partial t}\right). \tag{2.81}$$

Substitution of the above into the first equation of Eq. (2.79) results in:

$$i(1+\Lambda)\frac{\partial\psi_1}{\partial t} = \bar{H}\psi_1 \tag{2.82}$$

where

$$\Lambda = h\frac{1}{H_g^2}h^\dagger, \tag{2.83}$$

$$\bar{H} = H_1 - h\frac{1}{H_g}h^\dagger + h\frac{1}{H_g}H_2'\frac{1}{H_g}h^\dagger - ih\frac{1}{H_g^2}\frac{\partial h^\dagger}{\partial t} \tag{2.84}$$

Unfortunately, ψ_1 is not normalized. Disregarding terms of order higher than H_g^{-2},

$$1 = \langle\psi_1|\psi_1\rangle + \langle\psi_2|\psi_2\rangle = \langle\psi_1|1+\Lambda|\psi_1\rangle \tag{2.85}$$

and the normalized wavefunction is given by:

$$|\psi_{eff}\rangle = \left(1+\frac{\Lambda}{2}\right)|\psi_1\rangle \tag{2.86}$$

Using Eqs. (2.82) and (2.83) the effective Schrödinger equation in the conduction band subspace is given by:

$$\begin{aligned} i\frac{\partial\psi_{eff}}{\partial t} &= \left[H_1 - h\frac{1}{H_g}h^\dagger - \frac{\Lambda(H_1 - h\frac{1}{H_g}h^\dagger) + (H_1 - h\frac{1}{H_g}h^\dagger)\Lambda}{2}\right. \\ &\left. + h\frac{1}{H_g}H_2'\frac{1}{H_g}h^\dagger + \frac{i}{2}\left(\frac{\partial h}{\partial t}\frac{1}{H_g^2}h^\dagger - h\frac{1}{H_g^2}\frac{\partial h^\dagger}{\partial t}\right)\right]\psi_{eff} \end{aligned} \tag{2.87}$$

Nozières and Lewiner [19] constructed an effective Hamiltonian and showed the transformation necessary for all operators. With this construction, they have mapped the effects of the valence bands into the conduction band. For an operator O, the same procedure can be applied,

$$\langle O\rangle = \langle\psi_1|O|\psi_1\rangle + \langle\psi_2|O|\psi_2\rangle + \langle\psi_1|o|\psi_1\rangle + \langle\psi_1|o^\dagger|\psi_2\rangle \tag{2.88}$$

$$\langle O\rangle = \langle\psi_1|\bar{O}|\psi_1\rangle = \langle\psi_{eff}|O_{eff}|\psi_{eff}\rangle \tag{2.89}$$

where the effective operator is given in the conduction band subspace. Within this framework, and with the previous assumption that the material has a small band gap,

$$H_1 = H_2 = \frac{k^2}{2m_0} + g_0\frac{e}{2mc}\mathbf{S}\cdot\boldsymbol{B},\ h = \mathbf{k}\cdot\mathbf{\Pi} \tag{2.90}$$

where $\mathbf{\Pi}$ is the operator that couples the bands together. The matrix elements of $\mathbf{\Pi}$ are

$$\mathbf{\Pi}_{nn'} = \left\langle u_{n0}\left|-i\frac{\nabla}{m_0}\right|u_{n'0}\right\rangle \tag{2.91}$$

and the matrix elements of $\mathbf{\Pi}$ between the six valence bands and the two conduction bands are

$$\mathbf{\Pi}_\alpha \frac{1}{H_g^n} \mathbf{\Pi}_\beta = \frac{P^2}{3}\left[\delta_{\alpha\beta}\left(\frac{2}{(-\epsilon_g)^n}+\frac{1}{(-\epsilon_g-\Delta)^n}\right)+2i\epsilon_{\alpha\beta\gamma}S_\gamma\left(\frac{1}{(-\epsilon_g-\Delta)^n}-\frac{1}{(-\epsilon_g)^n}\right)\right], \tag{2.92}$$

where P is a parameter that for narrow gap semiconductors gives us an energy in the range $E_p = 2mP^2/\hbar^2 \approx (21, 25)$ eV.

Finally, the effective Hamiltonian is

$$\begin{aligned} H_{eff} &= \frac{\hbar^2k^2}{2m^*} + g^*\frac{e}{2mc}\mathbf{S}\cdot\boldsymbol{B} - e\frac{\hbar^2k^2}{4mm^*c}g^*\frac{\mathbf{S}\cdot\boldsymbol{B}}{E_0} - g^*\frac{e}{2mE_2}(\mathbf{k}\times\mathbf{E})\cdot\mathbf{S} \quad (2.93)\\ &= \frac{\hbar^2k^2}{2m^*} + \frac{1}{2}g^*\boldsymbol{\mu}\sigma\cdot\boldsymbol{B} - \frac{\hbar^2k^2}{4m^*E_0}g^*\boldsymbol{\mu}\,\boldsymbol{\sigma}\cdot\boldsymbol{B} \\ &\quad +\lambda^*(\boldsymbol{\sigma}\cdot(\mathbf{k}\times\nabla V(\mathbf{r})) + g_0\boldsymbol{\mu}(\mathbf{k}\times\boldsymbol{\sigma})\cdot(\mathbf{k}\times\boldsymbol{B})) \quad (2.94)\end{aligned}$$

with

$$\begin{aligned} E_0 &= \frac{E_g(E_g+\Delta)(3E_g+2\Delta)}{9E_g^2+11E_g\Delta+4\Delta^2}, \quad (2.95)\\ E_2 &= \frac{E_g(E_g+\Delta)}{2E_g+\Delta} \quad (2.96)\end{aligned}$$

and the renormalized quantities,

$$\begin{aligned} \frac{1}{m^*} &= \frac{1}{m_0}+\frac{2}{3}|P|^2\frac{3E_g+2\Delta}{E_g(E_g+\Delta)} \propto \frac{1}{E_g}, \quad (2.97)\\ g^* &= g_0 - \frac{4m_0}{3}|P|^2\frac{\Delta}{E_g(E_g+\Delta)} \propto \frac{\Delta}{E_g^2}, \quad (2.98)\\ \lambda^* &= \frac{P^2}{3}\left(\frac{1}{E_g^2}-\frac{1}{E_g+\Delta^2}\right) \propto \frac{\Delta}{E_g^3} \quad (2.99)\end{aligned}$$

We see how the effects of the valence band impart an effective spin-orbit coupling term in the conduction band. Given the renormalization of the parameters that show up in the Hamiltonian (effective mass $m^* < m_0$ and $g^* > g_0$), the SO term is strong

for narrow gap semiconductors.

D. Spin orbit coupling effects in confined (2D) semiconductors

The energy band structure can be modified intensely by the SO interaction. For instance, in Germanium, the SO coupling provides the splitting of the degenerate valence band (P-states) [20]. In heterostructures, the inversion asymmetry can induce a spin splitting. These systems with reduced dimensionality can exhibit bulk inversion asymmetry (BIA), as a consequence of the crystal structure, and structure inversion symmetry (SIA), due to the confinement potential [14]. The latter case is the focus of the current volume. The motion of electrons close to the atomic cores in a crystalline environment is what contributes to the SO coupling.

The emergence of fabrication techniques such as molecular beam epitaxy has made possible the growth of materials with electrical properties that can be engineered at will. For instance, a heterojunction is made by growing materials with similar lattice constants but different band gaps. An example of such new materials is the heterojunction made of the semiconductor gallium (Ga) and arsenide (As), and aluminium (Al) metal with the alloy composition GaAs/$Al_xGa_{1-x}As$, presented in Figure 3. The difference in the two alloys in lattice constant is about 1% but the difference between their band gaps can be significant and as such the conduction and valence bands edges do not align. This abrupt discontinuity in the bands is also known as the band offset [12]. When the material with the larger band gap is doped with donors (ions willing to give away their electrons), the Fermi energy moves from the middle of the band gap towards the donor levels. Since the chemical potential has to remain constant between the interface, electrons flow from the AlGaAs side to the GaAs. At the interface the band edges will bend and the electrons in the GaAs

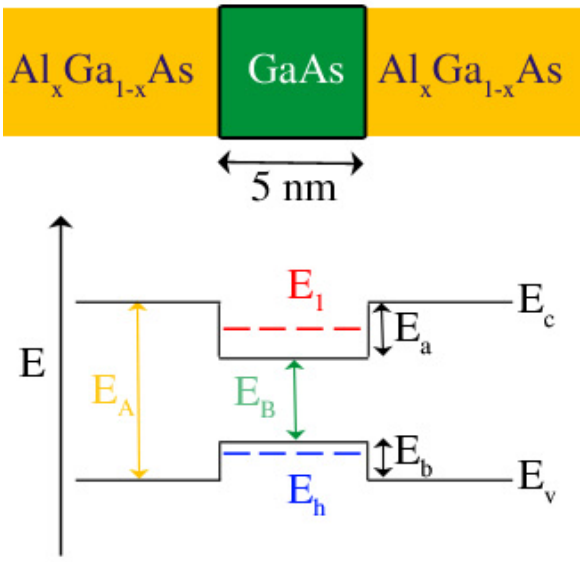

Fig. 3. Discontinuity in the energy bands for a heterojunction. (Top panel) A thin layer of GaAs sits between two larger layers of $Al_xGa_{1-x}As$. (Bottom panel) The mismatch between the bandgaps is significant and discrete states (E_1 and E_h) can be formed in the valence (E_c) and conduction (E_v) bands of the GaAs region.

are confined by a triangular potential near the interface of the two materials. The electrons are effectively confined to the discrete states and form a two-dimensional electron gas, as illustrated in Figure 4. Similarly, the preparation can be done such that the holes (electron missing from the valence band) are confined so that a two-dimensional hole gas is created. The confined electrons are separated from the ion impurities in the doped material and as such they are only weakly scattered from impurities producing highly mobile carriers [21].

As explained by Winkler [14], when there is inversion asymmetry, as there is in a triangular potential, the Bloch part of the wavefunction feels the atomic fields and the envelope function feels the macroscopic environment (electric field due to gates or

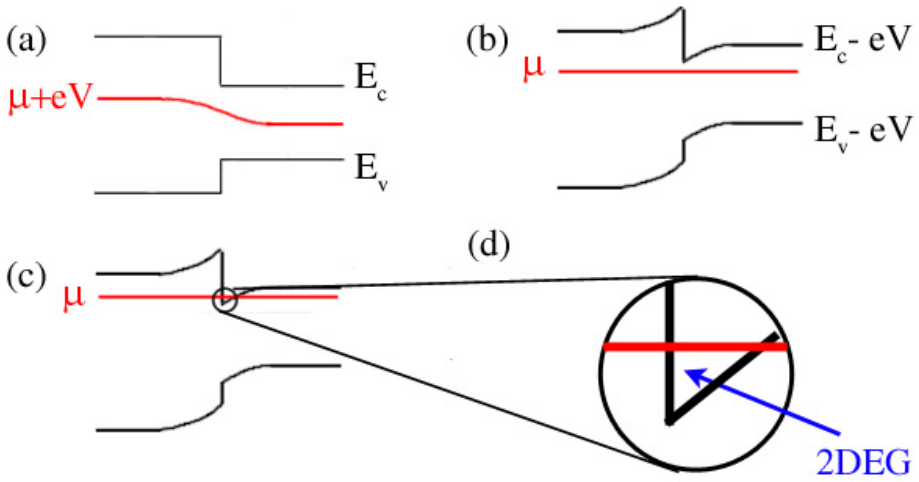

Fig. 4. Formation of a two-dimensional electron gas. A heterojunction of $Al_xGa_{1-x}As/GaAs$, where the bands are discontinuous near the junction. (a) The left side is doped with donors yet the chemical potential has to remain constant in both materials. (b) Similar schematic as the one in panel (a) but emphasizing the band bending. (c) An increase in the concentration of donors shifts the chemical potential above the conduction band of the material in the right. This confines the electrons to a triangular potential. (d) The inset shows the resulting triangular potential well formed at the interface. Note the presence of the spatial quantization level, the potential has confined the electrons into a 2D region, creating the 2DEG.

environment). The confinement makes for a macroscopic electric field and the atomic cores a microscopic electric field. Therefore, structure inversion symmetry (SIA) spin splitting is tunable via external gates that can modulate the electric field [14]. This spin-splitting leads to the Rashba type spin-orbit coupling term [22] that for narrow wells where the carriers are electrons (spin 1/2 particles):

$$H_{SO}^{e} = \frac{\alpha}{\hbar}\left(\hat{\sigma} \times \mathbf{p}\right)_z , \tag{2.100}$$

and for heavy holes carriers (spin 3/2 particles) [14],

$$H_{SO}^{hh} = \frac{\alpha}{\hbar}\left(\hat{\sigma}_{+}\mathbf{p}_{-}^{3} - \sigma_{-}\mathbf{p}_{+}^{3}\right), \tag{2.101}$$

where the strength of the spin-orbit interaction is given by α. If the confinement is not in narrow quantum wells the linear term mixes with the cubic term in the heavy holes case and the form of the spin-orbit term will be different.

CHAPTER III

REDUCED SKEW-SCATTERING IN TWO-DIMENSIONAL SYSTEMS: TESTING THE ORIGINS OF THE ANOMALOUS HALL EFFECT*

In 1879, Edwin Hall ran a current through a gold foil and discovered that a transverse voltage was induced when the film was exposed to a perpendicular magnetic field [23]. The ratio of this Hall voltage to the current density is the Hall resistivity. For paramagnetic materials, the Hall resistivity is proportional to the applied magnetic field, and Hall measurements give information about the concentration of free carriers and determine whether they are holes or electrons. Magnetic films exhibit both this ordinary Hall response and an extraordinary or anomalous Hall response that does not disappear at zero magnetic field and is proportional to the internal magnetization:

$$R_{\text{Hall}} = R_o H + R_s M, \tag{3.1}$$

where R_{Hall} is the Hall resistance, R_o and R_s are the ordinary and anomalous Hall coefficients, M is the magnetization, and H is the applied magnetic field. The anomalous Hall effect (AHE) is the consequence of spin-orbit (SO) coupling and allows an indirect measurement of the internal magnetization.

Despite the simplicity of the experiment, the theoretical basis of the AHE is still hotly debated and a source of conflicting reports [24]. Different mechanisms

---

*Part of this chapter is reprinted with permission from "Absence of Skew Scattering in Two-Dimensional Systems: Testing the Origins of the Anomalous Hall Effect" by Mario Borunda, Tamara S. Nunner, Thomas Lück, N. A. Sinitsyn, Carsten Timm, J. Wunderlich, T. Jungwirth, A. H. MacDonald, and Jairo Sinova, 2007. *Physical Review Letters* **99**, 066604, ©(2007) by The American Physical Society and from "Anomalous Hall Effect in a Two-Dimensional Electron Gas" by Tamara S. Nunner, N. A. Sinitsyn, Mario F. Borunda, V. K. Dugaev, A. A. Kovalev, Ar. Abanov, Carsten Timm, T. Jungwirth, Jun-ichiro Inoue, A. H. MacDonald, and Jairo Sinova, 2007. *Physical Review B* **76**, 235312, ©(2007) by The American Physical Society.

contribute to the AHE: an intrinsic mechanism and extrinsic mechanisms such as skew-scattering and side-jump contributions. The intrinsic mechanism is based solely on the topological properties of the Bloch states originating from the SO coupled electronic structure as first suggested by Karplus and Luttinger [25]. Their approach gives an anomalous Hall coefficient R_s proportional to the square of the ordinary resistivity, since the intrinsic AHE itself is insensitive to impurities. The skew-scattering mechanism, as first proposed by Smit [26], relies on an asymmetric scattering of the conduction electrons by impurities present in the material.[1] Not surprisingly, this skew scattering contribution to R_s is sensitive to the type and range of the scattering potential and, in contrast to the intrinsic mechanism, scales linearly with the diagonal resistivity. The presence of impurities also leads to a side-step type of scattering, which contributes to a net current perpendicular to the initial momentum. This is the so-called side-jump contribution, whose semi-classical interpretation was pointed out by Berger [27]. However, it is not trivial to correctly account for such contributions in the semiclassical procedure, making a connection to the microscopic approach very desirable.

The early theories of the AHE involved complex calculations with results that were not easy to interpret and often contradicting each other [19]. The adversities these theories had to overcome to obtain correct results stem from the origin of the AHE: it appears due to the interband coherence and not just due to simple changes in the occupation of Bloch states, as was recognized in the early works of

[1]Note that the origin of the asymmetry of this scattering arises from the spin-orbit coupling present in the Bloch states and not from the very weak spin-orbit coupling contribution of the disorder potential as noted originally by Smit. When projecting a multi-band system to an effective conduction band system one can obtain a term that looks as if it arises from such a spin-orbit coupling part of the disorder potential but it truly originates from spin-orbit coupling induced by the valence band states and the normal disorder that is felt by them.

Luttinger and Kohn [28, 29]. Nowadays, most treatments of the AHE either use the semiclassical Boltzmann transport theory or the diagrammatic approach based on the Kubo-Streda linear-response formalism. The equivalence of these two methods for the two-dimensional Dirac-band graphene system has recently been shown by Sinitsyn *et al.* [30], who explicitly identified various diagrams of the more systematic Kubo-Streda treatment with the physically more transparent terms of the semiclassical Boltzmann approach. So far a rigorous connection of the more intuitive semiclassical transport treatment with the more systematic diagrammatic treatment, providing a clear-cut interpretation of the intrinsic, skew, and side-jump AHE terms, has only been demonstrated for the Dirac Hamiltonian model [30]. It is therefore important to also obtain a similarly cohesive understanding of the AHE in other systems such as the two-dimensional (2D) spin-polarized electron gas with Rashba spin-orbit interaction in the presence of point-like potential impurities, where a series of previous studies has led to a multitude of results with discrepancies arising from the focus on different limits and/or subtle missteps in the calculations [31, 32, 33, 34, 35, 36, 37]. A similar debate over the origin of the AHE has carried over to the related phenomena of the spin Hall effect [38, 39, 40, 41].

In this chapter we calculate the transport coefficients in these two complementary approaches for asymmetrically confined 2D electron and hole gases in the presence of spin-independent disorder. The two approaches are in perfect agreement. The motivation for the study of these systems is threefold: First, they can be represented by simple spin-orbit-coupled bands which, similar to the Dirac Hamiltonian model, allows us to unambiguously identify the individual AHE contributions. Second, the extrinsic skew-scattering term is reduced for two-subband occupation in the Rashba 2D electron gas and for *any* band occupation in the studied 2D hole gas. This provides a clean test of the intrinsic AHE mechanism and of the transition between the intrinsic

and skew-scattering-dominated AHE. Finally, we propose a 2D electron gas/2D hole gas coplanar magneto-optical device in which the unique AHE phenomenology found in our theoretical models can be systematically explored experimentally.

A. Model Hamiltonians

We study the following 2D model Hamiltonians derived in the previous chapter:

$$H = \frac{\hbar^2 k^2}{2m}\boldsymbol{\sigma}_0 + i\alpha_n(\boldsymbol{\sigma}_+ k_-^n - \boldsymbol{\sigma}_- k_+^n) - h\boldsymbol{\sigma}_z + V(\mathbf{r})\boldsymbol{\sigma}_0 \tag{3.2}$$

with m being the effective in-plane mass, $\boldsymbol{\sigma}_0$ is the unity matrix, $\boldsymbol{\sigma}_i$ the 2×2 Pauli matrices, $\boldsymbol{\sigma}_\pm = \boldsymbol{\sigma}_x \pm i\boldsymbol{\sigma}_y$, $k_\pm = k_x \pm ik_y$, h the exchange field, α_n is the spin-orbit coupling parameter, and $V(\mathbf{r})$ a spin-independent disorder potential. The exponent $n = 1$ (3) describes a 2D electron (hole) gas [14]. The eigenenergies of Eq. (3.2) for a clean system ($V(\mathbf{r}) = 0$) are

$$E_\pm = \frac{\hbar^2 k^2}{2m} \pm \sqrt{h^2 + (\alpha_n k^n)^2}. \tag{3.3}$$

The eigenvectors in the clean system take the form $|\Psi_{\mathbf{k}}^\pm\rangle = \exp(i\mathbf{k}\cdot\mathbf{r})|u_{\mathbf{k}}^\pm\rangle$ with $\mathbf{k} = k\,(\cos\phi, \sin\phi)$ and

$$|u_{\mathbf{k}}^\pm\rangle = \frac{1}{\sqrt{2\lambda}} \begin{pmatrix} \pm ie^{-ni\phi}\sqrt{\lambda \pm h} \\ \sqrt{\lambda \mp h} \end{pmatrix}, \tag{3.4}$$

where $\lambda = \sqrt{h^2 + (\alpha_n k^n)^2}$. We now define $k_\pm(E)$ as the wave number for the $\pm$ band at a given energy E and define $\lambda_\pm \equiv \lambda(k_\pm)$. If E is not specified, it is assumed to be the Fermi energy. We consider the model of randomly located δ-function scatterers, $V(\mathbf{r}) = \sum_i V_i\,\delta(\mathbf{r} - \mathbf{R}_i)$, i enumerates impurities, and $\mathbf{R}_i$ is the random position of the impurities. The moments of the disorder satisfy $\langle V_i\rangle_{\text{dis}} = 0$, $\langle V_i^2\rangle_{\text{dis}} = V_0^2 \neq 0$, and $\langle V_i^3\rangle_{\text{dis}} = V_1^3 \neq 0$. In our model the first nonzero disorder correlators in the basis

Eq. (3.4) are

$$\langle V^{\mu,\mu'}_{\mathbf{k},\mathbf{k}'} V^{\mu',\mu}_{\mathbf{k}',\mathbf{k}} \rangle_{\rm dis} = n_i V_0^2 |\langle u^{\mu}_{\mathbf{k}} | u^{\mu'}_{\mathbf{k}'} \rangle|^2 \tag{3.5}$$

and

$$\langle V^{\mu,\mu'}_{\mathbf{k},\mathbf{k}'} V^{\mu',\mu''}_{\mathbf{k}',\mathbf{k}''} V^{\mu'',\mu}_{\mathbf{k}'',\mathbf{k}} \rangle_{\rm dis} = n_i V_1^3 \langle u^{\mu}_{\mathbf{k}} | u^{\mu'}_{\mathbf{k}'} \rangle \langle u^{\mu'}_{\mathbf{k}'} | u^{\mu''}_{\mathbf{k}''} \rangle \langle u^{\mu''}_{\mathbf{k}''} | u^{\mu}_{\mathbf{k}} \rangle, \tag{3.6}$$

where n_i is the impurity concentration. Note that the model we consider is different from the standard white-noise disorder ($V_1 = 0$). The deviation from white noise is quantified by $V_1 \neq 0$, and is necessary to capture part of the skew-scattering contribution to the AHE.

B. Calculations

1. Semiclassical approach

We give the details of the semiclassical procedure used in the calculation. Further details can be found in the work of Sinitsyn *et al.* [30] and a companion review by Sinitsyn [42]. The multi-band Boltzmann equation in a weak electric field $\mathbf{E}$ is given by

$$\frac{\partial f_l}{\partial t} + e\mathbf{E} \cdot \mathbf{v}_l \frac{df_l}{d\epsilon} = I[f]_{\rm coll} \tag{3.7}$$

where $l = (\mathbf{k}, \mu)$, $\mu = \pm$ is the subband index, and the impurity collision integral is

$$I[f]_{\rm coll} = -\sum_{\mu'} \int d^2\mathbf{k}'/(2\pi)^2 \, w_{ll'} \left(f_l - f_{l'} \right). \tag{3.8}$$

The distribution function f_l is the sum of the equilibrium function and a correction, $f_l = f_l^0 + g_l$. The angle between the direction of the velocity ($\mathbf{v}$) in a given phase space volume and the direction of the electric field is given by ϕ. The scattering rate encodes the details of the scattering potential. For the disorder potential considered (δ-function type) the quantum mechanical scattering matrix is given by the golden

rule [42]. The scattering rates $w_{ll'}$ are related to the T-matrix elements through

$$w_{ll'} = \frac{2\pi}{\hbar}|T_{l'l}|^2\delta(\epsilon_{l'} - \epsilon_l), \tag{3.9}$$

and we can use the expression of the T-matrix in terms of the Born series in powers of disorder potential matrix elements:

$$T_{l'l} = \langle l'|V|\psi_l\rangle \approx V_{l'l} + \sum_{l''} \frac{V_{l''l}V_{l'l''}}{\epsilon_l - \epsilon_{l''} + i\eta} + ..., \tag{3.10}$$

where the operator $\hat{V}$ is the impurity potential, $V_{l'l} = \langle l'|\hat{V}|l\rangle$, and $|\psi_l\rangle$ are eigenstates of the complete Hamiltonian, and $|l\rangle$ of the disorder free Hamiltonian.

2. Skew scattering

Skew scattering appears in the Boltzmann equation through the asymmetric part of the scattering rate, i.e., $w_{ll'} \neq w_{l'l}$ [26]. The scattering rates to second and third order in disorder strength are given by $w_{ll'} = w^{(2)}_{ll'} + w^{(3)}_{ll'} + \cdots$, where

$$w^{(2)}_{ll'} = \frac{2\pi}{\hbar}\langle|V_{ll'}|^2\rangle_{\rm dis}\delta(\epsilon_l - \epsilon_{l'}), \tag{3.11}$$

is symmetric. Here $V_{l'l} = \langle l'|V|l\rangle$. We break up the third-order contribution into symmetric and antisymmetric parts. We ignore the first, since only the second gives rise to skew scattering. This antisymmetric term is given by [30]:

$$w^{(3a)}_{ll'} = -\frac{(2\pi)^2}{\hbar}\sum_{l''}\delta(\epsilon_l - \epsilon_{l''})\mathrm{Im}\langle V_{ll'}V_{l'l''}V_{l''l}\rangle_{\rm dis}\delta(\epsilon_l - \epsilon_{l'}). \tag{3.12}$$

The solution of the Boltzmann equation Eq. (3.7) is found by first looking at the deviation of the distribution function from equilibrium [30],

$$g_l = -\frac{\partial f^0_\mu}{\partial\epsilon}\, eE|v_\mu|(A_\mu\cos\phi + B_\mu\sin\phi). \tag{3.13}$$

Assuming that the transverse conductivity is much smaller than the longitudinal one ($A_\mu \gg B_\mu$) and substituting Eq. (3.13) into Eq. (3.7) one finds $A_\mu = \tau_\mu^{\parallel}$ and $B_\mu = (\tau_\mu^{\parallel})^2/\tau_\mu^{\perp}$, where the above scattering times are given by:

$$\frac{1}{\tau_\mu^{\parallel}} = \sum_{\mu'} \int \frac{d^2\mathbf{k}'}{(2\pi)^2}\, w_{ll'}^{(2)} \left[1 - \frac{|v_{l'}|}{|v_l|}\cos(\phi - \phi')\right], \tag{3.14}$$

$$\frac{1}{\tau_\mu^{\perp}} = \sum_{\mu'} \int \frac{d^2\mathbf{k}'}{(2\pi)^2}\, w_{ll'}^{(3a)} \frac{|v_{l'}|}{|v_l|}\sin(\phi - \phi'), \tag{3.15}$$

where ϕ and ϕ' are the angles between the velocities $\mathbf{v}_l$ and $\mathbf{v}_{l'}$.

For symmetric Fermi surfaces, the skew-scattering contribution to the conductivity tensor at zero temperature can now be expressed using the scattering times,

$$\sigma_{xx} = e\sum_\mu \int \frac{d^2\mathbf{k}}{(2\pi)^2} g_\mu v_\mu \cos(\phi) = \frac{e^2}{4\pi\hbar}\sum_\mu \tau_\mu^{\parallel} v_{F,\mu} k_\mu, \tag{3.16}$$

$$\sigma_{xy}^{\text{skew}} = e\sum_\mu \int \frac{d^2\mathbf{k}}{(2\pi)^2} g_\mu v_\mu \sin(\phi) = \frac{e^2}{4\pi\hbar}\sum_\mu \frac{(\tau_\mu^{\parallel})^2}{\tau_\mu^{\perp}} v_{F,\mu} k_\mu. \tag{3.17}$$

where above we have assumed zero-temperature. Hence, within the semiclassical approach the focus is in calculating the scattering times from Eqs. (3.15) and (3.14). The calculation of $(\tau_\mu^{\parallel})^{-1}$ and $(\tau_\mu^{\perp})^{-1}$ uses the matrix elements of Eq. (3.12). To simplify the notation we define

$$\langle \mu\mu', \mu'\mu'', \mu''\mu\rangle \equiv \text{Im}\int_0^{2\pi} d\phi'' \langle u_{\mathbf{k}}^{\mu}|u_{\mathbf{k}'}^{\mu'}\rangle\langle u_{\mathbf{k}'}^{\mu'}|u_{\mathbf{k}''}^{\mu''}\rangle\langle u_{\mathbf{k}''}^{\mu''}|u_{\mathbf{k}}^{\mu}\rangle, \tag{3.18}$$

where all momenta are taken on the Fermi surface. Note that in Eq. (3.18) the magnitude of $\mathbf{k}''$ can be different from that of $\mathbf{k}'$ or $\mathbf{k}$ since the Fermi momenta of different bands do not coincide.

The matrix elements appearing in Eq. (3.18) can be calculated directly from the

basis functions $u_{\mathbf{k}}^{\pm}$ of Eq. (3.4),

$$\langle u_{\mathbf{k}}^{\mu}|u_{\mathbf{k}'}^{\mu}\rangle = \tfrac{1}{2\lambda_\mu}\left[A_\mu e^{-ni(\phi'-\phi)} + C_\mu\right], \tag{3.19}$$

$$\langle u_{\mathbf{k}}^{-}|u_{\mathbf{k}'}^{-}\rangle = \tfrac{1}{2\lambda_-}\left[C_- e^{-ni(\phi'-\phi)} + C_+\right], \tag{3.20}$$

$$\langle u_{\mathbf{k}}^{\mp}|u_{\mathbf{k}'}^{\pm}\rangle = \tfrac{1}{2\sqrt{\lambda_-\lambda_+}}\left[-B_+ e^{-ni(\phi'-\phi)} + B_-\right], \tag{3.21}$$

where $A_\mu = \lambda_\mu + \mu h$, $C_\mu = \lambda_\mu - \mu h$, and $B_\pm = \sqrt{(\lambda_- \mp h)(\lambda_+ \pm h)}$. This can be used to obtain the simplified result for Eq. (3.18):

$$\langle \mu\mu', \mu'\mu'', \mu''\mu\rangle = -\frac{h\pi\alpha_n^2 k_\mu^n k_{\mu'}^n}{2\lambda_\mu\lambda_{\mu'}\lambda_{\mu''}}\sin(n\phi - n\phi'), \tag{3.22}$$

from which we obtain the final expression for the skew-scattering rate, which yields the transverse relaxation time:

$$w_{ll'}^{(3a)} = -\frac{1}{\hbar} n_i V_1^3 \delta(\epsilon_l - \epsilon_{l'}) \sum_{\mu''} \nu^{\mu''} \langle \mu\mu', \mu'\mu'', \mu''\mu\rangle, \tag{3.23}$$

where $\nu^{\pm}$ is related to the density of states of each band at the Fermi energy,

$$(\nu^{\pm})^{-1} = \int k\ dk\ \delta(E_F - \epsilon^{\pm}(k)) = \hbar^2/m \pm n(\alpha_n k_{\pm}^{n-1})^2/\lambda_\pm \tag{3.24}$$

The relaxation times are found by inserting Eq. (3.24) into Eq. (3.14) and Eq. (3.23) into Eq. (3.15). For $n = 1$, i.e., for the 2D *electron* gas, the relaxation rates are then, from Eqs. (3.14) and (3.15),

$$\frac{1}{\tau_\mu^{\parallel}} = \frac{1}{\hbar} n_i V_0^2 \left[\frac{\nu^\mu}{\lambda_\mu}\left(\frac{h^2}{\lambda_\mu} + \frac{\alpha_1^2 k_\mu^2}{4\lambda_+} + \frac{\alpha_1^2 k_-^2}{4\lambda_-}\right) + \frac{\nu^{\bar\mu}}{2}\left(1 - \frac{h^2}{\lambda_-\lambda_+}\right)\right], \tag{3.25}$$

$$\frac{1}{\tau_\mu^{\perp}} = -\frac{n_i V_1^3 h \alpha_1^2 \nu^\mu}{8\hbar\lambda_\mu}\left(\frac{k_\mu^2}{\lambda_\mu} - \frac{k_{\bar\mu}^2}{\lambda_{\bar\mu}}\right)\left(\frac{\nu^\mu}{\lambda_\mu} - \frac{\nu^{\bar\mu}}{\lambda_{\bar\mu}}\right), \tag{3.26}$$

where $\bar\mu \equiv -\mu$. If both subbands are occupied, the last factor in Eq. (3.26) vanishes and there is no skew-scattering contribution. If only the majority subband is occupied ($E_F < h$), $(\tau_\mu^{\perp})^{-1}$ is non-zero and skew scattering contributes to the total

Hall conductivity. For the skew-scattering Hall conductivity and the longitudinal conductivity we obtain in this case, from Eqs. (3.25), (3.26), (3.16) and (3.17),

$$\sigma_{xx} = \frac{e^2}{\pi\hbar n_i V_0^2}\left(\frac{\lambda_- k_-}{\nu^-}\right)^2 \frac{1}{3h^2+\lambda_-^2}, \tag{3.27}$$

$$\sigma_{xy}^{\rm skew} = -\frac{e^2 V_1^3}{2\pi\hbar n_i V_0^4}\,\frac{h\lambda_-\alpha_1^2 k_-^4}{\nu_-(3h^2+\lambda_-^2)^2}. \tag{3.28}$$

If $n=3$, i.e., for the 2D *hole* gas, we obtain from Eqs. (3.14) and (3.15),

$$\frac{1}{\tau_\mu^{\parallel}} = \frac{1}{\hbar} n_i V_0^2 \left[\frac{\nu^\mu}{2\lambda_\mu^2}(\lambda_\mu^2+h^2) + \frac{\nu^{\bar\mu}(\lambda_-\lambda_+ - h^2)}{2\lambda_-\lambda_+}\right], \tag{3.29}$$

$$\frac{1}{\tau_\mu^{\perp}} = 0 \tag{3.30}$$

and skew scattering vanishes irrespective of band filling.

3. Microscopic approach

Within the diagrammatic Kubo formalism the skew-scattering contribution to the off-diagonal conductivity is obtained from the expression

$$\sigma_{xy}^{I(a)} = \frac{e^2\hbar}{2\pi V}\sum_k {\rm Tr}\left[v_x G_k^R(E_F) v_y G_k^A(E_F)\right], \tag{3.31}$$

where the bare velocity vertex factors in the linear-in-**k** Rashba model are given by

$$v_x = \frac{\hbar k_x}{m}\boldsymbol{\sigma}_0 - \frac{\alpha_1}{\hbar}\boldsymbol{\sigma}_y, \quad v_y = \frac{\hbar k_y}{m}\boldsymbol{\sigma}_0 + \frac{\alpha_1}{\hbar}\boldsymbol{\sigma}_x. \tag{3.32}$$

As shown in a previous study [30], the skew-scattering contribution proportional to $V_1^3/(n_i V_0^4)$ corresponds to the diagrams shown in Fig. 5. This diagram represents the conductivity, it has the current vertices $j_x,\ j_y$ on both sides thus it is the Hall conductivity and not the diagonal conductivity. The bare velocities $v_x,\ v_y$ are renormalized by ladder vertex corrections. Only the skew-scattering diagrams with a *single* third-order vertex, shown in Fig. 5, contribute to order $V_1^3/(n_i V_0^4)$. The disorder lines

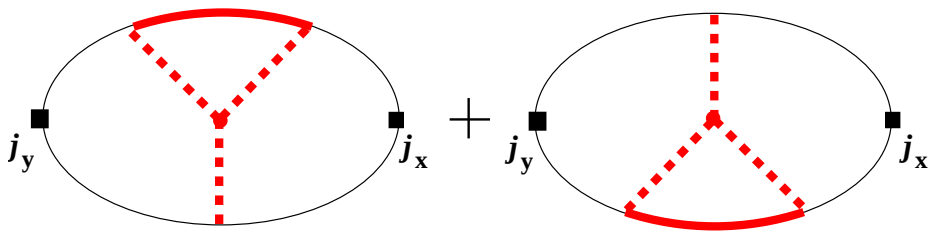

Fig. 5. Diagrammatic representation of the skew-scattering contribution to the Hall conductivity (σ_{yx}). Both current vertices, denoted by squares, are renormalized by ladder vertex corrections. Disorder lines represent the asymmetric scattering. The red part of the diagram represents Eq. (3.33), the sum of the skew-scattering vertices.

represent the type of asymmetric scattering rates that contribute to skew-scattering, which is third order in the Born approximation. All other terms from a ladder-type summation of third-order vertices are smaller because they are either not of the order $1/n_i$ or of higher order in V_1/V_0. Only the single third-order skew-scattering diagram contributes to order $V_1^3/(n_i V_0^4)$, whereas the summation of several third-order diagrams leads to terms of higher order in $n_i V_0^2$. The sum of the skew-scattering vertices (i.e., the bold/red part of Fig. 5) gives

$$\frac{i}{4} n_i V_1^3 h \left(\frac{\nu_-}{\lambda_-} - \frac{\nu_+}{\lambda_+} \right) (\boldsymbol{\sigma}_0 \otimes \boldsymbol{\sigma}_z - \boldsymbol{\sigma}_z \otimes \boldsymbol{\sigma}_0) \,. \tag{3.33}$$

In the linear Rashba model we find $\nu_+/\lambda_+ = \nu_-/\lambda_-$, implying that the contribution of order $V_1^3/(n_i V_0^4)$ of the skew scattering vanishes if both subbands are occupied. In the case that only one subband is occupied the evaluation of Fig. 5 to order $V_1^3/(n_i V_0^4)$ yields exactly the same expression for $\sigma_{xy}^{\text{skew}}$ as in the semiclassical Eq. (3.28). The only effect of the ladder vertex corrections is to renormalize each bare velocity by a factor of $2(h^2 + \lambda_-^2)/(3h^2 + \lambda_-^2)$ which reduces to a factor of 1 in the limit of small $\alpha_1 k_F$ and to a factor of 2 in the limit of small h.

For the 2D hole-gas model Hamiltonian, Eq. (3.2) with $n = 3$, the bare velocity

vertex factors are

$$v_{x,y} = \frac{\hbar k_{x,y}}{m}\boldsymbol{\sigma}_0 - \frac{6\alpha_3}{\hbar}k_x k_y \boldsymbol{\sigma}_{y,x} \pm \frac{3\alpha_3}{\hbar}(k_x^2 - k_y^2)\boldsymbol{\sigma}_{x,y}. \tag{3.34}$$

Here the vertex corrections disappear because integrals of the type $\sum_k G_k^R v_{x,y} G_k^A = 0$ vanish. This implies the absence of skew scattering for any subband filling [43], consistent with the semiclassical result. We note that the same consistency between semiclassical and microscopic quantum theory calculations for the studied 2D models is also obtained for the intrinsic and side-jump terms similar to the results in the graphene model [30]; the details of those calculations are shown in the next chapter [44] and are in general agreement with calculations by Inoue *et al.* [35].

The absence of skew scattering of order $V_1^3/(n_i V_0^4)$ is akin but not equivalent to the results of spin-Hall-effect calculations in 2D systems [45]. For the Rashba 2D electron gas the disappearance of the DC spin Hall conductivity is guaranteed by sum rules that relate the spin current to the dynamics of the induced spin polarization [46, 47]. In the case of a charge current no similar sum rule is known. As we have shown, the skew-scattering contribution in fact becomes finite when the minority band is depleted. Please note that we do not say that the Hall conductivity remains zero, since once higher order corrections are included, as was done by Kovalev *et al* [48], there will be a skew scattering contribution. Yet, Kovalev *et al* [48] find a contribution that is not of the order $V_1^3/(n_i V_0^4)$, rather, they find that it is proportional to $1/n_i$, independent of the strength of the impurity potential, V_0. Thus, this 'hybrid' skew scattering contribution is similar to the side-jump contribution in that it does not depend on the impurity strength but still has the $1/n_i$ dependence of the normal skew scattering. This calculation shows agreement with our expressions and by calculating these higher order terms, Kovalev *et al* [48] obtained agreement with the numerical results by Onoda *et al.* [36].

The reduction of the Hall conductivity in the Rashba 2D electron gas for $E_F > h$ is attributed to the simplicity of the Hamiltonian. In particular the relation $\nu_+/\lambda_+ = \nu_-/\lambda_-$ does not hold generally beyond the case of the linear-in-**k** Rashba coupling. The absence of skew scattering in the 2D hole system has a different origin: Due to the cubic dependence of spin-orbit coupling on momentum, the matrix elements, Eq. (3.22), in the antisymmetric part of the collision term behave like $\sin(3\phi - 3\phi')$. Together with the $\sin(\phi - \phi')$ dependence of the velocity factor in Eq. (3.15), this makes the integral over $\mathbf{k}'$ vanish.

Our results predict that the AHE in 2D electron and hole systems can be dominated by contributions independent of the impurity concentration, for which the anomalous Hall resistance is $\propto \sigma_{xx}^{-2}$. We also predict that in the Rashba 2D electron gas with only one subband occupied the extrinsic skew-scattering contribution, leading to anomalous Hall resistance proportional to σ_{xx}^{-1}, is non-zero. Note that this term has not been identified in previous works that considered only white-noise disorder [32, 33, 34, 35, 36]. Since the extrinsic skew scattering corresponding conductivity contribution is inversely proportional to the impurity concentration, the skew-scattering mechanism can dominate in clean samples. Finally, the recent result by Kovalev *et al* [48] shows that this hybrid skew scattering present when both subbands are occupied is weaker than the skew scattering contribution we have found in the case that one subband is occupied.

C. Proposed experimental setup

The unique phenomenology of the AHE in the studied 2D systems, in particular the sudden disappearance of skew scattering when the Fermi level crosses the depletion point of the minority 2D Rashba band, represents an opportunity for a clean test

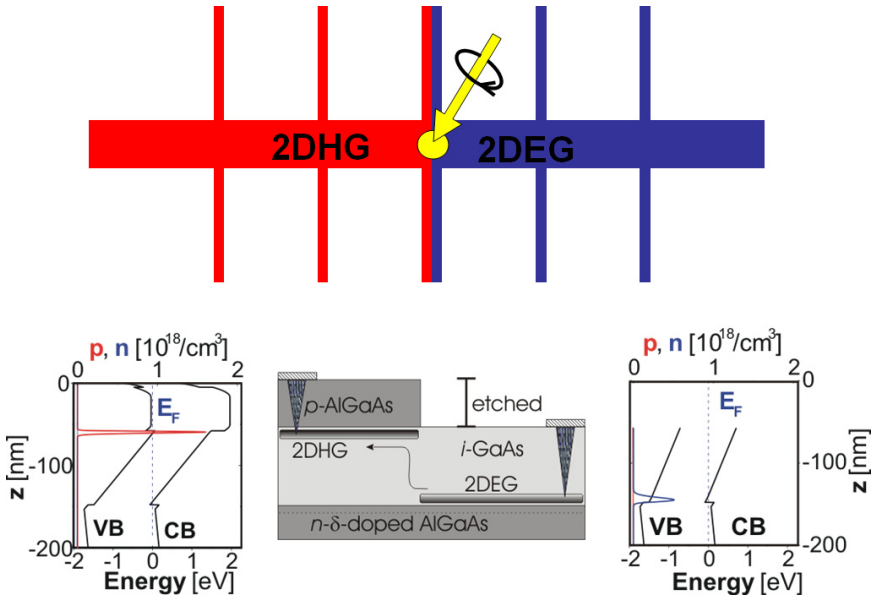

Fig. 6. Proposed experimental setup to test the anomalous Hall theory. Top panel: Schematics of the Hall bar with coplanar 2D hole and electron gases. Spin-polarized carriers are generated by shining circularly polarized light on the p-n junction. Center bottom panel: Cross section of the heterostructure containing p-type and n-type AlGaAs/GaAs single junctions. The left band diagram corresponds to the unetched part of the wafer with the 2D hole gas, the right band diagram shows the 2D electron gas in the etched section.

of the presence of intrinsic and extrinsic sources of the AHE and of the transition between these two regimes. In the absence of 2D ferromagnetic system with Rashba like spin-orbit interaction, we proposed an experimental setup for this test as shown in Fig. 6. The device is based on a AlGaAs/GaAs heterostructure containing a coplanar 2D hole gas/2D electron gas p-n junction [40]. The cross section of the heterostructure and corresponding band diagrams are shown in the lower panels of Fig. 6. Under a forward bias the junction was successfully utilized as a light-emitting-diode spin detector for the spin Hall effect [40]. Here we propose to operate the junction in the reverse-bias mode, while shining monochromatic, circularly polarized

light of tunable wavelength on the p-n junction. The photogenerated spin-polarized holes and electrons will propagate in opposite directions through the respective 2D hole and electron channels. The longitudinal voltage and the generated anomalous Hall voltage can be detected by the successive sets of Hall probes, as shown in the upper panel of Fig. 6. For the 2D electron gas the macroscopic spin diffusion length allows to use standard lithography for defining the Hall probes. Surface or back gates in close proximity to the 2D electron system can be used to modify the effective 2D confinements, carrier density, and spin-orbit coupling in order to control the transition between the intrinsic and extrinsic AHE regimes. The exploration of the AHE in the 2D hole gas is more challenging due to the expected sub-micron spin-diffusion length in this system but may still be feasible in the proposed experimental setup.

CHAPTER IV

ANOMALOUS HALL EFFECT IN A TWO-DIMENSIONAL ELECTRON GAS*

The observed Hall resistance of a magnetic film contains the ordinary Hall response to the external magnetic field and the anomalous Hall response to the internal magnetization. Although the anomalous Hall effect (AHE) has been used for decades as a basic characterization tool for ferromagnets, its origin is still being debated, also in the context of a closely related novel phenomenon, the spin Hall effect [38, 39, 40, 41]. Three mechanisms giving rise to AHE conductivity have been identified: (1) an intrinsic mechanism based solely on the topological properties of the Bloch states originating from the spin-orbit-coupled electronic structure [25], (2) a skew-scattering mechanism originating from the asymmetry of the scattering rate [26], and (3) a side-jump contribution, which semiclassically is viewed as a side-step-type of scattering and contributes to a net current perpendicular to the initial momentum [27]. Luttinger [29] uses quantum transport theory and calculates the conductivity exactly. He included impurity scattering as well as spin orbit coupling which causes the renormalization of the current operator. The interpretation by Berger [27] of the current renormalization is that when electrons scatter of impurities, in addition to the usual change of direction there is an additional side-jump (coordinate shift) during the collision.

---

*Part of this chapter is reprinted with permission from "Absence of Skew Scattering in Two-Dimensional Systems: Testing the Origins of the Anomalous Hall Effect" by Mario Borunda, Tamara S. Nunner, Thomas Lück, N. A. Sinitsyn, Carsten Timm, J. Wunderlich, T. Jungwirth, A. H. MacDonald, and Jairo Sinova, 2007. *Physical Review Letters* **99**, 066604, ©(2007) by The American Physical Society and "Anomalous Hall Effect in a Two-Dimensional Electron Gas" by Tamara S. Nunner, N. A. Sinitsyn, Mario F. Borunda, V. K. Dugaev, A. A. Kovalev, Ar. Abanov, Carsten Timm, T. Jungwirth, Jun-ichiro Inoue, A. H. MacDonald, and Jairo Sinova, 2007. *Physical Review B* **76**, 235312, ©(2007) by The American Physical Society.

Recent experimental and theoretical studies of transition-metal ferromagnets and of less conventional systems, such as diluted magnetic semiconductors, oxide and spinel ferromagnets, etc., have collected numerous examples of the intrinsic AHE and of the transition to the extrinsic AHE dominated by disorder scattering [49]. The unambiguous determination of the origin of the AHE in these experimental systems is hindered, in part, by their complex band structures, which has motivated studies of simpler model Hamiltonians, such as the two-dimensional (2D) Rashba and Dirac band models [32, 33, 34, 35, 36].

Since in the previous chapter it was demonstrated the equivalence of the Kubo-Streda formalism and the semiclassical Boltzmann approach with respect to skew scattering in the two-dimensional electron gas [50], we will focus here exclusively on the diagrammatic formalism based on the Kubo-Streda treatment. It is also the purpose of this chapter to review and analyze the previous attempts and to provide a detailed analysis of all contributions to the AHE in a two-dimensional electron gas.

The outline of the chapter is as follows. We start by reviewing and commenting on previous studies of the AHE in the two-dimensional electron gas in Sec. A, where we compare them with our results and discuss the discrepancies and their possible origins. In Sec. B we present details of our calculation within the diagrammatic Kubo-Streda formalism. In Sec. C we provide simple analytical limits of all terms of the anomalous Hall conductivity and discuss the full evaluation in Sec. D. Finally, in Sec. E we present our conclusions.

A. Comparison with previous approaches

Currently, there are several publications on the AHE in two dimensional systems reaching different quantitative predictions even in the same limits and parameters [31,

32, 33, 34, 35, 36, 37]. In this study we present a calculation with conclusions that are in disagreement with some previous studies. On such a background, we believe that previous articles have to be discussed in some detail. Below we review the history of the problem and explain why we think the subject has to be reconsidered.

A first study of the AHE in two dimensional systems was done by Culcer *et al.* [31], who calculated only the intrinsic contribution to the Hall conductivity for a wide class of two-dimensional systems, including the Rashba two-dimensional electron gas as a special case. The intrinsic contribution plays a special role in the theory of the AHE because it is not related to the scattering of electrons but is rather caused by the unusual trajectories of electrons under the action of the electric field. However, the disorder contributions can also be important and further insight was needed in the quest for a quantitatively rigorous theory of the dc-AHE.

The first attempts to understand the disorder effects were done independently by two groups [32, 33], each employing different approaches. Dugaev *et al.* [32] used the version of the Kubo formula which expresses the Hall conductivity in terms of the causal Green functions. The intrinsic contribution appears as a result of calculations with bare Green functions, while disorder effects renormalize the quasi-particle life time and the current vertex. This approach is formally rigorous and is similar to the one we adopt in our work. However, our results are quantitatively different from those found by Dugaev *et al.* [32] due to a subtlety in the calculation of the vertex at the Fermi surface which was later corrected in the appendix of a follow up article [30]. Starting with the equation for the renormalized vertex $T_x = ak_x + b\sigma_x + c\sigma_y$ and with the assumption that the density of impurities is low, Dugaev *et al.* [32] find correctly that $b = 0$ to leading order in n_i, i.e. $b/a \propto n_i$. However, such a term gets multiplied by an equivalent divergent term within the Kubo formula leading to a non-zero contribution to the AHE conductivity to zeroth order in n_i.

The expression for the Hall conductivity can be split into two parts as was done by Streda [51].

$$\sigma_{xy} = \sigma^{I}_{xy} + \sigma^{II}_{xy} \tag{4.1}$$

The first term is depends on the crystalline structure of the solid and the disorder potential. For the free electron model, in the limit where the vertex corrections are not considered, this term results in the classical Drude-Zener result [51]:

$$\sigma^{I}_{xy} \propto \tau\sigma_{xx} \tag{4.2}$$

where τ is the lifetime and σ_{xx} is the diagonal conductivity. The second term has no classical counterpart. It does not depend on the crystalline structure of the solid or the disorder present in the sample. Rather, the only material dependence is in the number of carriers in the sample [51]. Therefore, the breakup of the Hall conductivity (σ_{yx}) into the contribution from electrons at the Fermi surface (σ^{I}_{yx}) and the contribution of all states of the Fermi sea (σ^{II}_{yx}) [51].

The breakup of the Hall conductivity (σ_{yx}) into the contribution from electrons at the Fermi surface (σ^{I}_{yx}) and the contribution of all states of the Fermi sea (σ^{II}_{yx}) introduced by Streda [51] is not strictly followed by Dugaev *et al.* [32] who instead defined σ^{II}_{yx} to be all terms that arrive from the integration of the Fermi sea. This integration of the Fermi sea approach corresponds to the Hall conductivity in the clean limit and terms evaluated at the Fermi surface. As we show here and was also shown in the study of the Dirac Hamiltonian [30], σ^{II}_{yx} can be evaluated directly or as a subtraction of the clean limit σ_{yx} and σ^{I}_{yx}, leading to the correct result when both bands are occupied.

In contrast to the previous quantum mechanical approach, Sinitsyn *et al.* [33] employed the semiclassical wave-packet approach focusing only on the understanding

of the side-jump contribution and formulating the semi-classical problem in a gauge invariant form. That work [33] intentionally avoids a discussion of the skew-scattering contribution due to the asymmetry of the collision term kernel, which is also an important mechanism of the Hall current and can even be parametrically similar to all other contribution [30] in the case of Gaussian correlations. Therefore, the work by Sinitsyn *et al.* [33] was meant as an intuitive introduction into the physics of the anomalous velocity and the side-jump effect, but does not offer a rigorous quantitative comparison even in the considered limit of smooth disorder potential.

Subsequently, two papers by Liu *et al.* [34, 37] studied the problem using the Keldysh technique for linear transport. The Keldysh technique leads to the quantum Boltzmann equation for the diagonal elements of the density matrix in momentum space when only elastic scattering events are considered. In the steady state limit of a weak electric field this equation can be written as follows:

$$e\mathbf{E}\cdot\nabla_{\mathbf{p}}\hat{\rho}(\mathbf{p}) + i[\hat{H}_0, \hat{\rho}(\mathbf{p})] = \hat{I}_{col}(\hat{\rho}(\mathbf{p}))\,, \tag{4.3}$$

where $\hat{I}_{col}$ contains all disorder dependent terms that become zero when $\hat{\rho}(\mathbf{p})$ is the density matrix in thermodynamic equilibrium and $\hat{H}_0$ is the disorder free part of the Hamiltonian. The "hat" means that $\hat{\rho}$ and $\hat{I}_{col}$ are matrices in the band index space. The term containing the electric field is called the driving term. In the linear response approximation it only depends on the equilibrium part of the density matrix. To start with Eq. (4.3) is correct and is also the starting point of the pioneering work by Luttinger [29] and therefore one can compare Luttinger's work directly with the steps taken by Liu *et al.* [34, 37].

Luttinger split the density matrix into equilibrium and nonequilibrium parts $\hat{\rho} = \hat{\rho}_{\mathrm{eq}} + \hat{\rho}_{\mathrm{neq}}$, where $\hat{\rho}_{\mathrm{neq}}$ is linear in electric field, and is responsible for nonzero

currents. The quantum Boltzmann equation can be grouped as follows [42].

$$E[DT](\hat{\rho}_{\rm eq}) - i[\hat{H}_0, \hat{\rho}_{\rm neq}] = I_{col}(\hat{\rho}_{\rm neq}), \tag{4.4}$$

where $\hat{H}_0$ is the part of the Hamiltonian that is independent of the electric field and for the clean system ($V = 0$) since Luttinger used the disorder-free Bloch states in his calculation. The equilibrium term of the density matrix ($\hat{\rho}_{eq}$) contains the disorder. The driving term ($[DT]$) couples to the electric field (E). In the Bloch basis the driving term can be expressed as a series in powers of the disorder potential [42],

$$[DT](\hat{\rho}_{\rm eq}) = [DT]^{(0)} + V^2[DT]^{(2)} + \cdots \tag{4.5}$$

The collision term can also be expressed as a series in powers of V, but it starts at V^2 since it is the term with the information of the elastic scattering from the impurities in the system,

$$I_{col}(\hat{\rho}_{\rm neq}) = V^2 I^{(2)}_{col}(\hat{\rho}_{\rm neq}) + V^3 I^{(3)}_{col}(\hat{\rho}_{\rm neq}) + \cdots \tag{4.6}$$

For weak disorder potential $\hat{V}$, Luttinger looked for $\hat{\rho}_{neq}$ as a series in powers of the disorder potential. The equations can be ordered into terms of the same power of potential. Since the collision term is linear in the non-equilibrium part of the density matrix, Luttinger found that the non-equilibrium part of the density matrix series starts from the term of the order $\hat{V}^{-2}$,

$$\hat{\rho}_{\rm neq} = V^{-2}\hat{\rho}^{(-2)}_{\rm neq} + V^{-1}\hat{\rho}^{(-1)}_{\rm neq} + V^0\hat{\rho}^{(0)}_{\rm neq} + \cdots \tag{4.7}$$

As pointed out by Luttinger, the leading order term $\hat{\rho}^{(-2)}_{neq}$ does not contribute to the Hall effect and is only responsible for the longitudinal diffusive current. The term $\hat{\rho}^{(-1)}_{neq}$ was identified with skew scattering. This term, however, is parametrically very distinct and vanishes in the approximation of purely Gaussian correlations of disorder

Fourier components; therefore, Luttinger went to next order and calculated the term $\hat{\rho}^{(0)}_{\mathrm{n}eq}$. He found a number of contributions, whose physical meaning he did not clarify. The main conclusion was that at this order, both the diagonal and off-diagonal parts of the density matrix become nonzero and contribute to the Hall conductivity. The Hall conductivity becomes formally independent on the strength of disorder $\hat{V}$ in the DC limit, although disorder has to be included in the intermediate calculations.

Comparing the Luttinger approach with the first work of Liu and Lei [34], we find that they determined self-consistently only the off-diagonal part of the density matrix in band index. This is, however, not enough for a rigorous quantitative result because the diagonal part of the $\hat{\rho}^{(0)}_{neq}$ contribution has been known to be important since Luttinger's pioneering work. In their next effort Liu *et al.* [37] studied the problem of 2D Rashba systems in small gap semiconductor materials, in which a projection to the conduction band leads to extrinsic type spin-dependent contributions. In this work they noticed that the diagonal part is important and calculated it numerically. For the driving term in Eq. (4.3) Liu *et al.* assume that $\hat{\rho}_{eq}$ is just a diagonal equilibrium Fermi distribution. This assumption would be correct if one was using the basis of the eigenstates of the *full* Hamiltonian with impurities. However, both Liu *et al.* and Luttinger work in the chiral basis of the disorder free Hamiltonian $\hat{H}_0$. In this basis the *equilibrium* state density matrix is no longer diagonal and can also be written as a series in powers of the disorder potential:

$$\hat{\rho}_{eq} = \hat{\rho}^{(0)}_{eq} + \hat{\rho}^{(2)}_{eq} + \cdots \tag{4.8}$$

Luttinger has shown that in order to properly evaluate the non-equilibrium part $\hat{\rho}^{(0)}_{neq}$, one should include the second term $\hat{\rho}^{(2)}_{eq}$ of the expansion of the equilibrium density matrix in Eq. (4.8) into the driving term of Eq. (4.3). This was not done in the work of Liu *et al.* [37] and therefore we believe that their work is incomplete due to such

omission. We also note that the correction of order $\hat{V}^2$ in Eq. (4.8) leads to the Hall current contribution, which was identified in the semiclassical approach [52] as the anomalous distribution correction and if omitted leads to errors of factors of two in the typical side-jump type contributions [19]. In the Kubo formula approach, neglecting this correction would be equivalent to the unjustified omission of an important subset of Feynman diagrams [30]. Within the calculation presented here, all these terms are present.

Inoue *et al.* [35] calculated the AHE contribution using the same approach we use with a focus on the limit of both subbands being occupied and, in addition to the disorder that we consider, incorporating magnetic impurities in the model Hamiltonian. They found that for paramagnetic impurities the Hall conductivity vanishes. Our more general calculations confirm this result. However, we point to one important difference in its derivation. In both cases, the dc-limit Kubo formula, where the conductivity is expressed via retarded and advanced Greens functions, has been employed to calculate the Hall conductivity. As was shown by Streda [51], this version of the Kubo formula contains two parts: σ_{xy}^{I} a contribution from the Fermi surface and σ_{xy}^{II} a contribution from all states of the Fermi sea. The latter part is less known because it does not appear in the expression for the longitudinal conductivity. Inoue *et al.* [35] calculated only σ_{xy}^{I} and indeed we find that for their choice of parameters the second part of the conductivity σ_{xy}^{II} vanishes, explaining the agreement with our results. In a more general analysis, beyond the limit of weak spin-orbit and Zeeman couplings, we find a non-vanishing σ_{xy}^{II}. The present work provides the missing estimate of σ_{xy}^{II} and extends the calculations of Inoue *et al.* [35].

Finally, recent work by Onoda *et al.* [36] used a reformulated Keldysh technique appropriate for multiband problems in a gauge invariant formalism. They also derived a self-consistent equation, which is the analog of the standard quantum Boltz-

mann equation, and solved it numerically. Onoda *et al.* [36] find numerically a skew scattering contribution. We find that for the Rashba model with randomly placed delta-function impurities the leading part of the skew-scattering vanishes when both subbands are occupied. Onoda *et al* [36] consider the limit of dilute impurities $n_i \to 0$ independently of the disorder strength V_{imp}. Using the Keldysh formalism in the disorder free basis it has been possible to verify analytically our results [48]. Kovalev *et al* [48], find that a hybrid skew scattering appears when considering higher order terms of the Born series, these contributions do not depend on the disorder potential V_{imp}, and result in agreement with the work by Onoda *et al.* [36], putting an end to the discrepancies.

B. Anomalous Hall conductivity of the 2DEG

1. Model Hamiltonian

We consider a spin-polarized two dimensional electron gas with Rashba spin-orbit interaction, i.e. same model that what was considered in the previous chapter in Eq. (3.2) for $n = 1$,

$$H = \frac{k^2}{2m}\sigma_0 + \alpha(\sigma_x k_y - \sigma_y k_x) - h\sigma_z + V(\mathbf{r})\sigma_0 \tag{4.9}$$

where m is the effective in-plane mass of the quasiparticles, α the spin-orbit coupling parameter, h the exchange field, and σ_i the 2×2 Pauli matrices. The eigenenergies of the clean system are

$$E_{k\pm} = \frac{k^2}{2m} \pm \lambda_k \quad \text{with} \quad \lambda_k = \sqrt{h^2 + \alpha^2 k^2} \tag{4.10}$$

and are shown in Fig. 7.

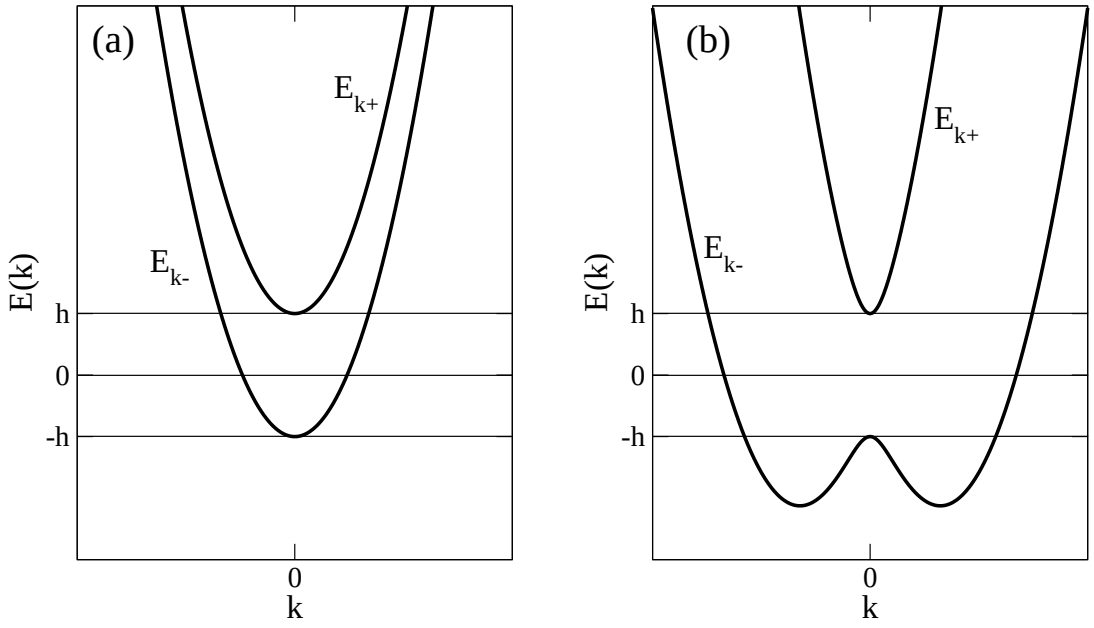

Fig. 7. Dispersion relations in two limits. (a) Single particle dispersion for small spin-orbit interaction $\alpha k_F/h = 0.2$ and (b) large spin-orbit interaction $\alpha k_F/h = 2.0$.

2. Green's functions

The retarded and advanced Green's functions are given by

$$G^{R/A}(E_F) = \frac{1}{E_F + H \pm i0^+} \tag{4.11}$$

In the chiral Bloch eigenstate basis, the retarded Greens function of the clean system (disorder free) is:

$$G_0^{R/A} = \frac{|u_k^+\rangle\langle u_k^+|}{E - E_k^+ \pm i0^+} + \frac{|u_k^-\rangle\langle u_k^-|}{E - E_k^- \pm i0^+} \tag{4.12}$$

$$\begin{aligned} G^{(0)R} &= \frac{\left(\omega - \frac{k^2}{2m} + i0^+\right)\sigma_0 + \alpha k_y \sigma_x - \alpha k_x \sigma_y - h\sigma_z}{\left(\omega - \frac{k^2}{2m} + i0^+\right)^2 - h^2 - \alpha^2 k^2} \\ &= G_0^{(0)R}\sigma_0 + G_x^{(0)R}\sigma_x + G_y^{(0)R}\sigma_y + G_z^{(0)R}\sigma_z\,, \end{aligned} \tag{4.13}$$

with

$$G_{\pm}^{(0)} = \frac{1}{\omega - E_{k\pm} + i0^{+}}, \quad G_{0}^{(0)R} = \frac{1}{2}\left(G_{+}^{(0)} + G_{-}^{(0)}\right) \tag{4.14}$$

$$G_{z}^{(0)R} = -\frac{1}{2}\frac{h}{\lambda_k}\left(G_{+}^{(0)} - G_{-}^{(0)}\right), \quad G_{x}^{(0)R} = \frac{1}{2}\frac{\alpha k_y}{\lambda_k}\left(G_{+}^{(0)} - G_{-}^{(0)}\right), \tag{4.15}$$

and

$$G_{y}^{(0)R} = -\frac{1}{2}\frac{\alpha k_x}{\lambda_k}\left(G_{+}^{(0)} - G_{-}^{(0)}\right). \tag{4.16}$$

The disorder potential $V(\mathbf{r})$ in Eq. (4.9) is assumed to be spin-independent. We consider the model of randomly located δ-function scatterers: $V(\mathbf{r}) = \sum_i V_i \delta(\mathbf{r} - \mathbf{R}_i)$ and strength distributions satisfying $\langle V_i \rangle_{\mathrm{d}is} = 0$, $\langle V_i^2 \rangle_{\mathrm{d}is} = V_0^2 \neq 0$ and $\langle V_i^3 \rangle_{\mathrm{d}is} = V_1^3 \neq 0$. This model is different from the standard white noise disorder model in which only the second order cumulant is nonzero; $\langle |V_{\mathbf{k}'\mathbf{k}}^0|^2 \rangle_{dis} = n_i V_0^2$ where n_i is the impurity concentration. This deviation from white noise disorder in our model is quantified by $V_1 \neq 0$ and is necessary to capture part of the skew scattering contribution to the anomalous Hall effect.

3. Self energy

Although the disorder-free Green's functions are simple in the basis we have chosen, the disorder matrix of the Hamiltonian now contains non-zero off-diagonal matrix elements. We first look at interband elements of the disorder which lead to a finite life time for the quasiparticles and a renormalization of the velocity vertex. This type of calculation allows us to write the self energy as:

$$\Sigma^{R} = \sum_{k'} V_{kk'}^{++} G^{R+} V_{k'k}^{++} \tag{4.17}$$

where the bare Green's function is given by:

$$G_{0}^{R+} = \frac{|u_k^{+}\rangle\langle u_k^{+}}{E - E_k^{+} \pm i0^{+}} \tag{4.18}$$

and the renormalization produces:

$$G^{R+} = \frac{|u_k^+\rangle\langle u_k^+}{E - E_k^+ + i(2\tau^+)^{-1}} \tag{4.19}$$

where

$$\frac{1}{\tau^+} = -2\mathrm{Im}(\Sigma^R) = 2\pi \int \frac{d^2\mathbf{k}'}{(2\pi)^2} |V_{k'k}^{++}|^2 \delta(E - E_{k'}^+). \tag{4.20}$$

The self energy can be rewritten as:

$$\Sigma^R = -i(\Gamma\sigma_0 + \Gamma_z\sigma_z) = -\frac{i}{4} n_i V_0^2 \left((\nu_+ + \nu_-)\sigma_0 - h \left[\frac{\nu_+}{\lambda_+} - \frac{\nu_-}{\lambda_-} \right] \sigma_z \right), \tag{4.21}$$

where $\nu_\pm$ is related to the density of states at the Fermi levels of the two subbands

$$\nu_\pm = k \left| \frac{dE_{k\pm}}{dk} \right|^{-1} = \frac{m\lambda_\pm}{\sqrt{\lambda_F^2 + (\alpha^2 m)^2}}, \tag{4.22}$$

with

$$\lambda_\pm = \sqrt{h^2 + \alpha^2 k_\pm^2} = \sqrt{\lambda_F^2 + (\alpha^2 m)^2} \mp \alpha^2 m \,, \tag{4.23}$$

where $\lambda_F = \sqrt{h^2 + 2\alpha^2 m \epsilon_F}$, and

$$k_\pm = \sqrt{2m \left(\epsilon_F + \alpha^2 m \mp \sqrt{\lambda_F^2 + (\alpha^2 m)^2} \right)} \tag{4.24}$$

are the Fermi momenta of the two subbands.

Including the self energy, the impurity averaged Green's function becomes:

$$\begin{aligned} G^R &= \frac{\left(\omega - \frac{k^2}{2m} + i\Gamma\right)\sigma_0 + \alpha k_y \sigma_x - \alpha k_x \sigma_y - (h + i\Gamma_z)\sigma_z}{\left(\omega - \frac{k^2}{2m} + i\Gamma\right)^2 - (h + i\Gamma_z)^2 - \alpha^2 k^2} \\ &= G_0^R \sigma_0 + G_x^R \sigma_x + G_y^R \sigma_y + G_z^R \sigma_z \,. \end{aligned} \tag{4.25}$$

By comparing this expression with Eq. (4.13) one observes that the impurity averaged Green's function can be obtained from the Greens function of the clean system by

the following replacements:

$$\omega \to \omega + i\Gamma\,, \quad h \to h + i\Gamma_z\,. \tag{4.26}$$

In the limit of small Γ_z one can therefore expand

$$\lambda_k \to \sqrt{(h+i\Gamma_z)^2 + \alpha^2 k^2} \approx \lambda_k \left(1 + i\frac{h\Gamma_z}{\lambda_k^2}\right)\,. \tag{4.27}$$

Using this approximation, and the following definitions,

$$G_\pm^R = \frac{1}{\omega - E_{k\pm} + i\Gamma_\pm} \tag{4.28}$$

and

$$\Gamma_\pm = \Gamma \mp \Gamma_z \frac{h}{\lambda_\pm} \tag{4.29}$$

the impurity averaged Green's function can also be written as

$$\begin{aligned} G_0^R &= \frac{1}{2}(G_+^R + G_-^R) \\ G_x^R &= \sin\phi\, \tilde{G}_x^R = \frac{1}{2}\frac{\alpha k_y \lambda_k}{\lambda_k^2 + i\Gamma_z h}(G_+^R - G_-^R) \\ G_y^R &= \cos\phi\, \tilde{G}_y^R = -\frac{1}{2}\frac{\alpha k_x \lambda_k}{\lambda_k^2 + i\Gamma_z h}(G_+^R - G_-^R) \\ G_z^R &= -\frac{1}{2}\frac{\lambda_k(h+i\Gamma_z)}{\lambda_k^2 + i\Gamma_z h}(G_+^R - G_-^R). \end{aligned} \tag{4.30}$$

4. General expression for the anomalous Hall conductivity

The fully quantum mechanical calculation for the conductivity is preformed using the linear response formalism of the Kubo formula. We use the approach that is suitable for the dc conductivity (no $\omega \to 0$ limit to worry about once the calculation is performed). The starting point is the Kubo-Streda formula at $T = 0$. According

to the Kubo-Streda formalism [51], the off-diagonal conductivity can be written as

$$\sigma_{yx} = \sigma_{yx}^{I(a)} + \sigma_{yx}^{I(b)} + \sigma_{yx}^{II} \tag{4.31}$$

where

$$\begin{aligned}
\sigma_{yx}^{I(a)} &= \frac{e^2}{2\pi V}\mathrm{Tr}\left\langle v_y G^R(\epsilon_F) v_x G^A(\epsilon_F)\right\rangle, && (4.32)\\
\sigma_{yx}^{I(b)} &= -\frac{e^2}{4\pi V}\mathrm{Tr}\left\langle v_y G^R(\epsilon_F) v_x G^R(\epsilon_F) + v_y G^A(\epsilon_F) v_x G^A(\epsilon_F)\right\rangle, && (4.33)\\
\sigma_{yx}^{II} &= \frac{e^2}{4\pi V}\int_{-\infty}^{\infty} d\epsilon f(\epsilon)\mathrm{Tr}\left\langle v_y G^R(\epsilon) v_x \frac{\partial G^R(\epsilon)}{\partial \epsilon} - v_y \frac{\partial G^R(\epsilon)}{\partial \epsilon} v_x G^R(\epsilon)\right. \\
&\qquad \left. - v_y G^A(\epsilon) v_x \frac{\partial G^A(\epsilon)}{\partial \epsilon} + v_y \frac{\partial G^A(\epsilon)}{\partial \epsilon} v_x G^A(\epsilon)\right\rangle. && (4.34)
\end{aligned}$$

Here, σ^I results from the electrons at the Fermi surface, whereas σ^{II} denotes the contribution of all states of the Fermi sea. For $\sigma^{I(b)}$ and σ^{II}, it is sufficient to calculate the bare bubble contribution in the weak scattering limit [30] because vertex corrections are of higher order in the scattering rate Γ. Substituting in the Green's function of Eq. (4.30) and using the velocity vertices

$$v_x = \frac{k_x}{m}\sigma_0 - \alpha\sigma_y, \quad v_y = \frac{k_y}{m}\sigma_0 + \alpha\sigma_x \tag{4.35}$$

one finds that $\sigma^{I(b)}$ vanishes

$$\sigma_{yx}^{I(b)} = \frac{e^2}{4\pi}\int \frac{d^2k}{(2\pi)^2}\left(i\alpha^2 G_0^R G_z^R - i\alpha^2 G_z^R G_0^R + i\alpha^2 G_0^A G_z^A - i\alpha^2 G_z^A G_0^A\right) = 0. \tag{4.36}$$

The bare contribution of σ^{II} in the clean limit, i.e., for $\Gamma_+ = \Gamma_- = 0^+$ can be calculated by integration (see Appendix A) and yields

$$\sigma_{yx}^{II} = \frac{e^2}{4\pi}\left(1 - \frac{h}{\sqrt{h^2 + 2\alpha^2 m\epsilon_F + (\alpha^2 m)^2}}\right)\Theta(h - \epsilon_F) \tag{4.37}$$

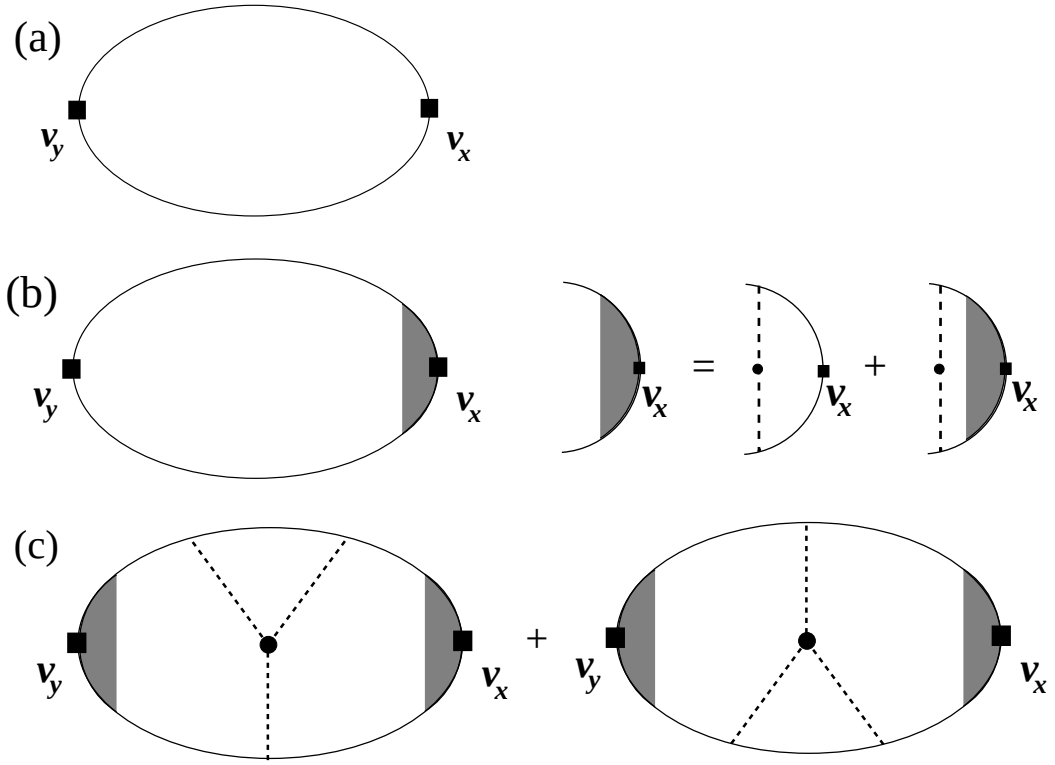

Fig. 8. Diagrammatic representation of the contributions to the conductivity. (a) the bare bubble diagram, representing Eq. 4.39, (b) the ladder vertex corrections, representing Eq. (4.44), with the expression on the right being given by Eq. (4.40), and (c) the skew scattering contribution, representing Eq. (4.47).

where $\partial G_{\pm}^{R/A}/\partial\epsilon = -(G_{\pm}^{R/A})^2$ has been used. Including the real scattering rates Γ_+ and Γ_- does not lead to qualitatively different results but mainly causes a slight smearing. Thus we consider it as sufficient to focus on the clean limit contribution of σ^{II}.

For $\sigma^{I(a)}$, vertex corrections can be of similar magnitude as the bare bubble and thus have to be considered carefully. In the weak scattering limit, contributions of higher order impurity scattering vertices are small leaving only ladder type vertex corrections and the $V_1^3/(n_i V_0^4)$ skew scattering contribution as the important terms [50].

Thus, we decompose $\sigma^{I(a)}$ in the following way:

$$\sigma_{yx}^{I(a)} = \sigma_{yx}^{I(a),b} + \sigma_{yx}^{I(a),l} + \sigma_{yx}^{I(a),s} \tag{4.38}$$

where $\sigma_{yx}^{I(a),b}$ is the bare bubble contribution (Fig. 8(a)), $\sigma_{yx}^{I(a),l}$ the ladder vertex corrections (Fig. 8(b)), and $\sigma_{yx}^{I(a),s}$ the skew-scattering contribution (Fig. 8(c)). With respect to the skew-scattering contribution we have shown in the previous chapter [50] that only the diagrams with a single third order vertex (see Fig. 8(c)) contribute to order $V_1^3/(n_i V_0^4)$. In this diagram both vertices have to be renormalized by ladder vertex corrections.

a. Bare bubble

The calculation of the bare bubble contribution proceeds as follows:

$$\begin{aligned}
\sigma_{yx}^{I(a),b} &= \frac{e^2}{2\pi}\int\int \frac{dkkd\phi}{(2\pi)^2}\mathrm{Tr}\left[v_y G^R(\epsilon_F) v_x G^A(\epsilon_F)\right] \\
&= 2i\alpha\int\frac{dkk}{2\pi}\left(\frac{k}{m}(\tilde{G}_y^R G_z^A - G_z^R\tilde{G}_y^A) - \alpha(G_0^R G_z^A - G_z^R G_0^A)\right) \\
&= 2i\alpha(2I_3 - \alpha I_2)
\end{aligned} \tag{4.39}$$

where $\tilde{G}_y^{R/A}$ are defined in Eq. (4.30) and each I_i represents the following integrals:

$$\begin{aligned}
I_1 &= \int\frac{dk}{2\pi}k\left(G_0^R G_0^A - G_z^R G_z^A\right) \approx \frac{1}{8}\left[\left(1-\frac{h^2}{\lambda_+^2}\right)\frac{\nu_+}{\Gamma_+} + \left(1-\frac{h^2}{\lambda_-^2}\right)\frac{\nu_-}{\Gamma_-}\right], \\
I_2 &= \int\frac{dk}{2\pi}k\left(G_0^R G_z^A - G_z^R G_0^A\right) \approx -\frac{i}{4}\left[\frac{\nu_+ h}{\lambda_+^2} + \frac{\nu_- h}{\lambda_-^2} - \frac{\Gamma_z}{\Gamma_+}\frac{\nu_+\alpha^2 k_+^2}{\lambda_+^3} + \frac{\Gamma_z}{\Gamma_-}\frac{\nu_-\alpha^2 k_-^2}{\lambda_-^3}\right], \\
I_3 &= \int\frac{dk}{2\pi}\frac{k^2}{2m}\left(\tilde{G}_y^R G_z^A - G_z^R\tilde{G}_y^A\right) \approx -\frac{i}{4}\alpha\Gamma_z\left[\frac{\nu_+}{\Gamma_+\lambda_+}\left(\frac{\epsilon_F}{\lambda_+}-1\right) + \frac{\nu_-}{\Gamma_-\lambda_-}\left(\frac{\epsilon_F}{\lambda_-}+1\right)\right], \\
I_4 &= \int\frac{dk}{2\pi}\frac{k^2}{2m}\left(G_0^R\tilde{G}_y^A + \tilde{G}_y^R G_0^A\right) \approx -\frac{1}{4}\alpha\left[\epsilon_F\left(\frac{\nu_+}{\Gamma_+\lambda_+} - \frac{\nu_-}{\Gamma_-\lambda_-}\right) - \left(\frac{\nu_+}{\Gamma_+} + \frac{\nu_-}{\Gamma_-}\right)\right].
\end{aligned}$$

The explicit evaluation of integrals I_1, I_2, I_3 and I_4 can be found in Appendix B.

b. Ladder diagrams

For the ladder terms $\sigma_{yx}^{I(a),l}$, we first need to sum the vertex corrections in front of the v_x vertex as indicated in Fig. 8(b). Starting from the momentum integrated bare velocity vertex, the expression corresponding to Fig. 8(b) is:

$$\int\int \frac{dkkd\phi}{(2\pi)^2} G^R(\epsilon_F) v_x G^A(\epsilon_F) = \gamma_x \sigma_x + \gamma_y \sigma_y, \tag{4.40}$$

with

$$\gamma_x = i(I_3 - \alpha I_2)\,, \quad \gamma_y = I_4 - \alpha I_1 \tag{4.41}$$

one finds for the renormalized vertex

$$\begin{aligned} \Gamma_{v_x} &= \Gamma_x \sigma_x + \Gamma_y \sigma_y \\ &= \gamma_x \sigma_x + \gamma_y \sigma_y + n_i V_0^2 \int\int \frac{dkkd\phi}{(2\pi)^2} G^R(\epsilon_F)(\gamma_x \sigma_x + \gamma_y \sigma_y) G^A(\epsilon_F) \\ &= \gamma_x \sigma_x + \gamma_y \sigma_y + n_i V_0^2 \left((I_1 \Gamma_x + i I_2 \Gamma_y)\sigma_x + (I_1 \Gamma_y - i I_2 \Gamma_x)\sigma_y\right) \end{aligned} \tag{4.42}$$

and thus

$$\begin{pmatrix} \Gamma_x \\ \Gamma_y \end{pmatrix} = \frac{1}{(1 - n_i V_0^2 I_1)^2 - (n_i V_0^2 I_2)^2} \begin{pmatrix} 1 - n_i V_0^2 I_1 & i n_i V_0^2 I_2 \\ -i n_i V_0^2 I_2 & 1 - n_i V_0^2 I_1 \end{pmatrix} \begin{pmatrix} \gamma_x \\ \gamma_y \end{pmatrix} \tag{4.43}$$

The complete expression for the ladder diagrams are given by

$$\begin{aligned} \sigma_{yx}^{I(a),l} &= \frac{e^2}{2\pi} \int\int \frac{dkkd\phi}{(2\pi)^2} \mathrm{Tr}[G^A(\epsilon_F) v_y G^R(\epsilon_F)(\Gamma_x \sigma_x + \Gamma_y \sigma_y)] = -\frac{e^2}{2\pi} 2(\gamma_y \Gamma_x + \gamma_x \Gamma_y) \\ &= -\frac{e^2}{\pi} \frac{n_i V_0^2 (2\gamma_x \gamma_y (1 - n_i V_0^2 I_1) + i n_i V_0^2 I_2 (\gamma_y^2 - \gamma_x^2))}{(1 - n_i V_0^2 I_1)^2 - (n_i V_0^2 I_2)^2}. \end{aligned} \tag{4.44}$$

In the weak scattering limit the above reduces to

$$\sigma_{yx}^{I(a),l} = -\frac{e^2}{\pi} \frac{n_i V_0^2 \left(2\gamma_x \gamma_y (1 - n_i V_0^2 I_1) + i n_i V_0^2 I_2 \gamma_y^2\right)}{(1 - n_i V_0^2 I_1)^2}. \tag{4.45}$$

c. Skew scattering

For skew-scattering we consider only diagrams with a single third order impurity vertex and both external current vertices renormalized by ladder vertex corrections as indicated in Fig. 8(c). In analogy to the renormalized v_x vertex in Eq. (4.42), also the renormalized v_y-vertex can be calculated and expressed via Γ_x and Γ_y as

$$\Gamma_{v_y} = -\Gamma_y \sigma_x - \Gamma_x \sigma_y \,. \tag{4.46}$$

Using these expressions the skew scattering diagram of Fig. 8(c) yields

$$\begin{aligned}
\sigma_{yx}^{I(a),s} &= \frac{e^2}{2\pi}\frac{n_i V_1^3}{2\pi}\int dk k \mathrm{Tr}[\Gamma_{v_y} G^R(\epsilon_F)\Gamma_{v_x} + \Gamma_{v_y}\Gamma_{v_x} G^A(\epsilon_F)] \\
&= \frac{e^2}{2\pi} i \frac{V_1^3}{V_0^2}\mathrm{Tr}[-\Gamma_{v_y}(\Gamma\sigma_0 + \Gamma_z\sigma_z)\Gamma_{v_x} + \Gamma_{v_y}\Gamma_{v_x}(\Gamma\sigma_0 + \Gamma_z\sigma_z)] \\
&= \frac{e^2}{2\pi} i \frac{V_1^3}{V_0^2}\Gamma_z \mathrm{Tr}[(\Gamma_y\sigma_x + \Gamma_x\sigma_y)(\sigma_z(\Gamma_x\sigma_x + \Gamma_y\sigma_y) - (\Gamma_x\sigma_x + \Gamma_y\sigma_y)\sigma_z)] \\
&= \frac{e^2}{2\pi}\frac{V_1^3}{V_0^2} 4\Gamma_z(\Gamma_y^2 - \Gamma_x^2). \qquad (4.47)
\end{aligned}$$

From this expression it is evident that the skew scattering contribution vanishes as soon as $\Gamma_z = 0$ implying that the lifetimes in both bands become equal since $\Gamma_- - \Gamma_+ = \Gamma_z(h/\lambda_- + h/\lambda_+)$ vanishes for $\Gamma_z = 0$. Plugging in Γ_x and Γ_y from Eq. (4.43) one finds [50] in the weak scattering limit, i.e., neglecting higher order impurity terms:

$$\sigma_{yx}^{I(a),s} = \frac{e^2}{2\pi}\frac{4V_1^3\Gamma_z\gamma_y^2}{V_0^2(1 - n_i V_0^2 I_1)^2} \tag{4.48}$$

$$= \frac{e^2}{2\pi}\frac{V_1^3}{n_i V_0^4}\frac{h\lambda_-\alpha^2 k_-^4}{\nu_-(3h^2 + \lambda_-^2)^2} \,. \tag{4.49}$$

When considering the weak scattering limit of the full vertex shown in Fig. 9, it yields exactly the same result as Eq. (4.48), i.e., to order $V_1^3/(n_i V_0^4)$ it reduces to the elementary skew scattering diagram depicted in Fig. 8(c).

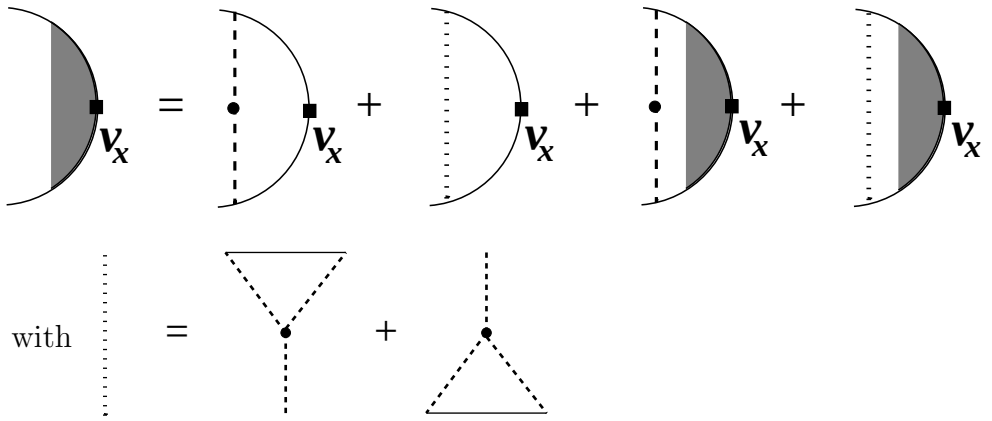

Fig. 9. Diagrammatic representation of the full vertex including ladder and skew scattering diagrams.

C. Simple limits

1. Both subbands occupied

In the situation that both subbands are partially occupied, i.e., $\epsilon_F > h$, all contributions to the anomalous Hall conductivity vanish. For σ_{yx}^{II}, this is immediately evident from Eq. (4.37). For the skew scattering contribution, which is proportional to Γ_z (see Eq. (4.48)), one observes that $\sigma_{yx}^{I(a),s} = 0$ because $\Gamma_z = 0$ (see Eq. (4.21)) due to $\nu_+/\lambda_+ - \nu_-/\lambda_- = 0$ (see Eq. (4.22)).

With respect to the bare bubble and ladder diagrams, we will show in the following that those contributions cancel each other. For $\epsilon_F > h$ the integrals in Eq. (4.40) simplify to

$$I_1 = \frac{\alpha^2 m^2 \epsilon_F}{2\lambda_F^2 \Gamma}\,, \quad I_2 = -\frac{ihm}{2\lambda_F^2}\,, \quad I_3 = 0\,, \quad I_4 = \frac{\alpha m}{2\Gamma} \tag{4.50}$$

and the bare momentum integrated vertices in Eq. (4.41) are

$$n_i V_0^2 \gamma_x = -\frac{\alpha h \Gamma}{\lambda_F^2}\,, \quad n_i V_0^2 \gamma_y = \alpha \left(1 - \frac{\alpha^2 m \epsilon_F}{\lambda_F^2}\right)\,. \tag{4.51}$$

This gives for the bare bubble in Eq. (4.39)

$$\sigma_{yx}^{I(a),b} = -\frac{e^2}{2\pi}\frac{\alpha^2 mh}{\lambda_F^2}\,. \tag{4.52}$$

For the ladder diagrams we need also

$$1 - n_i V_0^2 I_1 = \frac{n_i V_0^2 \gamma_y}{\alpha}\,, \quad -in_i V_0^2 I_2 = \frac{n_i V_0^2 \gamma_x}{\alpha}, \tag{4.53}$$

yielding

$$\sigma_{yx}^{I(a),l} \;=\; -\frac{e^2}{\pi}\frac{\alpha}{n_i V_0^2}\frac{2\gamma_x\gamma_y^2 - \gamma_x\gamma_y^2 + \gamma_x^3}{\gamma_x^2+\gamma_y^2} = -\frac{e^2}{\pi}\frac{\alpha\gamma_x}{n_i V_0^2} = \frac{e^2}{2\pi}\frac{\alpha^2 mh}{\lambda_F^2} \tag{4.54}$$

and thus

$$\sigma_{yx}^{I(a),b} + \sigma_{yx}^{I(a),l} = 0\,, \tag{4.55}$$

i.e., the contribution of the bare bubble and the ladder diagrams cancel mutually.

2. Only majority band occupied

In the opposite situation, where only the majority band is partially occupied, we have $\nu_+ = 0$ and therefore $\Gamma_z \neq 0$. In this case, all terms contribute to the anomalous Hall conductivity. In the following, we restrict our analysis to Fermi energies $\epsilon_F > -h$, i.e., we disregard the region of very small Fermi energies, where the valley structure of the majority band becomes important (see Fig. 7(b)) and discuss the results in two simple limits: (1) small spin orbit interaction, $\alpha k_F \ll h$, and (2) small magnetization, $h \ll \alpha k_F$.

In the limit of small spin-orbit interaction, $\alpha k_F \ll h$, the sum of bare bubble and ladder vertex corrections becomes

$$\sigma_{yx}^{I(a),b} + \sigma_{yx}^{I(a),l} = \frac{e^2}{2\pi}\frac{(\alpha k_F)^2}{16h\epsilon_F}\left(3\frac{\epsilon_F}{h}+1\right)\left(-\frac{\epsilon_F}{h}+1\right) \tag{4.56}$$

the contribution from the states of the full Fermi sea

$$\sigma_{yx}^{II} = -\frac{e^2}{4\pi}\frac{(\alpha k_F)^2}{2h^2}, \tag{4.57}$$

and the skew-scattering term

$$\sigma_{yx}^{I(a),s} = \frac{e^2}{2\pi}\frac{(\alpha k_F)^2}{8\epsilon_F n_i V_0}\frac{V_1^3}{V_0^3}\frac{(\epsilon_F + h)^2}{h^2}\,. \tag{4.58}$$

In the opposite limit of small exchange field $h \ll \alpha k_F$, considering first a spin-orbit interaction still smaller than the Fermi energy $\alpha k_F \ll \epsilon_F$, we find for the sum of bare bubble and ladder vertex corrections

$$\sigma_{yx}^{I(a),b} + \sigma_{yx}^{I(a),l} = -\frac{e^2}{2\pi}\frac{3h\epsilon_F}{(\alpha k_F)^2}, \tag{4.59}$$

for the contribution from the states of the full Fermi sea

$$\sigma_{yx}^{II} = \frac{e^2}{4\pi}\left(1 - \frac{h}{\alpha k_F}\right), \tag{4.60}$$

and for the skew scattering term

$$\sigma_{yx}^{I(a),s} = \frac{e^2}{2\pi}\frac{V_1^3}{V_0^3}\frac{2h\epsilon_F}{n_i V_0 \alpha k_F}\,. \tag{4.61}$$

In the same limit where the exchange field is small, $h \ll \alpha k_F$, but the spin-orbit interaction is now larger than the Fermi energy, $\alpha k_F \gg \epsilon_F$, we find for the sum of bare bubble and ladder vertex corrections

$$\sigma_{yx}^{I(a),b} + \sigma_{yx}^{I(a),l} = -\frac{e^2}{2\pi}\frac{2h\epsilon_F^3}{(\alpha k_F)^4}, \tag{4.62}$$

for the contribution from the states of the full Fermi sea

$$\sigma_{yx}^{II} = \frac{e^2}{4\pi}\left(1 - \frac{2h\epsilon_F}{(\alpha k_F)^2}\right), \tag{4.63}$$

and the for skew scattering term

$$\sigma_{yx}^{I(a),s} = \frac{e^2}{2\pi}\frac{V_1^3}{V_0^3}\frac{h}{n_i V_0}\,. \tag{4.64}$$

D. Discussion

We now discuss the full evaluation of the anomalous Hall conductivity in the limit of small spin orbit interaction $\alpha k_F \ll h$ and in the opposite limit of strong spin orbit interaction $\alpha k_F \gg h, \epsilon_F$. For the following discussion we will express all quantities in terms of the exchange field h, which we define as $h = 1$. Furthermore, we will set $m = 1$, we choose $V_1 = V_0$ and use an impurity concentration of $n_i = 0.1$.

In Fig. 10 we show the anomalous Hall conductivity for a small spin orbit interaction of $\alpha k_F/h = 0.2$ as a function of the Fermi energy ϵ_F/h and the scattering rate $1/\tau = n_i V_0^2 m$ for an impurity concentration of $n_i = 0.1$. Figure 10(a) shows the total anomalous Hall conductivity, i.e., the sum of skew scattering (shown in Fig. 10(b)), of bare bubble and ladder diagrams (shown in Fig. 10(c)) and of the contribution from the whole Fermi sea (Fig. 10(d)). All contributions to the total conductivity vanish for $\epsilon_F > h$, i.e., when both subbands are occupied in agreement with the analysis in Sec. 1. Furthermore, we observe that not only σ_{yx}^{II} but also the bare bubble and ladder vertex corrections $\sigma_{yx}^{I(a),b} + \sigma_{yx}^{I(a),l}$ (see Eq. (4.56)) are independent of impurity scattering. Both contributions are small: σ_{yx}^{II} contains a small prefactor of $(\alpha k_F/h)^2$ (see Eq. (4.57)) and $\sigma_{yx}^{I(a),b} + \sigma_{yx}^{I(a),l}$ a small prefactor of $(\alpha k_F)^2/(h\epsilon_F)$ (see Eq. (4.56)). The skew-scattering contribution, on the other hand, has a prefactor of $\alpha k_F/(n_i V_0)$ which diverges for $V_0 \to 0$, i.e, $1/\tau \to 0$ (see Eq. (4.58)), and therefore overcompensates the small prefactor of $\alpha k_F/\epsilon_F$ (see Eq. (4.58)) when the impurity potentials V_0 becomes small enough. Thus, for the parameters chosen in Fig. 10, the skew-scattering term outweighs the other contributions by orders of magnitude

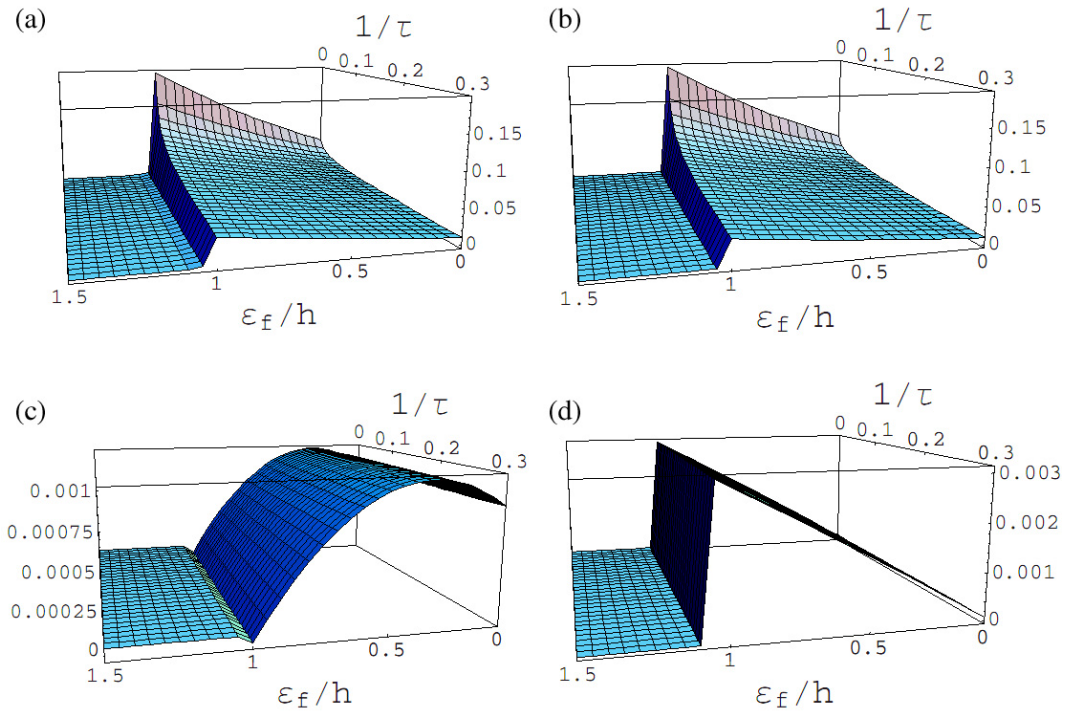

Fig. 10. The anomalous Hall conductivity in the limit of small spin-orbit coupling. Assuming that $\alpha k_F/h = 0.2$ and an impurity concentration of $n_i = 0.1$ the anomalous Hall conductivity is plotted as a function of ϵ_F/h (from right to left) and as a function of $1/\tau = n_i m V_0^2$ in units of h (from back to front). (a) Total anomalous Hall conductivity (Eq. (4.31)), (b) skew scattering contribution (Eq. (4.48)), (c) bare bubble plus ladder vertex corrections (Eq. (4.39)+Eq. (4.44)), (d) σ^{II} (Eq. (4.37)). All conductivities are plotted in units of e^2.

and therefore the total anomalous Hall conductivity is almost identical to the skew scattering term. The anomalous Hall conductivity increases quadratically with ϵ_F/h (see Eq. (4.58)) and then vanishes suddenly for $\epsilon_F > h$.

Figure 11 displays the anomalous Hall conductivity in a similar way as Fig. 10 only for a large spin orbit interaction of $\alpha k_F/h = 10$. Again, $\sigma_{yx}^{I(a),b} + \sigma_{yx}^{I(a),l}$ turns out to be independent of the impurity parameters and even smaller in magnitude as before because now it is suppressed by a small prefactor of $(h\epsilon_F^3)/(\alpha k_F)^4$ (see Eq. (4.62)).

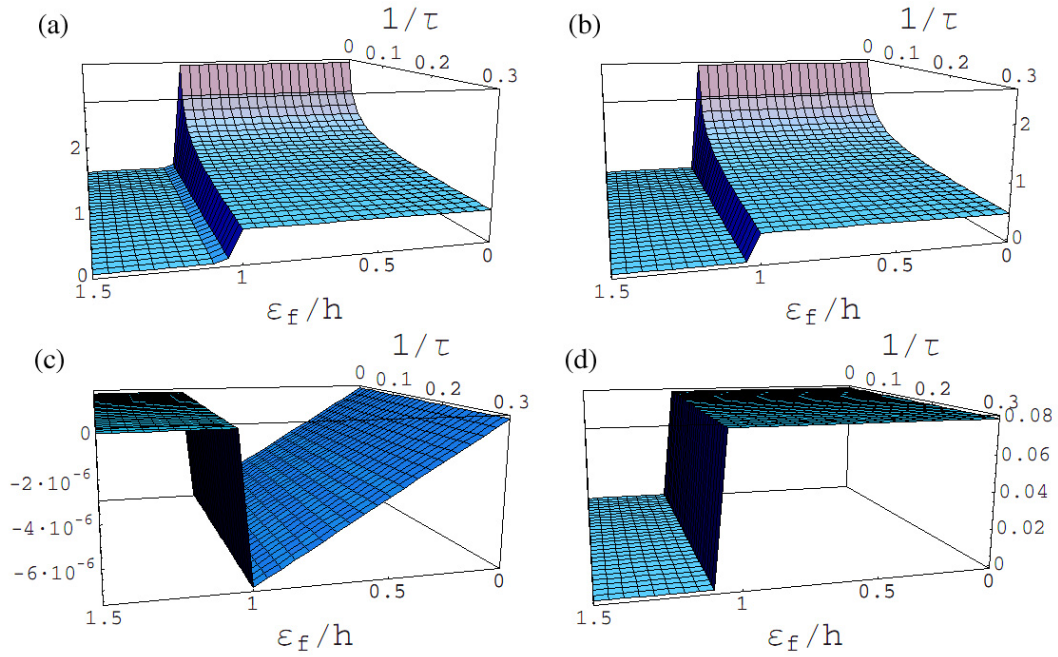

Fig. 11. The anomalous Hall conductivity in the limit of large spin-orbit coupling. Assuming that $\alpha k_F/h = 10.0$ and an impurity concentration of $n_i = 0.1$, the anomalous Hall conductivity is plotted as a function of ϵ_F/h (from right to left) and as a function of $1/\tau = n_i m V_0^2$ in units of h (from back to front): (a) total anomalous Hall conductivity (Eq. (4.31)), (b) skew scattering contribution (Eq. (4.48)), (c) bare bubble plus ladder vertex corrections (Eq. (4.39)+Eq. (4.44)), and (d) σ^{II} (Eq. (4.37)). All conductivities are plotted in units of e^2.

Analogously to the limit of small spin orbit interaction, the total anomalous Hall conductivity is dominated by the skew-scattering contribution, which contains no small prefactor and, due to the factor of $h/(n_i V_0)$, grows rapidly for small impurity potentials $V_0 \to 0$, i.e., $1/\tau \to 0$ (see Eq. (4.64)). In the limit of large spin-orbit interaction, $\alpha k_F \gg \epsilon_F$, the skew-scattering and thus the total anomalous Hall conductivity is independent of the Fermi energy ϵ_F for $\epsilon_F < h$ (see Eq. (4.64)) and then abruptly drops to zero for $\epsilon_F > h$.

E. Conclusions

In summary, we have investigated the anomalous Hall conductivity in a spin-polarized two-dimensional electron gas with Rashba spin-orbit interaction in the presence of pointlike potential impurities. Our calculations have been performed within diagrammatic perturbation theory based on the Kubo-Streda formula, an approach which has previously been shown to yield equivalent results to the semiclassical Boltzmann treatment [30, 50].

Comparing our results with previous calculations, we have been able to sort out contradictions existing in the literature. We have found that within the model Hamiltonian considered, all contributions to the anomalous Hall conductivity vanish as soon as the minority band becomes partially filled, i.e., as soon as the Fermi energy becomes larger than the internal Zeeman field. For smaller Fermi energies, all contributions are finite with σ_{yx}^{II}, the contribution from all states of the Fermi sea, being the smallest term at least in the limits of weak and of strong spin orbit interaction. The vertex corrections, which represent disorder contributions, can be of similar magnitude as the intrinsic contribution and turn out to be independent of the impurity concentration and impurity potential at least in the limits of small and of strong spin orbit interaction. In the weak scattering limit, the dominant contribution originates from skew-scattering; due to its $1/(n_i V_0)$-dependence, skew-scattering outweighs all other terms. Moreover, the intrinsic and the side jump terms contain higher orders of small prefactors than the skew scattering contribution.

CHAPTER V

MESOSCOPIC RINGS*

In recent decades, advances in technology have allowed the fabrication of electronic components of mesoscopic dimensions. Given the nanometer spatial confinement of the charge carriers, some of the important features exhibited are due entirely to quantum mechanical effects. Notwithstanding the future applications that will exploit such effects, several areas of fundamental physics will benefit from the study of such devices [53].

One such area is the study of geometric phases [54]. When a quantum particle undergoes cyclic evolution motion in the system's parameter space, it acquires a geometric phase that will strongly influence the transport properties of the system. Pancharatnam [55], when studying polarized light in crystals, found from interference experiments that the path that the light travels (or the sequence of measurements performed during that path) was responsible for an additional phase component. In the same manner, the path taken by a beam of electric charges is important when in the presence of electromagnetic vector potentials. Even in the case of the potential not producing a field that results in a force acting on the particles, the particles may gain a quantum phase that depends on the path traversed. Examples of such phase gains are the Aharonov-Bohm (AB) effect and its relativistic cousin the Aharonov-Casher (AC) effect. In the AB effect the particle gains a phase as it moves in a path enclosing a magnetic flux [56]. In the AC effect the phase acquired follows readily from spin-orbit

*Part of this chapter is reprinted with permission from "Aharonov-Casher and spin Hall effects in mesoscopic ring structures with strong spin-orbit interaction" by M. F. Borunda, Xin Liu, A. A. Kovalev, Xiong-Jun Liu, T. Jungwirth, and Jairo Sinova, 2008. *Physical Review B* in press, ©(2008) by The American Physical Society.

(SO) coupling instead of a magnetic field [57]. The generalized explanation to these phase dependent phenomena in adiabatically and non-adiabatically evolving quantum systems was given by Berry [58] and by Aharonov and Anandan [59], respectively.

These geometric phases can be studied most readily in mesoscopic ring structures. Studies on mesoscopic rings with inhomogeneous magnetic fields showed analogies between geometric phases due to SO interaction and the phases acquired by moving electrons in an effective inhomogeneous magnetic field with opposite sign for each spin [60]. At the same time, it was found that SO interaction shifts the AB oscillations and adds destructive interference to the conducting rings [61].

Applications arising from tuning the phase of the carriers have been widely discussed [62, 63, 64, 65, 66, 67], starting with the proposal by Nitta *et. al.* of an spin-interference device to modulate the current flow [62]. The proposed device consists of a paramagnetic electrode lead injecting charge into a ring section fitted with a gate and another lead that would extract the charge carriers. In narrow-gap semiconductor systems (electron or heavy hole) the SO coupling strength can be controlled by applying a gate voltage [68]. Thus, the phase difference acquired in each of the arms of the ring and the ensuing interference effect can be modified by the gate voltage which results in periodic oscillations of the conductance [62].

Recent experiments have confirmed that a gate bias modifies the oscillations in the magneto-conductance curves which demonstrates gate-controlled changes in the geometric phase [69, 70, 71]. The magneto-conductance oscillations as a function of both magnetic field and gate voltage that controls the SO interaction strength in HgTe ring structures have been studied by König and coworkers [70]. Their measurements exhibit a nonmonotonic phase change as a function of the gate voltage and establish the connection between this observation and the AC effect by finding a quantitative agreement between their experimental results and Landauer-Büttiker

numerical calculations of a multichannel ring with Rashba SO interaction [70]. Koga *et. al.* measured the sheet conductivity of square loops arrays observing a gate voltage mechanism influencing the spin interference of electrons [69]. Habib *et. al.* also measured resistance oscillations in a two-dimensional hole ring structure [71]. The oscillations depend on a front gate voltage but are not completely attributed to SO splitting due to asymmetry in the structure and the low density of the system [71]. Similarly AB oscillations in the magneto-conductance have been measured in p-type ring structures lacking a gate to control the SO splitting but in systems with considerable SO splitting ($\Delta_{SO}/E_F \sim 0.3$) where the SO induced field is reported to be as strong as $B_{eff} = 0.25T$ [72].

In the theoretical front the modulation of the electric current driven by quantum interference effects in 1D coherent electron systems was calculated analytically and compared to numerical simulations of a 2D ring in which only one mode is conducting [63, 64]. Both calculations confirmed that the spin-dependent transport results in strong quasiperiodic modulations to the conductivity. Molnár and coworkers calculated the conductance as a function of the Fermi wave vector of the incident electrons and the SO coupling in the mesoscopic rings [64]. Souma and Nikolić numerically compared the conductance modulation of the mesoscopic rings as more channels open for conduction and they found that the modulation pattern remains but is affected as more modes become available. Moreover, they concluded that the spin-interference of the channels is not cumulative, given that for single-channel devices the conductivity can be null at certain values of the SO interaction and the same does not hold in the multi-channel devices [65]. In addition, Souma and Nikolić calculated the spin-Hall conductance of ring structures and found that the spin Hall conductance is also modulated by the SO interaction [66]. In their proposed four-probe ring, a pure spin current is induced in the transverse probes when unpolarized current flows in the lon-

gitudinal probes. A recent calculation also considers the effect of an inhomogeneous SO coupling in the 2DEG ring structures [67]. By mapping the SO interaction to a spin dependent magnetic field, Tserkovnyak and Brataas found that in the weak SO regime quantum-interference effects can be stronger due to the inhomogeneity of the field [67].

In this chapter, we revisit the problem of transport characteristics of ring structures in electron and hole doped system. In section A we present Hamiltonians that describe electron and heavy-hole systems in thin ring geometries and outline the two methods used to calculate their transport properties. In section B we confirm numerically analytical results [73] for a single channel ring embedded in a narrow quantum well. The first part of the section focuses on the consequences for the conductance of the change in the Hamiltonian from wave-vector k-linear spin splitting term compared to a k-cubic term. In the second part of the section we explain the results and the dependence on the carrier concentration. In the last part of section B we present the calculation of the spin Hall conductivity in a four probe ring geometry for heavy-hole carriers and compare it to the conductivity obtained for electrons. Section C explores numerically the effect of inhomogeneous SO in mesoscopic rings. We study how the AC effect is affected by having a region with no SO coupling within the ring and show increases in the strength of the signals obtained from the conductivities. In this section we also demonstrate that devices with inhomogeneous SO interaction exhibit an electrically controlled spin-flipping mechanism not present in the case of homogeneous SO coupling. In section D we summarize the results and present our conclusions.

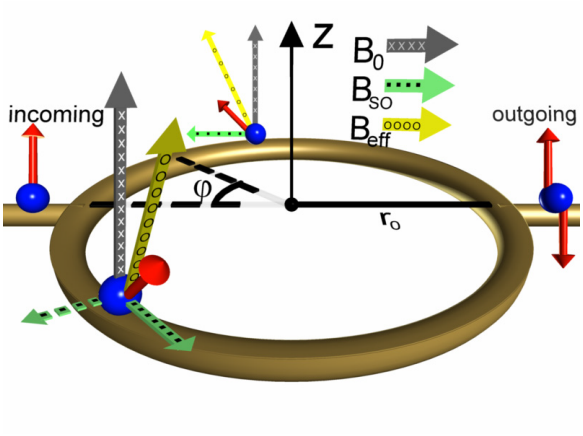

Fig. 12. Semiconductor quantum well patterned as a ring. Semiconductor quantum well patterned as a ring of radius r_0 in the presence of a magnetic field B_0 and of spin-orbit coupling. An electron(hole) spin traveling around the ring acquires phase due to the sum of the magnetic fields acting on it. The effective field, B_{eff}, is given by the yellow(o markings) arrow, the applied out-of-plane magnetic field, B_0, is represented by the gray(x markings) arrow, and the momentum dependent in-plane magnetic field due to spin-orbit interaction, B_{SO}, seen in green(• markings) arrow. The orientation of the spin-orbit field changes at different rates depending on the carriers, due to the holes (solid arrow) having a cubic in momentum spin splitting and the electrons (dashed arrow) having a spin splitting that depends linearly on the momentum.

A. Model Hamiltonians and calculation methods

1. Hamiltonians

In two-dimensional systems the effective mass Hamiltonian in the presence of both SO coupling and a perpendicular magnetic field, B_z, is:

$$H = \frac{\mathbf{\Pi}^2}{2m} + H_z + H_{conf} + H_{SO} \tag{5.1}$$

where $\mathbf{\Pi} = \mathbf{p} + (e/c)\mathbf{A}$, $H_z = \frac{1}{2} g \mu_g \sigma_z B_z$, and the electrostatic confining potential is given by H_{conf}. The SO terms in the single particle Hamiltonian is given by $H^e_{SO} = \alpha_1 \left(\hat{\sigma} \times \mathbf{\Pi}\right)_z / \hbar$ for electrons and $H^{hh}_{SO} = \alpha_3 \left(\hat{\sigma}_+ \Pi^3_- - \sigma_- \Pi^3_+\right) / \hbar^3$ for heavy holes. We limit our study to Rashba type SO coupling in narrow quantum wells, i.e. the structure inversion asymmetry is responsible for SO. The strength of the spin-orbit interaction is given by α_n. The system is illustrated in Fig. 12.

As outlined by Meijer *et al.* [74], to obtain the effective 1D Hamiltonian and due to the subtleties introduced by the SO interactions, it does not suffice to discard the derivatives in the radial direction and set $r = r_0$ in the 2D Hamiltonian. The single particle 1D Hamiltonian is found by assuming that the confining potential of the 2D system is such that the electron wave functions are confined to a 1D ring [74]:

$$H^e(\varphi, \Phi) = \frac{(\hbar\, \tilde{\partial}_\varphi)^2}{2m^* r_0^2} + H_z - \frac{\hbar^2 Q_e}{2m^* r_0^2} \left(\hat{\sigma}_{1,r} \tilde{\partial}_\varphi - \frac{i}{2} \hat{\sigma}_{1,\varphi} \right) \tag{5.2}$$

where $Q_e \equiv 2m^* \alpha_1 r_0 / \hbar^2$ characterized the strength of the spin-orbit coupling splitting in the thin ring limit relative to the angular leading term. The same process was used in finding the effective 1D heavy-hole Hamiltonian [73]:

$$\begin{aligned} H^{hh}(\varphi, \Phi) \;=\; & \frac{(\hbar\, \tilde{\partial}_\varphi)^2}{2m^* r_0^2} + \frac{\alpha_3}{r_0^3} \hat{\sigma}_{3,r} \left((\tilde{\partial}_\varphi)^3 + \tilde{\partial}_\varphi \left[\frac{3r_0^3}{w^2} - \frac{7}{2} \right] \right) \\ & + \frac{i\alpha_3}{2r_0^3} \hat{\sigma}_{3,\varphi} \left(\frac{3r_0^3}{w^2} + 1 + 3(\tilde{\partial}_\varphi)^2 \right) + H_z \end{aligned} \tag{5.3}$$

with r_0 being the radius of the ring, w is the half width of the ring channel, m^* the effective particle mass, φ the angular coordinate, $\tilde{\partial}_\varphi = i \frac{\partial}{\partial \varphi} + \Phi$, the Pauli spin operators ($\hat{\sigma}_x$ and $\hat{\sigma}_y$) assume their usual values. To allow a cleaner notation, we use the following generalization of the Pauli spin operators in cylindrical coordinates: $\hat{\sigma}_{n,r} = \cos(n\varphi)\, \hat{\sigma}_x + \sin(n\varphi)\, \hat{\sigma}_y$ and $\hat{\sigma}_{n,\varphi} = \cos(n\varphi)\, \hat{\sigma}_y - \sin(n\varphi)\, \hat{\sigma}_x$. The magnetic field is included by its corresponding magnetic flux, $\Phi = \pi r_0^2 B / \Phi_0$, where $\Phi_0 = hc/e$ is the

magnetic flux quantum. We model the heavy hole character of the band in that the SO interaction is cubic in momentum and the 2D Hamiltonian contains terms with r^n and nth derivatives with respect to r, $n = 1, 2, 3$. The projection of the lowest radial solution of the 2D Hamiltonian into a 1D Hamiltonian has as a consequence that in the heavy-hole calculation there are terms that depend on the width of the channel. As a contrast, in the electron system there are only terms dependent on the first power of r and the first derivatives with respect to r, thus the desired 1D Hamiltonian does not have the dependence on the width. In order to have a fully 1D systems the radius of the ring has to be larger than the width of the arms. In the electron systems the limit $w = 0$ can be taken; this is not possible in the heavy-hole systems. Nevertheless, we can obtain a simpler Hamiltonian than the one in Eq. (5.3) by assuming that the width of the channel is of the order of the Fermi wavelength ($k_f w \lesssim 1$) [73]:

$$H^{hh}(\varphi, \Phi) = \frac{(\hbar\ \tilde{\partial}_\varphi)^2}{2m^* r_0^2} + H_z + \frac{\hbar^2 Q_{hh}}{2m^* r_0^2}\left(\hat{\sigma}_{3,r}\tilde{\partial}_\varphi + \frac{3i}{2}\hat{\sigma}_{3,\varphi}\right) \tag{5.4}$$

where $Q_{hh} \equiv 6\alpha_3 m^* r_0/(\hbar^2 w^2)$ characterized the strength of the spin-orbit coupling splitting in the thin ring limit relative to the angular leading term and controls the precessions angle over the circumference of the ring. If the lateral confinement is not very strong leading to thick rings (the width of the channel is comparable to the Fermi wavelength), then we are not truly in the lowest radial mode. Although from Eq. (5.3) it is possible to write a Hamiltonian where the terms w^{-2} are not dominant, this will not be realistic unless those higher radial modes are taken into account. Unfortunately, current experiments have not reached the limit of single channel rings. We also consider structures where the SO interaction varies along the

azimuthal direction. Then an additional term appears in the Hamiltonian:

$$\begin{aligned} H^e(\varphi,\Phi) &= -\frac{\hbar}{2m^* r_0^2}\tilde{\partial}_\varphi^2 - \frac{i}{r_0}\alpha_1(\varphi)\left(\hat{\sigma}_{1,r}\tilde{\partial}_\varphi + \frac{1}{2}\hat{\sigma}_{1,\varphi}\right) \\ &\quad -\frac{i\hat{\sigma}_{1,r}}{2r_0}\frac{\partial\alpha_1(\varphi)}{\partial\varphi}, \end{aligned} \tag{5.5}$$

Our calculations do not consider the mixing of heavy-hole and light-hole states that is induced by the confinement. This neglected coupling has been shown to be responsible for an additional energy dependent non-adiabatic phase [75].

2. Landauer-Büttiker formalism

Numerical modeling of the rings is performed using the Landauer-Büttiker formalism [65, 76, 77]. We assume that the ring is attached to semi-infinite paramagnetic leads that act as reservoirs for the quasiparticles. The procedure is as follows. First, the 1D Hamiltonians of the ring structure are discretized in a tight-binding model [78], and used to find the retarded/advanced Green's function:

$$G^{R/A}(E) = (E - H - \Sigma^{R/A})^{-1} \tag{5.6}$$

The last term is the self-energy ($\Sigma^{R/A}$). It holds the connection between the structure and the semi-infinite leads. $\Sigma^R = \sum_p \Sigma_p^R$ involves a sum over all leads because we are assuming that all the leads are independent and thus their effects are additive. The description of the probes attached to our sample is made by solving the Green's function of a semi-infinite strip analytically. To do so, we need to calculate the self-energy terms which involves solving for the wave functions of the quasiparticles flowing from each lead into and out of the sample. With both the Green's functions and the self-energies at hand, we can write the transmission function:

$$T_{pq} = \mathrm{Tr}\left[\Gamma_p G^R \Gamma_q G^A\right] \tag{5.7}$$

where

$$\Gamma_p = i\left[\Sigma_p^R - \Sigma_p^A\right] \tag{5.8}$$

The Green's function describes the dynamics of the charge carrier in the conductor taking the leads into account where Γ_p represents the strength of the coupling of the leads to the sample. The total current flowing in each lead is obtained from the Landauer-Büttiker formula:[76, 77]

$$I_p = \frac{e^2}{h}\sum_{q\neq p} T_{pq}(V_p - V_q) = I_p^{\uparrow} + I_p^{\downarrow} \tag{5.9}$$

The spin current can be defined as:[79, 80]

$$I_{p,\sigma}^{\text{spin}} = \frac{\hbar}{2e}(I_p^{\uparrow} - I_p^{\downarrow}) = \frac{e}{4\pi}\sum_{q\neq p,\sigma'} T_{pq}^{\sigma\sigma'}(V_p - V_q) \tag{5.10}$$

where σ, σ' are the spin indices and the transmission function $T_{pq}^{\sigma\sigma'}$ gives us the probability of a particle with spin σ' injected in lead q is extracted from lead p with spin σ. In the four probe structure current is injected in the right lead and extracted in the left lead. The transverse leads (top and bottom) act as voltage probes. Thus, the longitudinal and spin Hall conductance are [80]:

$$G_L = \frac{I_R}{V_L - V_R} \tag{5.11}$$

$$G_{sH} = \frac{I_{T,\uparrow}^{\text{spin}} - I_{T,\downarrow}^{\text{spin}}}{V_L - V_R} \tag{5.12}$$

3. Boundary condition tight-binding model

In a ring system, the point where a lead and a ring subsection join can be considered as a three-way junction, as illustrated in Fig. 13. In this section we show how this method works in one dimensional structures but it can be easily extended to more dimensions. We first find the boundary condition for a three-way junction by assum-

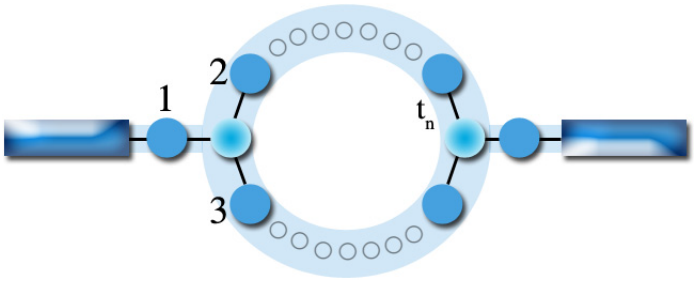

Fig. 13. Tight-binding representation of a ring attached to two leads. The ring attached to two leads can be modeled as two three-way junctions. Each of this three-way junctions connects to one lead and the subsections corresponding to each of the arm in the ring.

ing that the wave function used in the scattering S-matrix is also the eigenfunction of the system. Generally, the lattice distance in the three leads are a_1, a_2, and a_3, with $t_n = \hbar^2/2m_n a_n$ and $n = 1, 2, 3$. The potential at the joint point, where the three leads come together, is t_0. Under this assumption, the eigenfunction and eigenenergy of the electron in each lead can be obtained except at the joint point. Our aim is to find the boundary condition that will combine the three eigenfunctions in the leads and at the joint point to obtain the wave function for the whole system. Let us assume that the three eigenfunction corresponding to the three leads are Ψ_1, Ψ_2 and Ψ_3 and the function at the joint point is $\Psi(0)$. Thus, we have four equations:

$$(E - 2t_n)\Psi_n(a_n) + t_n\Psi_n(2a_n) + t_n\Psi(0) = 0 \tag{5.13}$$

$$(E - 2t_0)\Psi(0) + \sum_{i=1,2,3} t_i\Psi_i(a_i) = 0 \tag{5.14}$$

where $n = 1, 2, 3$ represents each of the leads. Since Ψ_n satisfies $(E - 2t_n)\Psi_n(a_n) - t_n\Psi_n(2a_n) - t_n\Psi_n(0) = 0$ and comparing this with Eq. (5.13), we obtain the first

boundary condition:

$$\Psi_1(0) = \Psi_2(0) = \Psi_3(0), \tag{5.15}$$

which is equivalent to the condition that the wave function is continuous at the boundary. As a result, Eq. (5.14) can be rewritten as

$$\begin{aligned}
&(E - (2t_0 - t_1 - t_2 - t_3))\Psi(0) \\
&+t_1(\Psi_1(a_1) - \Psi_1(0)) + t_2(\Psi_2(a_2) - \Psi_2(0)) \\
&+t_3(\Psi_3(a_3) - \Psi_3(0)) = 0
\end{aligned} \tag{5.16}$$

and we see that Eq. (5.16) is equivalent with saying that the first derivative is continuous except for a δ function at the junction point [81].

Using these boundary conditions in the tight binding model, the S-matrix of a three-way or multi-way junction can be calculated. It should be noted that the matrix we directly calculate is the so called S'-matrix which is not unitary [77]. The relation between the S-matrix and the S'-matrix can be given as

$$S_{mn} = S'_{mn}\sqrt{\frac{v_m}{v_n}}, \tag{5.17}$$

where $v_{m,n}$ is the velocity of the particle in the $m(n)$-th lead. The ring system attached to two leads can be considered as two three-way junctions each of which connects to one lead. These two junction S-matrices can be combined using the boundary conditions (Eqs. 5.13 and 5.14). With both S-matrices, the transmission function can be calculated by combining S-matrices with the advantage that we are able to see the contribution of each Feynman paths, as outlined in the book by Datta [77]. Having computed this S-matrix under proper boundary conditions, we can use it recursively to compute the transmission probabilities in order to study the effects of

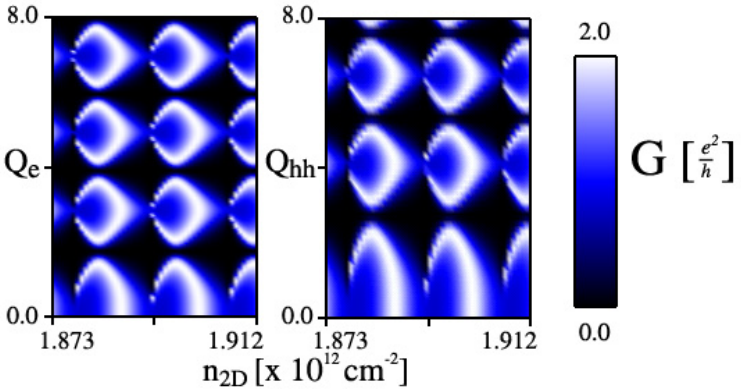

Fig. 14. Interference effects seen in the conductivity of mesoscopic rings. Calculation of the zero temperature conductance in a single-moded ring connected to two leads based on the Landauer-Büttiker formula. The conductance in both electron and heavy-hole systems is modulated as a function of the spin-orbit coupling and the carrier concentration. In the left panel we present the result for an electron system and in the right panel for a heavy-hole system; both systems have an effective mass of $m^* = 0.031\ m_0$.

the transparent lead approximation done in prior analytical works.

B. Effects due to the heavy-hole nature of the carriers

1. Aharonov-Casher effect

Approximate analytical forms for the conductance in ring structures have been found for electrons [62, 63, 64] and heavy-hole systems [73]:

$$G = \frac{e^2}{h}\left[1 - \cos\left(\pi\sqrt{1+Q_e^2}\right)\right] \tag{5.18}$$

$$G = \frac{e^2}{h}\left[1 - \cos\left(3\pi\sqrt{1+\frac{Q_{hh}^2}{9}}\right)\right] \tag{5.19}$$

The key approximation of the formulas above is that the coupling between the lead and the ring is perfectly transparent, neglecting backscattering effects that may lead

to resonances and other self-interference effects. Another assumption is that the transport of the quasiparticles is just from one lead to the other, traveling in one of the two arms only once, i.e. it does not take into account that the quasiparticles could wind around the ring structure more than half the ring's circumference. Eq. (5.19) is derived under an the assumption of a thin channel ring ($k_F w \lesssim 1$) [73].

In Figure 14 we show the contour plot of the zero temperature conductance in a single moded rings as a function of both the electron density and the dimensionless SO interaction strength using the full Landauer-Buttiker formalism. The left plot corresponds to electrons traveling in the ring (uses the Hamiltonian in Eq. (5.2)), and the right plot corresponds to the heavy-hole system (uses the Hamiltonian in Eq. (5.4)). In this and all subsequent calculations we considered a ring of radius $r_0 = 1\mu m$, an effective mass $m^* = 0.031\ m_0$, and starting from zero, we ramp up the dimensionless parameter controlling the strength of the SO splitting energy to 8. In the plots presented in Figure 14, we vary the carrier concentration from $n_{2D} = 1.873 \times 10^{12} cm^{-2}$ to $n_{2D} = 1.912 \times 10^{12} cm^{-2}$. These parameters correspond to the system measured in Ref. [70]. Further, we have chosen the carrier concentration assuming an infinite two-dimensional (2D) gas, the situation in the semi-infinite leads which are the particle reservoirs. As is evident in Fig. 14, the character of the SO coupling of the particles traversing the ring is of importance. As a function of the dimensionless parameter Q_e/Q_{hh} the heavy holes start at a slower rate reaching the same rate at higher values as the electron system. However, in experiments, where these parameters are a function of the gate voltage, we speculate that the oscillations as a function of gate voltage will likely be higher in the thin ring heavy hole system since the effective spin-orbit coupling is enhance with respect to the bulk value due to the confinement.

A comparison of the relative oscillation frequency in experiments, assuming a

splitting proportional to the top gate voltage in most set-ups where spin-orbit coupling can be tuned, would require a translation of the above figures to those parameters together with an accounting of the rate of change of the carrier density with gate voltage. For typical parameters, ignoring the carrier dependence on the oscillations, same parameters for electrons give a slower frequency of oscillation in the conductance as compared to the heavy-holes system when ($k_F \lesssim 1$) [73].

Our calculation is in partial agreement with the analytical formulas in that the conductance is modulated by the strength of the SO parameter and also exhibits, at certain values of Q (but independent of the particle density, i.e. Fermi energy), a zero conductance. As Souma and Nikolić [65] pointed out, these null values correspond to the zeroes of Eq. (5.18) and in the heavy-hole case to zeroes of Eq. (5.19). Similarly, the numerical results of Molnár and coworkers [64] found a dependence of the conductance in the Fermi wave-vector. These conductance oscillations as a function of the particle concentration not captured by the analytical treatment are due the neglect of backscattering from the leads and related to resonance energies of the rings as we show below.

Using a recursive S-matrix method we have performed calculations assuming the boundary condition tight-binding model to study the effects of backscattering at the leads and the validity of the transparent leads approximation. With this method we are able to obtain the conductance for different paths taken by the particles. In Fig. 15 we present contour plots of the conductance as a function of both the electron density and the dimensionless SO interaction strength for the same electron system as in Fig. 14 while increasing the number of allowed backscattering events. In this calculations, one lead is used for injecting electrons and the other will allow the electrons to exit the ring once they completed at most N scattering events from that same lead. The transparent leads case corresponds to Fig. 15 (a), where no

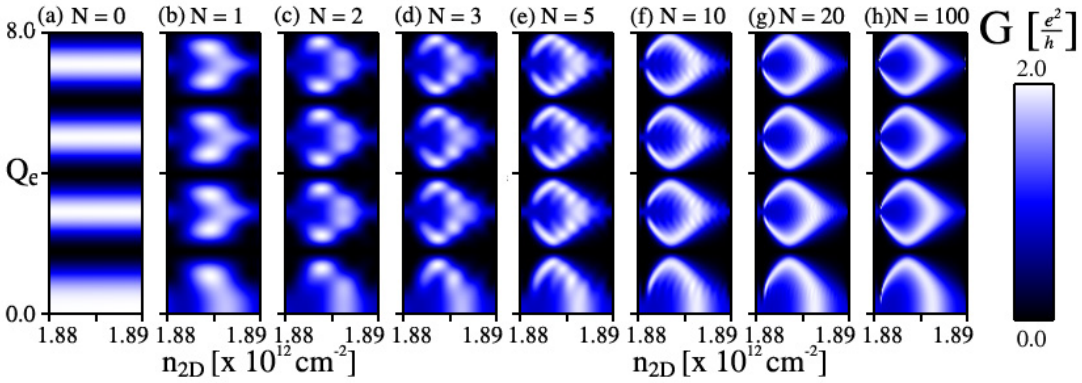

Fig. 15. Conductivity analysis based on the path taken by the charge carriers. Calculation based on the tight-binding model of the zero temperature conductance in a single-moded ring connected to two leads using a recursive S-matrix method. Each panel shows the conductance modulation as a function of both the spin-orbit interaction and the carrier density of the electrons when backscattering from the exit lead N times. $N \to \infty$ corresponds to the full calculation shown in Fig. 14.

backscattering is allowed in exact agreement with Eq. (5.18). If we allow for at most a single scattering event at the right lead before exiting the structure while accounting for all such possible paths, we obtain the contour plot in Fig. 15 (b). The continuous structure now gives way to a conductance that depends on the carrier density and it is further divided into periodic sub-structures. Each of these sub-structures shows that as a function of the SO coupling the conductance has either one or two peaks, depending on the carrier density. If the carrier concentration is chosen so that the Fermi energy is in resonance with an eigenenergy of the discretized ring then there is only one peak in the substructure and it happens at the same maximum value as when the lead was transparent. When the carrier density is chosen so that the Fermi energy is not very close to a value of the eigenvalues of the ring then the electron gets backscattered once and as it travels around the ring the path taken and the same

path but time-reversed are interfering with each other, similar to weak localization corrections to the conductance [82]. The $Q_e = 0$ result is also in agreement with the results obtained by Lucignano *et. al.* [83] for AB rings where once they allowed scattering at the leads, the Fourier spectrum of the magneto-conductance displays an additional peak at double the fundamental frequency ($2/\Phi_0$).

The rest of the panels show the result of more backscattering events being allowed. Finally, the periodic structures seen with this "path" calculations get closer to the structures found using the full Landauer-Büttiker calculation and these two methods are the same in the limit where the number of allowed backscattering events is taken to infinity. One thing we need to note is that in the heavy-hole calculation, as $Q_h h$ is increased there is a small curvature followed by the sub-structures in the SO coupling axis. The reason for that deviation is a numerical artifact. We have repeated the calculation varying the number of lattice points used to represent the discretized ring and as more points are used the sub-structures shift is reduced. This curvature is apparent in previous numerical calculations [65] but not recognized as numerical artifact. In our calculations we have chosen the carrier concentration such that the Fermi energy of the system is close to the bottom of the band and hence model in this way the continuous effective mass model appropriate for these semiconductor systems.

2. Spin Hall effect

The proposal of intrinsic spin Hall effect [84] and the experimental observation of the effect (both extrinsic and intrinsic) [39, 40] has generated a lot of interest in the semiconductor spintronics community. Numerical calculations based on the Landauer-Büttiker formalism on quantum coherent ballistic rings have shown that the spin Hall conductance exhibits quasi-periodic oscillations as a function of the Rashba SO

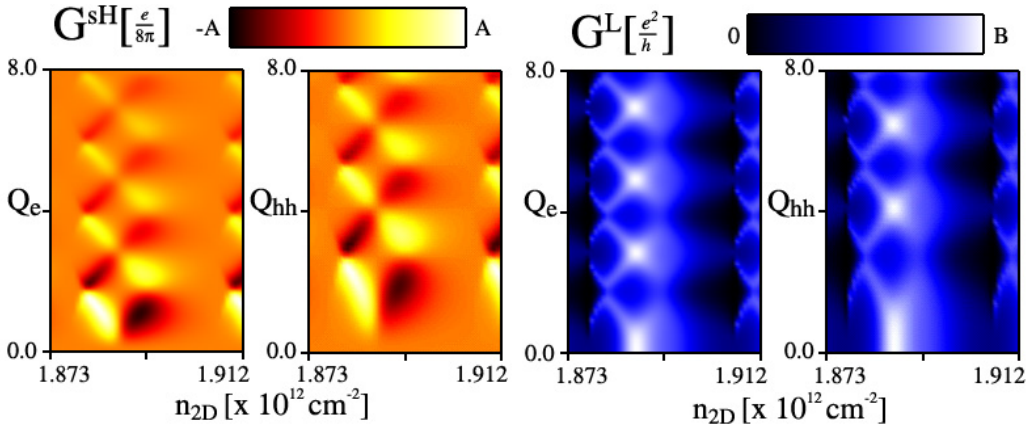

Fig. 16. Interference effects seen in the spin Hall conductivity. Calculation of the zero temperature spin-Hall and longitudinal conductance in four terminal ring structure based on the Landauer-Büttiker formula. The spin-Hall conductance (top panels) and longitudinal conductance (bottom panels) in electron and heavy-hole systems is modulated as a function of the spin-orbit coupling and carrier concentration. We present on the left the electron system where the spin Hall conductivity has a maximum value of $A = 0.72 \times e/(8\pi)$ and the longitudinal conductance has a maximum value of $B = 1.2 \times e^2/h$. In the heavy-hole system, shown on the right, the maximum value of the spin Hall conductivity is $A = 1.0 \times e/(8\pi)$ and the longitudinal conductance reaches a maximum value of $B = 1.7 \times e^2/h$.

coupling [66]. The calculation found several interesting predictions including the possibility of generating a spin Hall current in a ring with two longitudinal probes that inject/extract current and two transverse probes that would measure the voltage. Although experimental realization of such four-probe rings could prove difficult, we are interested in how the cubic SO term would affect the spin Hall effect.

As we show in Fig. 16, there are oscillations in the spin Hall conductance as the carrier density is increased. This oscillations have similar nature as those found in the conductance of the two-probe rings. The pattern seen by Souma and Nikolić [66]

is recognized from the figure, as we also observe that the spin Hall conductance oscillates in sign and that as the SO interaction increases the oscillations in the spin Hall conductance dampen. The longitudinal conductance of the four-probe ring shows common features with the conductance of the two-probe ring with two distinct features: (1) it does not vanish at specific values of the SO interaction and (2) the maximum value of the conductance is now lower than $2e^2/h$ due to the dephasing effects of the additional voltage probes. The addition of the transverse leads has shifted the structures to the left and now the structures we see are overlapping. It is at this overlap that the spin Hall conductance shows the x-like structures. The parameters used in these plots are similar to those used in the two-probe rings: the effective mass $m^* = 0.031\ m_0$ is the same in both systems, we vary the carrier concentration from $n_{2D} = 1.873 \times 10^{12} cm^{-2}$ to $n_{2D} = 1.912 \times 10^{12} cm^{-2}$, and starting from zero, we ramp up the dimensionless parameter controlling the strength of the SO splitting energy to 8. We note that the strength of the signal is larger for the heavy-hole system: maximum spin Hall conductance is $G_e^{sH} = 0.72 \times e/(8\pi)$ for electrons and $G_{hh}^{sH} = e/(8\pi)$ for heavy-hole system and the longitudinal conductance has a maximum value of $G_e^L = 1.2 \times e^2/h$ and $G_{hh}^L = 1.7 \times e^2/h$. As explained in the previous section, the curvature followed by the sub-structures as SO increases in the heavy-hole plots is a numerical artifact.

C. Inhomogeneous spin orbit coupling

Experimental efforts in mesoscopic rings have manipulated the SO splitting (in both the ring structure and the leads) via a gate voltage. Since the SO interaction depends on the surface electric field, there is a natural interest in studying the effects of a gate that covers only part of the system [85, 86]. Tserkovnyak and Brataas have predicted

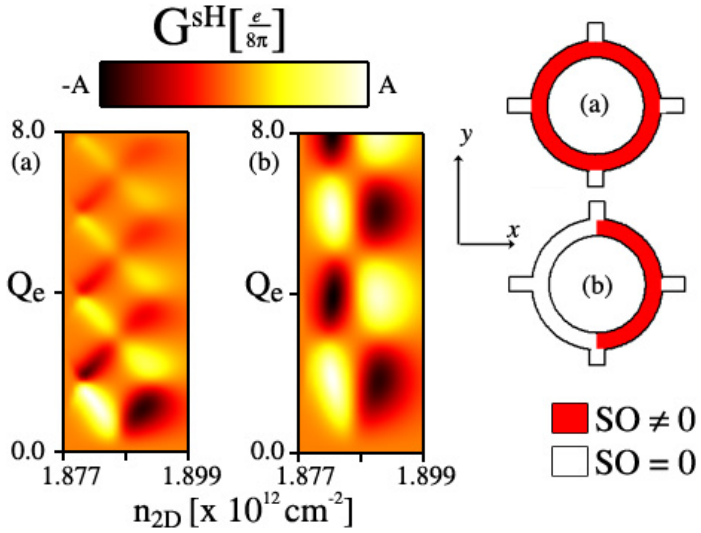

Fig. 17. Interference effects seen in the spin Hall conductivity of structures with inhomogeneous spin-orbit coupling. Calculation of the zero temperature spin-Hall conductance (four terminal device) based on the Landauer-Büttiker formula. The spin-Hall conductance in electron systems is modulated as a function of the spin-orbit coupling and electron density. When the spin-orbit coupling is homogeneous (Left picture), the spin Hall conductivity has a maximum value of $A = 0.72 \times e/(8\pi)$. When the spin-orbit coupling is present in only one half of the ring structure (Right picture), the maximum value of the spin Hall conductivity is $A = 1.07 \times e/(8\pi)$.

and enhancement of the interference effects in mesoscopic rings with inhomogeneous SO splitting for weak SO coupling systems [67]. We study those effects with our numerical techniques in spatially varying SO coupling systems. We observe an enhancement in the spin Hall conductivity in the four-probe rings and an unexpected modulation of the conductivity in the two-probe rings.

In the last two figures, we present the conductivities for a ring with a constant SO coupling (α_o) and compare it to the conductivities obtained in a ring where the electrostatic gate covers half of the ring. The SO coupling depends on the position

as:

$$\alpha(x) = \frac{\alpha_o}{2}\left(1 + \tanh\frac{x - x_o}{\Delta}\right) \tag{5.20}$$

Although not shown in the sketches in Figures 17 and 18, the value of Δ in the calculation allows for a transition region in the range of one tenth of the radius of the ring. This transition region would account for the electric field from the gate affecting parts of the ring not covered by the gate. Previous studies have shown that if the SO interaction is turned on abruptly there are strong scattering effects in the two regions [80, 87]. We have found that the sharpness of the transition region does not significantly change the conductivity patterns apart from the noticeable effect of a higher 'effective' SO coupling along the ring.

Fig. 17 shows the spin Hall conductivity as a function of Q_e and carrier density for a fully covered and a partially covered configuration. The oscillations are slower in the partially covered one due to the fact that the configuration of the right ring has a lower effective SO coupling. Yet, the pattern is significantly stronger ($\sim 35\%$). Also important is that the spin Hall conductivity does not dampen as the SO interaction is raised.

Next we study the spin-dependent conductivity for inhomogeneous SO interaction. The configuration we consider for the measurement would require the injection of spin polarized electrons into the ring structure and a means to detect their polarization as they exit the ring. Both the spin injection and the detection of the spin direction could be probed by electrical [88] or optical [89] means with current experimental techniques.

In Fig. 18, we show the contour plot of zero temperature conductances (total and spin resolved) in single moded rings as a function of both the electron density and the dimensionless SO interaction strength for three different spatial configurations of

the SO interaction. In the top panel we show the homogeneous case, which has been previously analyzed [65]. As the SO increases from zero, the injected electrons flip their spin direction. While the total conductance has the familiar periodic structure, these oscillations are only present in the spin-flipped (spin up injected on left lead and spin down detected on the right lead) conductivity. The spin conductivity for spin-conserved components (spin up injected and spin up detected) decays rapidly. The next two panels present the same calculation when only half of the ring is covered by the gate. As we see, the total conductivity is devoid of null values and is identical for the two configurations. In contrast, the spin-flipped and the same-spin conductivity show a marked difference from the homogeneous SO case. The spin-conserved conductivity does not decay as the SO increases but rather oscillates. Meanwhile, the spin-flipped conductivity is also oscillating and both conductivities contribute to the total value equally. This behavior illustrates that the reversal of the spin polarization could be controlled in ring structures by changing the voltage in a top-gate.

D. Summary

We have studied the quantum interference effects induced by the Aharonov-Casher phase in asymmetrically confined two-dimensional electron and heavy-hole ring structure systems taking into account the electrically tunable SO interaction. We calculated the non-adiabatic transport properties of charges in ring structures and confirm the analytic result [73]. We have found that the interference effects depend both on the SO splitting of the bands and the carrier density. Further, we are able to show that the contribution to the conductivity of non-transparent leads affect the conductivity and fully explains the Landauer-Büttiker result dependence on carrier density. We have calculated the spin Hall conductivity and longitudinal conductivity in four-

probe rings. Our analysis suggests that for hole doped systems both conductivities are stronger than the conductivities found in electron doped system. Finally, we have investigated the conductance of mesoscopic rings with spatially inhomogeneous SO coupling. In this case the spin Hall conductivity oscillates in a similar fashion as in the homogeneous SO case but, as the gate voltage is increased, the signal strength does not weaken in contrast to the homogeneous case. We have also found that devices with inhomogeneous SO interaction exhibit intriguing spin resolved conductivities which could lead to the modulation of the spin direction of polarized carriers.

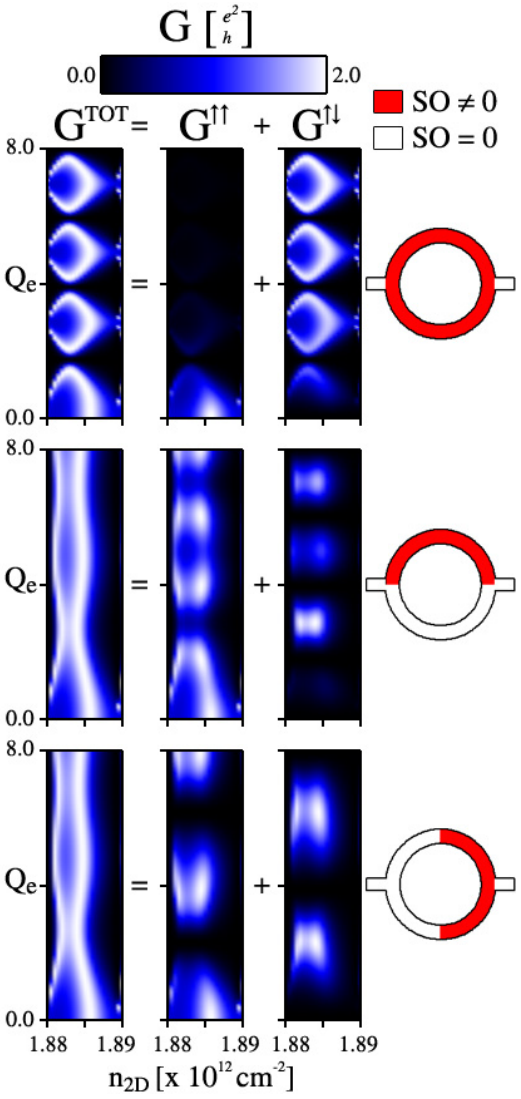

Fig. 18. Spin flipping mechanism seen in ring structures with spatially varying spin-orbit interaction.

CHAPTER VI

SUMMARY

A. Spin-orbit coupling in the weak relativistic limit

We have studied the Dirac equation to second order in the weak relativistic limit. We obtained the corrections to the kinetic energy terms, the Zeeman term and its second order corrections and by going to this order we have derived the spin-orbit coupling: $\hbar e(2mc)^{-2}\boldsymbol{\sigma}\cdot\mathbf{E}\times\boldsymbol{\pi}=\hbar e(2mc)^{-2}\boldsymbol{\sigma}\times\nabla V\cdot\mathbf{p}$. We also describe how this term is important in semiconductors and how the structure inversion symmetry of the systems studied gives origin to the Rashba term used in throughout the calculations.

B. Reduction of skew scattering in two-dimensional systems: testing the origins of the anomalous Hall effect

We have studied the anomalous Hall conductivity in spin-polarized, asymmetrically confined two-dimensional electron and hole systems, taking into account the intrinsic, side-jump, and skew-scattering contributions to the transport. We found that the skew scattering, principally responsible for the extrinsic contribution to the anomalous Hall effect, is reduced for the two-dimensional electron system if both chiral Rashba subbands are partially occupied, and vanishes always for the two-dimensional hole gas studied here, regardless of the band filling. Our prediction can be tested with the proposed coplanar two-dimensional electron-hole gas device and can be used as a benchmark to understand the crossover from the intrinsic to the extrinsic anomalous Hall effect.

C. Anomalous Hall effect in a two-dimensional electron gas

We have studied the anomalous Hall effect in a magnetic two-dimensional electron gas with Rashba spin-orbit coupling within the Kubo-Streda formalism in the presence of pointlike potential impurities. We find that all contributions to the anomalous Hall conductivity vanish to leading order in disorder strength when both chiral subbands are occupied. In the situation that only the majority subband is occupied, all terms are finite in the weak scattering limit and the total anomalous Hall conductivity is dominated by skew scattering. We compare our results to previous treatments and resolve some of the discrepancies present in the literature.

D. Transport in two-dimensional mesoscopic ring structures with strong spin-orbit interaction

We have studied the quantum interference effects induced by the Aharonov-Casher phase in asymmetrically confined two-dimensional electron and heavy-hole ring structures systems taking into account the electrically tunable spin-orbit (SO) interaction. We have calculated the non-adiabatic transport properties of charges (heavy-holes and electrons) in two-probe thin ring structures and compare how the form of the SO coupling of the carries affects it. We show that both the SO splitting of the bands and the carrier density can be used to modulate the conductance through the ring. We show that the dependence on carrier density is due to the backscattering from the leads which shows pronounce resonances when the Fermi energy is close to the eigenenergy of the ring. We also calculate the spin Hall conductivity and longitudinal conductivity in four-probe rings as a function of the carrier density and SO interaction, demonstrating that for heavy-hole carriers both conductivities are larger than for electrons. Finally, we investigate the transport properties of mesoscopic rings with

spatially inhomogeneous SO coupling. We show that devices with inhomogeneous SO interaction exhibit an electrically controlled spin-flipping mechanism.

REFERENCES

[1] W. M. Saslow, *Electricity, Magnetism, and Light*, (Academic Press, Amsterdam, 2002).

[2] S. A. Wolf, D. D. Awschalom, R. A. Buhrman, J. M. Daughton, S. von Molnar, M. L. Roukes, A. Y. Chtchelkanova, and D. M. Treger, Science **294**, 1488 (2001); I. Zutic, J. Fabian, and S. Das Sarma, Rev. Mod. Phys. **76**, 323 (2004).

[3] M. N. Baibich, J. M. Broto, A. Fert, F. Nguyen Van Dau, F. Petroff, P. Eitenne, G. Creuzet, A. Friederich, and J. Chazelas, Phys. Rev. Lett. **61**, 2472 (1988); G. Binasch, P. Grnberg, F. Saurenbach, and W. Zinn, Phys. Rev. B **39**, 4828 (1989); S. S. Parkin, N. More, and K. P. Roche, Phys. Rev. Lett. **64**, 2304 (1990).

[4] S. S. P. Parkin, *Applications of Magnetic Nanostructures*, (Taylor & Francis, New York , 2002).

[5] J. J. Sakurai, *Modern Quantum Mechanics*, (Addison-Wesley, Reading MA, 1994).

[6] R. Shankar, *Principles of Quantum Mechanics*, (Plenum, New York, 1994).

[7] L. H. Thomas, Nature **117**, 574 (1926).

[8] A. S. Davydov, *Quantum Mechanics*, (Pergamon, Oxford, 1965); P. Strange, *Relativistic Quantum Mechanics*, (Cambridge University, UK, 1998).

[9] B. Thaller, *The Dirac Equation*, (Springer-Verlag, Berlin, 1992).

[10] M. E. Peskin and D. V. Schroeder, *An Introduction to Quantum Field Theory*, (Addison-Wesley, Reading MA, 1995).

[11] F. Bloch, Zeitschrigt für Physik **52**, 555 (1928).

[12] P. Y. Yu and M. Cardona, *Fundamentals of Semiconductors*, (Springer, Berlin, 2001).

[13] E. O. Kane, J. Phys. Chem. Solids **1**, 249 (1957).

[14] R. Winkler, *Spin-Orbit Coupling Effects in Two-Dimensional Electron and Hole Systems*, (Springer, Berlin, 2003).

[15] J. M. Luttinger and W. Kohn, Phys. Rev. **97**, 869 (1955).

[16] M. Abolfath, T. Jungwirth, J. Brum, and A. H. MacDonald, Phys. Rev. B **63**, 054418 (2001).

[17] S.-R. E. Yang, J. Sinova, T. Jungwirth, Y. P. Shim, and A. H. MacDonald, Phys. Rev. B **67**, 045205 (2003).

[18] R. C. Fivaz, Phys. Rev. **183**, 586 (1969).

[19] P. Nozieres and C. Lewiner, Le Journal de Physique **34**, 901 (1973).

[20] E. N. Adams, II, (as pointed out by R. J. Elliot in footnote 7) Phys. Rev. **92**, 1063 (1953).

[21] J. Singh, *Physics of Semiconductors and their Heterostructures*, (McGraw-Hill International, New York, 1993); K. F. Brennan, *Physics of Semiconductors with Applications to Optoelectronic Devices*, (Cambridge University Press, Cambridge, 1999); B. G. Streetman and S. K. Banerjee, *Solid State Electronic Devices*, (Prentice Hall, NJ, 2006);

[22] Y. A. Bychkov and E. I. Rashba, J. Phys. C **17**, 6039 (1984).

[23] E. H. Hall, Philos. Mag. **10**, 301 (1880); E. H. Hall, Philos. Mag. **12**, 157 (1881).

[24] J. Sinova, T. Jungwirth, and J. Cerne, Int. J. Mod. Phys. B **18**, 1083 (2004).

[25] R. Karplus and J. M. Luttinger, Phys. Rev. **95**, 1154 (1954).

[26] J. Smit, Physica **21**, 877 (1955).

[27] L. Berger, Phys. Rev. B **2**, 4559 (1970).

[28] W. Kohn and J. M. Luttinger, Phys. Rev. **108**, 590 (1957).

[29] J. M. Luttinger, Phys. Rev. **112**, 739 (1958).

[30] N. A. Sinitsyn, A. H. MacDonald, T. Jungwirth, V. K. Dugaev, and J. Sinova, Phys. Rev. B **75**, 045315 (2007).

[31] D. Culcer, A. H. MacDonald, and Q. Niu, Phys. Rev. B **68**, 045327 (2003).

[32] V. K. Dugaev, P. Bruno, M. Taillefumier, B. Canals, and C. Lacroix, Phys. Rev. B **71**, 224423 (2005).

[33] N. A. Sinitsyn, Q. Niu, J. Sinova, and K. Nomura, Phys. Rev. B **72**, 045346 (2005).

[34] S. Y. Liu and X. L. Lei, Phys. Rev. B **72**, 195329 (2005).

[35] J.-I. Inoue, T. Kato, Y. Ishikawa, H. Itoh, G. E. W. Bauer, and L. W. Molenkamp, Phys. Rev. Lett. **97**, 046604 (2006).

[36] S. Onoda, N. Sugimoto, and N. Nagaosa, Phys. Rev. Lett. **97**, 126602 (2006).

[37] S. Y. Liu, N. J. M. Horing, and X. L. Lei, Phys. Rev. B **74**, 165316 (2006).

[38] M. I. Dyakonov and V. I. Perel, JETP **33**, 467 (1971); S. Murakami, N. Nagaosa, S.-C. Zhang, Science **301**, 1348 (2003); J. Sinova, D. Culcer, Q. Niu, N. A. Sinitsyn, T. Jungwirth, and A.H. MacDonald, Phys. Rev. Lett. **92**, 126603 (2004).

[39] Y. K. Kato, R. C. Myers, A. C. Gossard, and D.D. Awschalom, Science, **306**, 1910 (2004).

[40] J. Wunderlich, B. Kaestner, J. Sinova, and T. Jungwirth, Phys. Rev. Lett. **94**, 047204 (2005).

[41] V. Sih, R. C. Myers, Y. K. Kato, W. H. Lau, A. C. Gossard, and D. D. Awschalom, Nature Physics **1**, 31 (2005).

[42] N. A. Sinitsyn, J. Phys.: Condens. Matter **20**, 023201 (2008).

[43] B. A. Bernevig and S.-C. Zhang, Phys. Rev. Lett. **95**, 016801 (2005).

[44] T. S. Nunner, N. A. Sinitsyn, M. F. Borunda, V. K. Dugaev, A. A. Kovalev, Ar. Abanov, C. Timm, T. Jungwirth, J.-I. Inoue, A. H. MacDonald, and J. Sinova, Phys. Rev. B **76**, 235312 (2007).

[45] J. Inoue, G. E. W. Bauer, and L. W. Molenkamp, Phys. Rev. B **70**, 041303 (2004).

[46] A. A. Burkov, A. S. Nunez, and A. H. MacDonald, Phys. Rev. B **70**, 155308 (2004).

[47] O. Chalaev and D. Loss, Phys. Rev. B **71**, 245318 (2004).

[48] A. A. Kovalev, K. Výborný, and J. Sinova, Phys. Rev. B **78**, 041305(R) (2008).

[49] J. Banhart and H. Ebert, Europhys. Lett. **32**, 517 (1995); J. Ye, Y. B. Kim, A. J. Millis, B. I. Shraiman, P. Majumdar, and Z. Teanovic, Phys. Rev. Lett. **83**, 3737 (1999); T. Jungwirth, Q. Niu, and A. H. MacDonald, *ibid.* **88**, 207208 (2002); Y. Yao, L. Kleinman, A. H. MacDonald, J. Sinova, T. Jungwirth, D.-S. Wang, E. Wang, and Q. Niu, *ibid.* **92**, 037204 (2004); Y. Taguchi, Y. Oohara, H. Yoshizawa, N. Nagaosa, and Y. Tokura, Science **291**, 5513 (2001); W.-L. Lee, S. Watauchi, V. L. Miller, R. J. Cava, and N. P. Ong, *ibid.* **303**, 1647 (2004); J. Kötzler and W. Gil, Phys. Rev. B **72**, 060412(R) (2005); B. C. Sales, R. Jin, D. Mandrus, *ibid.* **73**, 224435 (2006); C. Zeng, Y. Yao, Q. Niu, and H. H. Weitering, Phys. Rev. Lett. **96**, 037204 (2006); S. H. Chun, Y. S. Kim, H. K. Choi, I. T. Jeong, W. O. Lee, K. S. Suh, Y. S. Oh, K. H. Kim, Z. G. Khim, J. C. Woo, and Y. D. Park, *ibid.* **98**, 026601 (2007); J. Cumings, L. S. Moore, H. T. Chou, K. C. Ku, G. Xiang, S. A. Crooker, N. Samarth, and D. Goldhaber-Gordon, *ibid.* **96**, 196404 (2006); T. Miyasato, N. Abe, T. Fujii, A. Asamitsu, S. Onoda, Y. Onose, N. Nagaosa, and Y. Tokura, *ibid.* **99**, 086602 (2007).

[50] M. F. Borunda, T. S. Nunner, T. Lück, N. A. Sinitsyn, C. Timm, J. Wunderlich, T. Jungwirth, A. H. MacDonald, and J. Sinova, Phys. Rev. Lett. **99**, 066604 (2007).

[51] P. Streda, J. Phys. C **15**, L717 (1982).

[52] N. A. Sinitsyn, Q. Niu, and A. H. MacDonald Phys. Rev. B **73**, 075318 (2006).

[53] Y. Imry, *Introduction to Mesoscopic Physics* (Oxford, New York, 1997).

[54] J. Anandan, Nature **360**, 307 (1992).

[55] S. Pancharatnam, Proc. Ind. Acad. Sci., **44 A**, 247 (1956).

[56] Y. Aharonov and D. Bohm, Phys. Rev. **115**, 485 (1959).

[57] Y. Aharonov and A. Casher, Phys. Rev. Lett. **53**, 319 (1984).

[58] M.V. Berry, Proc. R. Soc. A **392**, 45 (1984).

[59] Y. Aharonov and J. Anandan, Phys. Rev. Lett. **58**, 1593 (1987).

[60] D. Loss, P. Goldbart, and A. V. Balatsky, Phys. Rev. Lett. **65**, 1655 (1990).

[61] A.G. Aronov and Y.B. Lyanda-Geller, Phys. Rev. Lett. **70**, 343 (1993).

[62] J. Nitta, F.E. Meijerand, and H. Takayanagi, Appl. Phys. Lett. **75**, 695 (1999).

[63] D. Frustaglia, K. Richter, Phys. Rev. B **69**, 235310 (2004).

[64] B. Molnar, F.M. Peeters, and P. Vasilopoulos, Phys. Rev. B **69**, 155335 (2004).

[65] S. Souma and B.K. Nikolić, Phys. Rev. B **70**, 195346 (2004).

[66] S. Souma and B.K. Nikolić, Phys. Rev. Lett. **94**, 106602 (2005).

[67] Y. Tserkovnyak and A. Brataas, Phys. Rev. B **76**, 155326 (2007).

[68] G. Lommer, F. Malcher, and U. Rossler, Phys. Rev. Lett. **60**, 728 (1988); J. Nitta, T. Akazaki, H. Takayanagi, and Takatomo Enoki, *ibid* **78**, 1335 (1997); J. P. Lu, J. B. Yau, S. P. Shukla, M. Shayegan, L. Wissinger, U. Rössler, and R. Winkler, *ibid* **81**, 1282 (1998).

[69] T. Koga, Y. Sekine, and J. Nitta, Phys. Rev. B **74**, 041302(R) (2006).

[70] M. König, A.Tschetschetkin, E.M. Hankiewicz, J. Sinova, V.Hock, V. Daumer, M. Schäfer, C.R. Becker, H. Buhmann, and L.W.Molenkamp, Phys. Rev. Lett. **96**, 076804 (2006).

[71] B. Habib, E. Tutuc, and M. Shayegan, Appl. Phys. Lett. **90**, 152104 (2007).

[72] B. Grbic, R. Leturcq, T. Ihn, K. Ensslin, D. Reuter, and A.D. Wieck, Phys. Rev. Lett. **99**, 176803 (2007).

[73] A.A. Kovalev, M.F. Borunda, T. Jungwirth, L.W. Molenkamp, and J. Sinova, Phys. Rev. B **76**, 125307 (2007).

[74] F.E. Meijer, A.F. Morpurgo, and T.M. Klapwijk, Phys. Rev. B **66**, 033107 (2002).

[75] M. Pletyukhov and U. Zülicke, Phys. Rev. B **77**, 193304 (2008).

[76] M. Büttiker, Phys. Rev. Lett. **57**, 1761 (1986).

[77] S. Datta, *Electronic Transport in Mesoscopic Systems* (Cambridge University Press, Cambridge, 1995).

[78] A. Aldea, P. Gartner, and I. Corcotoi, Phys. Rev. B **45**, 14122 (1992).

[79] T.P. Pareek, Phys. Rev. Lett. **92**, 076601 (2004).

[80] B.K. Nikolić, L.P. Zârbo, and S. Souma, Phys. Rev. B **72**, 075361 (2005).

[81] Jian-Bai Xia, Phys. Rev. B, **45**, 3593(1992).

[82] E. Abrahams, P. W. Anderson, D. C. Licciardello, and T. V. Ramakrishnan, Phys. Rev. Lett. **42**, 673 (1979).

[83] P. Lucignano, D. Giuliano, and A. Tagliacozzo, Phys. Rev. B **76**, 045324 (2007).

[84] S. Murakami, N. Nagaosa, S.-C. Zhang, Science **301**, 1348 (2003); J. Sinova, D. Culcer, Q. Niu, N. A. Sinitsyn, T. Jungwirth, and A.H. MacDonald, Phys. Rev. Lett. **92**, 126603 (2004).

[85] M. Khodas, A. Shekhter, and A. M. Finkelstein, Phys. Rev. Lett. **92**, 086602 (2004).

[86] Y. Tserkovnyak, B. I. Halperin, A. A. Kovalev, and A. Brataas, Phys. Rev. B **76**, 085319 (2007).

[87] A. Reynoso, G. Usaj, and C. A. Balseiro, Phys. Rev. B **73**, 115342 (2006).

[88] X. Lou, C. Adelmann, S. A. Crooker, E. S. Garlid, J. Zhang, K. S. Madhukar Reddy, S. D. Flexner, C. J. Palmstrm, and P. A. Crowell, Nature Phys. **3**, 197 (2007).

[89] B. T. Jonker, G. Kioseoglou, A. T. Hanbicki, C. H. Li, and P. E. Thompson, Nature Phys. **3**, 542 (2007).

[90] A. Crepiux and P. Bruno, Phys. Rev. B **64**, 014416 (2001).

APPENDIX A

DEFINITIONS AND INTEGRATION OF σ^{II}

Here, we discuss and further clarify the meaning of the contributions from all states of the Fermi sea (σ^{II}_{yx}) to the anomalous Hall conductivity presented in Chapter IV. The definition of the conductivity tensor in the form of a sum, $\sigma_{yx} = \sigma^{I}_{yx} + \sigma^{II}_{yx}$, was proposed by Streda [51]. The idea behind this separation is that the first term, σ^{I}_{yx}, corresponds to the classical Drude-Zener formula of conductivity, whereas the second term, σ^{II}_{yx}, has no classical analogy. Another important point is that σ^{II}_{yx} does not depend on scattering from impurities. Later on, Streda's separation of the off-diagonal conductivity in two parts was rederived using the Kubo formalism [90].

The contribution σ^{I}_{yx} (see Chapter IV) is related only to the states at the Fermi surface, whereas σ^{II}_{yx} formally includes the contribution of all states with energies below the Fermi level. However, in the integral over energy in σ^{II}_{yx}, a part with $\epsilon = \epsilon_F$ can be additionally separated so that we can present σ^{II}_{yx} as

$$\sigma^{II}_{yx} = \sigma^{(\text{ int})}_{yx} - \sigma^{I(\text{ int})}_{yx}, \tag{A.1}$$

where $\sigma^{(\text{int})}_{yx}$ includes integration over all states with $\epsilon < \epsilon_F$. Mathematically, the reason for this is a singularity at the point $\epsilon = \epsilon_F$ related to the Fermi function $f(\epsilon)$ in the zero temperature limit. It was already discussed in Appendix C of Ref. [30] in the context of the two-dimensional Dirac model.

A. σ^{II}_{yx} Calculation: using the theorem of residues

Let us demonstrate it now within the model of two-dimensional electron gas with Rashba SO interaction. Starting from Eq. 4.34 with the Green's functions of a clean

crystal (Eq. 4.13),and calculating the trace, we can rewrite it as

$$\sigma_{yx}^{II} = -\frac{ie^2\alpha^2 h}{2\pi}\int\frac{d^2k}{(2\pi)^2}\frac{1}{\lambda_k}\int_{-\infty}^{\infty}d\epsilon f(\epsilon)\left(-G_-^{(0)R}\frac{\partial G_+^{(0)R}}{\partial\epsilon}+G_+^{(0)R}\frac{\partial G_-^{(0)R}}{\partial\epsilon}\right.$$
$$\left.+G_-^{(0)A}\frac{\partial G_+^{(0)A}}{\partial\epsilon}-G_+^{(0)A}\frac{\partial G_-^{(0)A}}{\partial\epsilon}\right) \quad (A.2)$$

The integral over energy runs over the real axis, while the poles of the Green's function are located in the plane near the real axis. Assuming that the temperature is very small but finite, the poles of the Fermi function, $f(\epsilon)$, are located at a finite distance form the real axis, $\epsilon_n = \epsilon_F + i(2n+1)\pi T$. Using Eq. (4.16) as the definition of the Green's functions and substituting in the above equation, along with the identity $G_\pm^{(0)A} = (G_\pm^{(0)R})^{*^\pm}$, we present

$$\sigma_{yx}^{II} = -\frac{ie^2\alpha^2 h}{2\pi}\int\frac{d^2k}{(2\pi)^2}\frac{1}{\lambda_k}\int_{-\infty}^{\infty}d\epsilon f(\epsilon)\left[\frac{1}{(\epsilon-E_{k-}+i0^+)(\epsilon-E_{k+}+i0^+)^2}\right.$$
$$-\frac{1}{(\epsilon-E_{k+}+i0^+)(\epsilon-E_{k-}+i0^+)^2}-\frac{1}{(\epsilon-E_{k-}-i0^+)(\epsilon-E_{k+}-i0^+)^2}$$
$$\left.+\frac{1}{(\epsilon-E_{k+}-i0^+)(\epsilon-E_{k-}-i0^+)^2}\right] \quad (A.3)$$

The integral over ϵ contains simple and double poles, and they can be shifted to the real axis. Correspondingly, the integration contour should be deformed to encircle each singularity in the complex plane. Thus, the contour would consist of some lines at the real axis and half circles around the poles. Each of the half circles gives half of the whole residue associated with the pole. Only the contribution of the poles give a real value for σ_{yx}. Thus, we take into account only this contribution. Then, we find

$$\sigma_{yx}^{II} = -\frac{ie^2\alpha^2 h}{2\pi}\int\frac{d^2k}{(2\pi)^2}\frac{1}{\lambda_k}\int_{-\infty}^{\infty}d\epsilon\left\{f(\epsilon)\left[4\frac{-i\pi\delta(\epsilon-E_{k-})}{(E_{k-}-E_{k+})^2}-4\frac{-i\pi\delta(\epsilon-E_{k+})}{(E_{k+}-E_{k-})^2}\right]\right.$$
$$\left.+\frac{\partial f(\epsilon)}{\partial\epsilon}\left[2\frac{-i\pi\delta(\epsilon-E_{k+})}{E_{k+}-E_{k-}}+2\frac{-i\pi\delta(\epsilon-E_{k-})}{E_{k-}-E_{k+}}\right]\right\} \quad (A.4)$$

The terms with $\partial f(\epsilon)/\partial\epsilon$ are related to the contribution from the Fermi surface. We obtain

$$\sigma_{yx}^{II-\text{ clean}} = \sigma_{yx}^{\text{clean}} - \sigma_{yx}^{I-\text{ clean}}, \tag{A.5}$$

where

$$\sigma_{yx}^{\text{clean}} = 4e^2\alpha^2 h \int \frac{d^2k}{(2\pi)^2} \frac{f(E_{k+}) - f(E_{k-})}{E_{k+} - E_{k-}}, \tag{A.6}$$

and

$$\sigma_{yx}^{I-\text{ clean}} = -2e^2\alpha^2 h \int \frac{d^2k}{(2\pi)^2} \left[\left(\frac{\partial f(E_{k+})}{\partial\epsilon} \right) + \left(-\frac{\partial f(E_{k-})}{\partial\epsilon} \right) \right] \frac{1}{(E_{k+} - E_{k-})^2} \tag{A.7}$$

Equation (A.6) is the formula for the intrinsic Hall conductivity in the clean limit. Iti is relates to all filled states (Fermi sea). From Eq. (A.5), the contribution to $\sigma_{yx}^{II-\text{ clean}}$ from the Fermi surface defined as $\sigma_{yx}^{I-\text{ clean}}$ partly compensates the intrinsic Hall conductivity $\sigma_{yx}^{\text{clean}}$. By integrating Eq. (A.5) we obtain

$$\sigma_{yx}^{\text{clean}} = -\frac{e^2}{4\pi} \left[1 - \frac{h}{\lambda_-} - \Theta(\epsilon_F - h) \left(1 - \frac{h}{\lambda_+} \right) \right] \tag{A.8}$$

Using Eq. (A.7) and the one presented above, we find

$$\sigma_{yx}^{I-\text{ clean}} = -\frac{e^2\alpha^2 h}{4\pi} \left(\frac{\nu_+}{\lambda_+^2} \Theta(\epsilon_F - h) + \frac{\nu_+}{\lambda_+^2} \right) \tag{A.9}$$

and with Eqs (A.5), (A.8), and (e:A9), Eq. (4.37) is obtained.

Let us emphasize that σ_{yx}^{II} corresponds to Streda's definition [51]. Dugaev *et al.* used a different method in their calculation [32]. In principle, both methods lead to the same result for the conductivity, as demonstrated in the two-dimensional Dirac model [30]. However, the contribution to the conductivity from the filled states, which was identified as σ_{yx}^{II} by Dugaev and coworkers [32], corresponds only to the "Fermi sea" term of Eq. (A.6) which corresponds to the clean limit calculation of the anomalous Hall conductivity calculated by Culcer *et al.* [31]. In turn, the contribution $\sigma_{yx}^{I-\text{ clean}}$

related to the Fermi surface but not affected by impurities was included into the σ_{yx}^{I} by Dugaev *et al.* [32] and the vertex correction should not appear in this term as was corrected later [30]. Hence, although initially the σ_{yx}^{I} and σ_{yx}^{II} are defined in Ref. [32] as in this work, in that article, their actual definitions were changed to terms only including Fermi sea integrals and Fermi surface integrals. Hence, they are not defined by Eqs. (A.5) and (A.6). We should emphasize here this difference of notations to avoid possible misunderstandings.

B. σ_{yx}^{II} Calculation: using the eigenstates

An alternative to the contour integration is to use the disorder free eigenstates of the Rashba Hamiltonian,

$$|\pm\rangle = e^{\pm i\phi/2}\begin{pmatrix} \pm e^{\pm i\phi/2}\left(\cos\frac{\gamma}{2} \pm \sin\frac{\gamma}{2}\right) \\ e^{i\phi/2}\left(\cos\frac{\gamma}{2} \mp \sin\frac{\gamma}{2}\right) \end{pmatrix}, \tag{A.10}$$

where $\sin\gamma = h/\lambda$ and $\tan\phi = k_y/k_x$ to calculate the clean limit of $\sigma_{yx}^{II-\text{ clean}}$ as the difference given in Eq. (A.5). In the clean limit, the calculation of σ_{yx} is as follows:

$$\begin{aligned}
\sigma_{yx}^{clean} &= \frac{e^2}{m^2 V}\sum_{\mathbf{k},n\neq n'}\frac{(f_{nk}-f_{n'k})\mathrm{Im}\left[\langle n'k|\hat{p}_x|nk\rangle\langle nk|\hat{p}_y|n'k\rangle\right]}{(E_{nk}-E_{n'k})^2} \\
&= -\frac{e^2}{(2\pi)^2}\int d\mathbf{k}\sum_n f_{nk}2\mathrm{Im}\left\langle\frac{\partial u_{n,k}}{\partial k_y}\middle|\frac{\partial u_{n,k}}{\partial k_x}\right\rangle \\
&= -\frac{e^2}{(2\pi)^2}\sum_n\int_C d\mathbf{k}\cdot f_{nk}\left\langle nk\middle|i\frac{\partial}{\partial\mathbf{k}}\middle|nk\right\rangle \\
&= -\frac{e^2}{(2\pi)^2}\sum_n\int_0^{2\pi} d\phi f_{nk}\left\langle nk\middle|i\frac{\partial}{\partial\phi}\middle|nk\right\rangle,
\end{aligned} \tag{A.11}$$

where, got the eigenstates given in Eq. (A.10), one finds

$$\left\langle\pm,k\middle|i\frac{\partial}{\partial\phi}\middle|\pm,k\right\rangle = \mp\frac{\lambda-h}{2\lambda} \tag{A.12}$$

thus

$$\sigma_{yx}^{clean} = -\frac{e^2}{4\pi}\left[\frac{\lambda_- - h}{2\lambda_-} - \Theta(\epsilon - h)\frac{\lambda_+ - h}{2\lambda_+}\right] \tag{A.13}$$

which is identical to the result obtained in Eq. (A.8).

The clean limit contribution to σ_{yx}^{I} is

$$\begin{aligned}\sigma_{yx}^{I-clean} &= \frac{e^2}{m^2 V}\mathrm{Tr}\left[\hat{v}_y G^{(0)R}(\epsilon_F)\hat{v}_x G^{(0)A}(\epsilon_F)\right] \\ &= \frac{e^2}{2\pi V}\sum_{\mathbf{k},s,s'}\langle s\,|\hat{v}_y|\,s'\rangle\, G_{s'}^{(0)R}\,\langle s'\,|\hat{v}_x|\,s\rangle\, G_s^{(0)A},\end{aligned} \tag{A.14}$$

using the eigenstates of the Rashba Hamiltonian, one finds

$$\begin{aligned}\sigma_{yx}^{I-clean} &= \frac{e^2}{2\pi V}\sum_{\mathbf{k}}(\langle +|\hat{v}_y|-\rangle\langle -|\hat{v}_x|+\rangle\, G_-^{(0)R}G_+^{(0)A} \\ &\qquad + \langle -|\hat{v}_y|+\rangle\langle +|\hat{v}_x|-\rangle\, G_+^{(0)R}G_-^{(0)A}) \\ &= \frac{e^2}{2\pi V}\sum_{\mathbf{k}} 2\mathrm{Im}\left[\langle +|\hat{v}_y|-\rangle\langle -|\hat{v}_x|+\rangle\right]\left(\frac{\pi\delta(\epsilon - E_{k-})}{\epsilon - E_{k+}} - \frac{\pi\delta(\epsilon - E_{k+})}{\epsilon - E_{k-}}\right) \\ &= \frac{e^2}{4\pi}\left\langle \mathrm{Im}\langle +|\hat{v}_y|-\rangle\langle -|\hat{v}_x|+\rangle\right\rangle_\phi\left(\frac{\nu_+}{\lambda_+} + \frac{\nu_-}{\lambda_-}\right),\end{aligned} \tag{A.15}$$

where the subscript ϕ indicates averaging over the momentum angle ϕ. For the Rashba model, one finds

$$\left\langle \mathrm{Im}\langle +|\hat{v}_y|-\rangle\langle -|\hat{v}_x|+\rangle\right\rangle_\phi = -\frac{\alpha^2 h}{\lambda}, \tag{A.16}$$

therefore Eq. (A.15) simplifies to Eq. (A.8). The two methods yield the same expressions for the contributions from all states of the Fermi sea (σ_{yx}^{II}).

APPENDIX B

INTEGRALS IN THE WEAK SCATTERING LIMIT

In the weak scattering limit (Γ, Γ_z small) the integrals over two Greens functions simplify to:

$$\begin{aligned}\frac{1}{2\pi}\int dk k f(k) G_+^R(k) G_+^A(k) &= \frac{1}{2\pi}\int dk k f(k) \frac{1}{\epsilon_F - E_{k+} + i\Gamma_+} \frac{1}{\epsilon_F - E_{k+} - i\Gamma_+} \\ &= \frac{1}{2\pi}\int dE_{k+} \nu_+ f(k(E_{k+})) \frac{1}{\Gamma_+} \frac{\Gamma_+}{(E_{k+}^2 - \epsilon_F^2)^2 + \Gamma_+^2} \\ &\approx \frac{\nu_+ f(k_+)}{2\Gamma_+}, \end{aligned} \tag{B.1}$$

similarly,

$$\frac{1}{2\pi}\int dk k f(k) G_-^R(k) G_-^A(k) \approx \frac{\nu_- f(k_-)}{2\Gamma_-}, \tag{B.2}$$

and

$$\begin{aligned}\frac{1}{2\pi}\int dk k f(k) G_+^R(k) G_-^A(k) &= \frac{1}{2\pi}\int dk k f(k) \frac{1}{\epsilon_F - E_{k+} + i\Gamma_+} \frac{1}{\epsilon_F - E_{k-} - i\Gamma_-} \\ &\approx \frac{1}{2\pi}\int dk k f(k) \left(\frac{1}{\epsilon_F - E_{k+}} - i\pi\delta(\epsilon_F - E_{k+})\right)\left(\frac{1}{\epsilon_F - E_{k-}} + i\pi\delta(\epsilon_F - E_{k-})\right) \\ &\approx \frac{i}{2}\int dk k f(k) \left(\delta(\epsilon_F - \epsilon_k + \lambda_k)\frac{1}{\epsilon_F - \epsilon_k - \lambda_k} - \delta(\epsilon_F - \epsilon_k - \lambda_k)\frac{1}{\epsilon_F - \epsilon_k + \lambda_k}\right) \\ &\quad + \frac{1}{2\pi}\int dk k f(k) \frac{1}{\epsilon_F - \epsilon_k - \lambda_k}\frac{1}{\epsilon_F - \epsilon_k + \lambda_k} \end{aligned} \tag{B.3}$$

yielding

$$\begin{aligned}&\frac{1}{2\pi}\int dk k f(k)(G_+^R(k)G_-^A(k) - G_-^R(k)G_+^A(k)) \\ &\quad \approx i\int dE_{k-} \frac{\nu_- f(k(E_{k-}))\delta(\epsilon_F - E_{k-})}{\epsilon_F - E_{k-} - 2\lambda_{k(E_{k-})}} - i\int dE_{k+} \frac{\nu_+ f(k(E_{k+}))\delta(\epsilon_F - E_{k+})}{\epsilon_F - E_{k+} + 2\lambda_{k(E_{k+})}} \\ &\quad = -\frac{i}{2}\left(\frac{\nu_+ f(k_+)}{\lambda_+} + \frac{\nu_- f(k_-)}{\lambda_-}\right). \end{aligned} \tag{B.4}$$

Now we find for the integrals I_1, I_2, I_3 and I_4 in the weak scattering limit:

$$\begin{aligned}
I_1 &= \frac{1}{2\pi}\int dkk\left(G_0^RG_0^A - G_z^RG_z^A\right)\\
&= \frac{1}{4}\frac{1}{2\pi}\int dkk\left(G_+^RG_+^A + G_-^RG_-^A + G_+^RG_-^A + G_-^RG_+^A - (h^2+\Gamma_z^2)\right.\\
&\quad \left.\times\frac{\lambda_k^2}{\lambda_k^4+h^2\Gamma_z^2}\left(G_+^RG_+^A + G_-^RG_-^A - G_+^RG_-^A - G_-^RG_+^A\right)\right)\\
&\approx \frac{1}{4}\frac{1}{2\pi}\int dkk\left(1-\frac{h^2}{\lambda_k^2}\right)\left(G_+^RG_+^A + G_-^RG_-^A\right)\\
&\approx \frac{1}{8}\left(\left(1-\frac{h^2}{\lambda_+^2}\right)\frac{\nu_+}{\Gamma_+} + \left(1-\frac{h^2}{\lambda_-^2}\right)\frac{\nu_-}{\Gamma_-}\right), \qquad \text{(B.5)}\\
I_2 &= \frac{1}{2\pi}\int dkk\left(G_0^RG_z^A - G_z^RG_0^A\right)\\
&= -\frac{1}{2}\frac{1}{2\pi}\int dkk\frac{\lambda_k}{\lambda_k^4+\Gamma_z^2h^2}\left(h(\lambda_k^2+\Gamma_z^2)(G_-^RG_+^A - G_+^RG_-^A)\right.\\
&\qquad\qquad \left.+i\Gamma_z(h^2-\lambda_k^2)(G_+^RG_+^A - G_-^RG_-^A)\right)\\
&\approx -\frac{1}{2}\frac{1}{2\pi}\int dkk\frac{1}{\lambda_k^3}\left(h\lambda_k^2(-G_+^RG_-^A + G_-^RG_+^A) + i\Gamma_z(h^2-\lambda_k^2)(G_+^RG_+^A - G_-^RG_-^A)\right)\\
&\approx -\frac{i}{4}\left(\frac{\nu_+h}{\lambda_+^2} + \frac{\nu_-h}{\lambda_-^2} + \frac{\Gamma_z}{\Gamma_+}\frac{\nu_+(h^2-\lambda_+^2)}{\lambda_+^3} - \frac{\Gamma_z}{\Gamma_-}\frac{\nu_-(h^2-\lambda_-^2)}{\lambda_-^3}\right) \qquad \text{(B.6)}\\
I_3 &= \frac{1}{2\pi}\int dk\frac{k^2}{2m}\left(\tilde{G}_y^RG_z^A - G_z^R\tilde{G}_y^A\right)\\
&= -\frac{i}{2}\frac{1}{2\pi}\int dkk\frac{k^2}{2m}\frac{\alpha\Gamma_z\lambda_k^2}{\lambda_k^4+\Gamma_z^2h^2}(G_+^RG_+^A + G_-^RG_-^A - G_+^RG_-^A - G_-^RG_+^A)\\
&\approx -\frac{i}{2}\frac{1}{2\pi}\int dkk\frac{k^2}{2m}\frac{\alpha\Gamma_z}{\lambda_k^2}(G_+^RG_+^A + G_-^RG_-^A)\\
&\approx -\frac{i}{4}\alpha\Gamma_z\left(\epsilon_F\left(\frac{\nu_+}{\Gamma_+\lambda_+^2} + \frac{\nu_-}{\Gamma_-\lambda_-^2}\right) - \frac{\nu_+}{\Gamma_+\lambda_+} + \frac{\nu_-}{\Gamma_-\lambda_-}\right). \qquad \text{(B.7)}\\
I_4 &= \frac{1}{2\pi}\int dk\frac{k^2}{2m}\left(G_0^R\tilde{G}_y^A + \tilde{G}_y^RG_0^A\right)\\
&= -\frac{1}{2}\frac{1}{2\pi}\int dkk\frac{k^2}{2m}\frac{\alpha\lambda_k}{\lambda_k^4+\Gamma_z^2h^2}\left(\lambda_k^2(G_+^RG_+^A - G_-^RG_-^A) + i\Gamma_zh(G_-^RG_+^A - G_+^RG_-^A)\right)\\
&\approx -\frac{1}{2}\frac{1}{2\pi}\int dkk\frac{k^2}{2m}\frac{\alpha}{\lambda_k}(G_+^RG_+^A - G_-^RG_-^A)\\
&\approx -\frac{1}{4}\alpha\left(\epsilon_F\left(\frac{\nu_+}{\Gamma_+\lambda_+} - \frac{\nu_-}{\Gamma_-\lambda_-}\right) - \left(\frac{\nu_+}{\Gamma_+} + \frac{\nu_-}{\Gamma_-}\right)\right). \qquad \text{(B.8)}
\end{aligned}$$

VITA

Mario Francisco Borunda Bermúdez was born in Acapulco de Juárez, Guerrero, Mexico on 1978. His parents are Mario Elías Borunda Escobedo and Silvia Lorenza Bermúdez de Borunda. He attended public schools in Mexico City, Ciudad Juárez, Chihuahua, Mexico and in El Paso, Texas, USA. He obtained his Bachelor in Science degree in physics and mathematics at The University of Texas at El Paso, in 2003 and became a Doctor of Philosophy specializing in theoretical condensed matter physics under the supervision of Professor Jairo Sinova at Texas A&M University, in 2008.

Contact information: Department of Physics, Texas A&M University, 4242 TAMU, College Station, TX 77843-4242.